Threshold Resummation Effects
on the Parton Distribution Function of the Pion and
Time-Reversal-Odd Single-Spin Asymmetries

Dissertation

zur Erlangung des
Doktorgrades der Naturwissenschaften
(Dr. rer. nat.)
der Fakultät für Physik
der Universität Regensburg

vorgelegt von
Matthias Aicher
aus Regenstauf

Juni 2011

Contents

1. Motivation

Over the last fifty years a huge effort in both experimental and theoretical physics has been made to shed light on the internal structure of the constituents of nuclei, the protons and neutrons. In the 1960s, it was Murray Gell-Mann [1], and independently Georg Zweig [2], who proposed the quark model originally as a classification scheme for the large number of different hadrons identified in accelerator experiments by that time. In this model the hadrons are no elementary particles but bound states of quarks and antiquarks. In 1969, on the experimental side groundbreaking results were obtained at the Stanford Linear Accelerator Center (SLAC), where high-energy electrons were scattered off a nuclear target in a so-called deep-inelastic scattering (DIS) experiment. The measured data unambiguously showed that the electrons interacted with point-like spin-1/2 particles within the protons, which were called *partons* and later identified with the quarks in Gell-Mann's model.

This observation laid the ground for the development of *Quantum Chromodynamics* (QCD), the quantum field theory describing the strong interaction of color-charged particles which build up nuclear matter, namely quarks and gluons. However, theorists were facing immense problems in modeling the quarks' and gluons' behavior as they seemed to posses ambiguous properties: On the one hand, the SLAC experiment suggested that quarks in the proton behave as almost free particles on short time or distance scales, on the other hand, all experimental efforts to detect isolated free quarks failed. More precisely, quarks and gluons can only be observed in color-neutral combinations, the hadrons. This remarkable feature of strong interaction physics is referred to as *color confinement*. The problem of the almost vanishing interaction at short distance scales was successfully resolved in 1973 when Gross, Wilczek, and Politzer [3, 4] discovered that QCD, as a non-abelian quantum field theory, possesses another fundamental property: *asymptotic freedom*. I.e. on large momentum scales or, equivalently, short time or distance scales the strength of the coupling between quarks and gluons decreases and quarks and gluons become quasi-free particles. This feature allows to treat the strong interaction perturbatively as a power series in the strong coupling α_s. Perturbation theory was then successfully applied to the derivation of corrections to the structure functions measured in the SLAC DIS experiment. Later, advanced experimental setups enabled physicists to precisely measure these corrections in DIS. The observed data clearly verified the theoretical predictions.

Due to this successful application to DIS, perturbative QCD was used to predict cross sections for more sophisticated hadronic processes. However, perturbation theory is only

valid if in the derivation of a hadronic observable the perturbatively calculable hard part, i.e. the process associated with a large momentum transfer, is separated from the soft part including the momentum distribution of quarks and gluons inside the hadron. In field theory this separation is known as *factorization*. For inclusive processes, such as DIS and the Drell-Yan process, elaborate factorization theorems have been worked out, while for several exclusive hadronic processes reasonable factorization arguments exist, but have not been proven to all orders. A factorized hadronic cross section σ can schematically be written as a convolution,

$$\sigma = f^H \otimes \hat{\sigma}, \tag{1.1}$$

where f^H is referred to as parton distribution function (PDF) and parameterizes the distribution of quarks and gluons in the hadron H. The hard-scattering function $\hat{\sigma}$ can be calculated in perturbation theory as a series expansion in α_s. For most processes calculations of the hard-scattering function have been performed to leading order (LO) or next-to-leading order (NLO) in the strong coupling. It turns out that the soft functions are universal and do not depend on the considered hadronic process. This feature makes perturbative QCD a powerful and indispensable tool in the exploration of the internal structure of hadrons. In part I of this thesis we outline the fundamental concepts needed for such a perturbative calculation, namely factorization, regularization and renormalization. The framework which we introduce in principle allows to calculate hard-scattering functions for any high-energy process involving strongly interacting particles.

By means of Eq. (1.1) an analysis of all available experimental data from different hadronic processes can be employed to extract one set of universal parton distributions. Several such *global* analyses have been performed to determine the parton distributions of the proton to a very good accuracy [5–7]. The same approach has also been used to uncover the internal structure of mesons, especially the pion. Due to its dual role as the lightest quark-antiquark bound state and the Nambu-Goldstone boson of dynamical chiral symmetry breaking in QCD it plays a significant role in strong-interaction physics. It is therefore all the more regrettable that its internal structure is still rather poorly known. The reason for that is the lack of reliable experimental data. Since the pion is a short-lived particle, the experimental setup for measuring processes with a pion in the initial state is more involved than for stable particles, such as the proton. Most of the available information comes from Drell-Yan dimuon production. That is the production of a virtual massive photon, which subsequently creates a pair of muons, in the collision of two hadrons. These data have been analyzed using LO and NLO cross sections [8–11]. However, the behavior of the extracted pion PDFs is at odds with theoretical predictions based on perturbative QCD and several low-energy effective models of hadronic structure [12]. This discrepancy is an important long-standing problem in strong-interaction physics and challenges our understanding of hadronic structure.

In part II we try to resolve this issue. We find that in the kinematic regime accessed by the available pion Drell-Yan data perturbative corrections beyond NLO are significant. In the Drell-Yan process, the relation $z = Q^2/x_1 x_2 S = 1$ sets a threshold for the partonic reaction, where Q and $\sqrt{S}$ denote the invariant mass of the lepton pair and the overall hadronic center-of-mass energy, respectively, and x_1 and x_2 are the momentum fractions of the partons participating in the hard-scattering reaction. Near the threshold the cross section receives large logarithmic corrections of the form

$$\alpha_s^n \left(\frac{\ln^{2n-1}(1-z)}{1-z} \right)_+ \tag{1.2}$$

at the nth order of perturbation theory. These so-called threshold logarithms become particularly important in the fixed-target regime, because here the ratio Q^2/S is relatively large. It then becomes necessary to take these large corrections into account to all orders by resumming the perturbative series, a technique known as *threshold resummation*. For the Drell-Yan process threshold resummation was originally derived by Sterman [13] and Catani and Trentadue [14] more than 20 years ago. The techniques developed in these seminal papers have later been extended and successfully applied to the resummation of large logarithmic corrections in numerous other hard QCD processes. In this thesis, we perform a new analysis of pion Drell-Yan data including threshold-resummation effects in the calculation of the cross section. In contrast to all previous fixed-order analyses, the extracted valence PDF of the pion agrees with predictions based on the QCD parton model and perturbative QCD.

Part III of this thesis is dedicated to a quite different topic. We study so-called single-spin asymmetries. These are asymmetric observables in high-energy processes with one polarized initial-state particle. The phenomenology of single-spin asymmetries is generally different for transversely and longitudinally polarized particles. While large single transverse-spin asymmetries were already measured in the 1970s in processes involving electromagnetic and strong interactions [15], single longitudinal-spin asymmetries in hadronic collisions were only recently detected in parity-violating observables in the production of $W^{\pm}$-bosons at RHIC [16, 17]. Since in hadronic processes weak interaction is strongly suppressed at momentum transfer $Q \ll M_W$, parity-violating observables can generally only be observed at very large momentum scales. By contrast, observed single transverse-spin asymmetries are associated with so-called naive-time-reversal-odd (T-odd) observables, i.e. quantities which change sign under simultaneous reversal of both spins and three-momenta. T-odd effects are generally not forbidden in strong interaction physics and may therefore also be detected in fixed-target experiments. To explain the large size of the asymmetries theorists have developed certain QCD-based mechanism over the last 20 years, which rely on the use of transverse-momentum dependent parton distributions and include higher-twist effects.

However, higher-order perturbative corrections can also account for T-odd effects, even in the longitudinally polarized case. Although these perturbative corrections are rather small, the predicted T-odd single longitudinal-spin asymmetries can still be measured by means of accurate experiments foreseen for the planned high-luminosity electron-ion collider at RHIC (eRHIC), and may serve as a thorough test for the validity of higher-order QCD predictions. In this thesis we calculate the lowest-order non-vanishing perturbative contribution to the single longitudinal-spin asymmetry in semi-inclusive deep-inelastic scattering and perform a numerical analysis of the results in the kinematic regime relevant for the eRHIC project.

Part I.

Introduction

2. Foundations of Perturbative Quantum Chromodynamics

In this first chapter, we present the general framework needed for perturbative calculations in QCD. The starting point for our considerations is the Lagrangian density of QCD. As for any quantum field theory, all properties of the respective theory can be deduced from this single expression. Particularly, in perturbative QCD the Lagrangian serves as a 'book of rules': The so-called Feynman rules provide a framework, which allows to write down an analytic expression for any given partonic process to any given order in perturbation theory. The Lagrangian and the deduced rules are characterized by the symmetries of the theory. The fundamental symmetry of QCD is SU(3) gauge symmetry. In Sec. 2.2 we therefore study the properties of the group SU(3) and its underlying algebra. Section 2.3 deals with the running of the coupling α_s in QCD. It exhibits asymptotic freedom, which is a necessary condition for a perturbative treatment of gauge theories at high energies.

2.1. The Lagrangian

As mentioned above, the form of the Lagrangian density is determined by the symmetries of the corresponding theory. For example, Poincare symmetry implies that the Lagrangian density is invariant under Lorentz transformations and hence has to be a Lorentz scalar. Another symmetry which is fundamental to QCD is SU(3) color gauge symmetry, i.e. the Lagrangian density is invariant under a local SU(3) gauge transformation of the fermionic (spin-$\frac{1}{2}$) quark fields $\Psi_f(x)$,

$$\Psi_f(x) \rightarrow e^{ig\theta^a(x)t^a}\Psi_f(x), \tag{2.1}$$

where $\theta^a(x)$ are position-dependent scalar functions with the index a running from 1 to 8. The subscript f denotes the quark flavor. The generators of the gauge transformation t^a obey the commutator relation

$$\left[t^a, t^b\right] = if^{abc}t^c \tag{2.2}$$

with f^{abc} structure constants which define the underlying SU(3) Lie algebra. Respecting both the Poincare and the SU(3) gauge symmetry, the classical Lagrangian density of

QCD reads

$$\mathcal{L}_{\text{cl}} = \sum_f \bar{\Psi}_f(x) \left(i\gamma^\mu D_\mu - m_f\right) \Psi_f(x) - \frac{1}{4} F^a_{\mu\nu}(x) F^{a\mu\nu}(x), \tag{2.3}$$

where the sum runs over all active quark flavors f with masses m_f. The vector D_μ denotes the covariant derivative and is defined as

$$D_\mu = \partial_\mu - ig A^a_\mu(x) t^a, \tag{2.4}$$

where the bosonic fields A^a_μ are the massless spin-1 gluon fields. The field strength tensor $F^a_{\mu\nu}$ of these bosonic fields is defined as

$$F^a_{\mu\nu}(x) = \partial_\mu A^a_\nu(x) - \partial_\nu A^a_\mu(x) + g f^{abc} A^b_\mu(x) A^c_\nu(x). \tag{2.5}$$

The third term in the field strength tensor implies that the gluon fields interact with themselves, in contrast to the photon fields in Quantum Electrodynamics (QED), which only couple to electromagnetically charged fermions. This self-interaction of the gauge fields is due to the non-abelian character of the underlying gauge group SU(3), manifest in the commutator relation in Eq. (2.2).

Owing to the invariance of the classical Lagrangian under gauge transformations the gauge fields cannot be uniquely determined by physical observables. This freedom results in an infinite number of possible gauge choices for the gluon fields. Quantization of the Lagrangian of QCD, however, requires to eliminate those unphysical degrees of freedom. This is done by adding a gauge-fixing term to the Lagrangian. Since we want the gauge condition to be invariant under Lorentz transformations, we choose the covariant gauge $\partial^\mu A^a_\mu = 0$. This special gauge is implemented in the Lagrangian by adding the term

$$\mathcal{L}_{\text{gf}} = -\frac{1}{2\xi} \left(\partial^\mu A^a_\mu\right) \left(\partial^\nu A^a_\nu\right) \tag{2.6}$$

with a gauge parameter ξ. As physical observables are independent of the choice of gauge, the value of the parameter ξ is arbitrary. It is convenient to choose $\xi = 1$, referred to as Feynman gauge. The prize of a covariant gauge-fixing term in a non-abelian gauge theory is that the unphysical degrees of freedom remain for the self-interaction of gauge fields. To eliminate these degrees of freedom additional anti-commuting scalar particles, which couple to the gluon fields, have to be introduced to the theory. This is done by adding the ghost Lagrangian

$$\mathcal{L}_{\text{ghost}} = g f^{abc} \bar{\chi}^a \partial^\mu (A^c_\mu \chi^b) - \bar{\chi}^a \partial^\mu \partial_\mu \chi^a \tag{2.7}$$

with the anti-commuting Faddeev-Popov ghost fields χ^a [18].

Altogether the Lagrangian of QCD in covariant gauge takes the form,

$$
\begin{aligned}
\mathcal{L}_{\text{QCD}} =& \mathcal{L}_{\text{cl}} + \mathcal{L}_{\text{gf}} + \mathcal{L}_{\text{ghost}} \\
=& \sum_f \bar{\Psi}_f(x) \left(i\gamma^\mu D_\mu - m_f\right) \Psi_f(x) - \frac{1}{4} F^a_{\mu\nu}(x) F^{a\mu\nu}(x) \\
& - \frac{1}{2\xi} \left(\partial^\mu A^a_\mu\right) \left(\partial^\nu A^a_\nu\right) \\
& + g f^{abc} \bar{\chi}^a \partial^\mu (A^c_\mu \chi^b) - \bar{\chi}^a \partial^\mu \partial_\mu \chi^a.
\end{aligned}
\tag{2.8}
$$

From this expression our main tool in perturbative QCD, the Feynman rules, can be deduced. They are defined from the action of the theory

$$
S_{\text{QCD}} = i \int \mathrm{d}^4 x \, \mathcal{L}_{\text{QCD}}.
\tag{2.9}
$$

In case the interaction of fields can be treated as a perturbation of the corresponding interaction-free theory, it is intuitive to split up the action into two terms,

$$
S_{\text{QCD}} = S_0 + S_{\text{int}},
\tag{2.10}
$$

where S_{int} contains all terms of the Lagrangian describing the interaction of fields. Of course, a necessary condition for treating the interaction as a perturbation is that the coupling between the fields is small. We will come back to this point later. The propagators of the fields are now deduced from the free part S_0 of the action. For example, the fermion propagator is given by the inverse of the Dirac operator in momentum space,

$$
iS(p) = \frac{i}{\slashed{p} - m + i\eta},
\tag{2.11}
$$

where we use the symbolic notation $\slashed{p} = \gamma_\mu p^\mu$. The $i\eta$ prescription in the denominator preserves causality. Similarly, the propagator for the gluon fields is derived from S_0 and rules for the interaction of quarks and gluons (and ghost fields) are deduced from S_{int}. In Appendix A.1 we present all Feynman rules and corresponding diagrams in QCD.

2.2. The Group SU(3)

As we have seen above, the symmetry under SU(3) gauge transformations is a striking property of the QCD Lagrangian. Another classic example for a gauge theory is QED and its local gauge group U(1). The properties of the gauge-group algebra can directly be translated to the properties of the corresponding gauge fields. E.g. since U(1) is an abelian group, the photons in electromagnetism do not interact with each other. By contrast, SU(3) is a non-abelian group and hence self-interaction of gluon fields occurs.

In the following, we state some major properties of the algebra and the representations of the group SU(3). An extensive review on group theory can be found in Ref. [19].

Let us first consider the most intuitive and also most important representation of the group SU(3): the fundamental representation. Group elements can be visualized as unitary 3×3 - matrices with complex arguments and determinant 1,

$$U = \begin{pmatrix} u_{11} & u_{12} & u_{13} \\ u_{21} & u_{22} & u_{23} \\ u_{31} & u_{32} & u_{33} \end{pmatrix}, \quad UU^\dagger = \mathbb{1}, \quad \det U = 1. \tag{2.12}$$

Due to the two constraints the matrix has $18 - 9 - 1 = 8$ degrees of freedom. An important property of a unitary matrix is that it can be expressed in terms of a hermitian matrix H as

$$U = e^{iH}. \tag{2.13}$$

The determinant of the unitary matrix then takes the form

$$\det U = e^{iTr(H)}. \tag{2.14}$$

Each element of the group can be represented by 8 real numbers θ^a as

$$U = e^{i\theta^a t^a}, \tag{2.15}$$

with the generators t^a. As we have already stated above, the generators obey the SU(3) Lie algebra

$$[t^a, t^b] = i f^{abc} t^c. \tag{2.16}$$

From Eq. (2.12) and Eq. (2.15) we see that in the fundamental representation the generators t_a are expressed as a set of 8 linearly independent hermitian and traceless matrices. In principle, there exists an infinitesimal number of sets of matrices satisfying Eq. (2.16). The most convenient choice for the generators t^a are the Gell-Mann matrices $\frac{\lambda^a}{2}$ defined as

$$\lambda_1 = \begin{pmatrix} 0 & 1 & 0 \\ 1 & 0 & 0 \\ 0 & 0 & 0 \end{pmatrix}, \quad \lambda_2 = \begin{pmatrix} 0 & -i & 0 \\ i & 0 & 0 \\ 0 & 0 & 0 \end{pmatrix}, \quad \lambda_3 = \begin{pmatrix} 1 & 0 & 0 \\ 0 & -1 & 0 \\ 0 & 0 & 0 \end{pmatrix},$$

$$\lambda_4 = \begin{pmatrix} 0 & 0 & 1 \\ 0 & 0 & 0 \\ 1 & 0 & 0 \end{pmatrix}, \quad \lambda_5 = \begin{pmatrix} 0 & 0 & -i \\ 0 & 0 & 0 \\ i & 0 & 0 \end{pmatrix}, \quad \lambda_6 = \begin{pmatrix} 0 & 0 & 0 \\ 0 & 0 & 1 \\ 0 & 1 & 0 \end{pmatrix},$$

$$\lambda_7 = \begin{pmatrix} 0 & 0 & 0 \\ 0 & 0 & -i \\ 0 & i & 0 \end{pmatrix}, \quad \lambda_8 = \frac{1}{\sqrt{3}} \begin{pmatrix} 1 & 0 & 0 \\ 0 & 1 & 0 \\ 0 & 0 & -2 \end{pmatrix}. \tag{2.17}$$

In this context we state another important property of the Lie algebra which is very useful for the calculation of color factors: The generators fulfill the Jacobi identity

$$\left[[t^a, t^b], t^c\right] + \left[[t^b, t^c], t^a\right] + \left[[t^c, t^a], t^b\right] = 0. \tag{2.18}$$

This representation, generated by 3×3 matrices, is called fundamental since the quantum-mechanical state, on which the elements of the group act, has the least number of degrees of freedom (in our matrix representation the state is a vector with three elements). The three degrees of freedom are referred to as colors red (R), blue (B) and green (G). States which belong to higher representations of the group SU(3) are obtained by coupling fundamental triplets. The easiest way of coupling fundamental triplets is

$$3 \otimes \bar{3} = 1 \oplus 8, \tag{2.19}$$

where 3 denotes the fundamental triplet, $\bar{3}$ is its conjugate (referred to as anti-colors carried by antiquarks). 1 is the color singlet $(1/\sqrt{3})(R\bar{R} + B\bar{B} + G\bar{G})$, which transforms trivial under SU(3). 8 denotes the color octet, it transforms under the so-called adjoint representation of the group. The generators of the adjoint representation are 8×8-matrices satisfying the SU(3) Lie algebra, for example

$$(t^a)^{bc} = -if^{abc}, \quad a, b, c = 1\ldots8, \tag{2.20}$$

where b and c denote the matrix indices. This procedure of combining multiplets is similar to the coupling of spins in quantum mechanics. For example, coupling two spin-$\frac{1}{2}$ doublets yields four possible states, the spin-0 singlet and the spin-1 triplet.

For the special unitary group SU(N), there exists a set of distinguished elements, the Casimir operators, which commute with all generators t^a of the algebra. The number of these operators depends on the dimension N of the group. In the case of SU(3) there are two Casimir operators, namely

$$C_1 = \sum_a t^a t^a, \quad C_2 = \sum_{abc} d^{abc} t^a t^b t^c, \tag{2.21}$$

where d^{abc} are the so-called symmetric structure constants, which are defined by the anti-commutation relation

$$\left\{t^a, t^b\right\} = \frac{1}{3}\delta^{ab}\mathbb{1} + d^{abc}t^c. \tag{2.22}$$

The eigenvalues of the Casimir operators are characteristic for the representations of the group. When calculating color factors of Feynman diagrams we will often encounter the Casimir operator C_1 in the fundamental and adjoint representation. For our choice of generators of the algebra, the operators C_1 in the fundamental and adjoint representation are diagonal 3×3 and 8×8 matrices, respectively,

$$(C_1)_F = \frac{4}{3}\mathbb{1}_{3\times3} \equiv C_F \mathbb{1}_{3\times3}, \quad (C_1)_A = 3\mathbb{1}_{8\times8} \equiv C_A \mathbb{1}_{8\times8}. \tag{2.23}$$

For arbitrary N the eigenvalues of the Casimir operator are given by

$$C_F = \frac{N^2 - 1}{2N}, \quad C_A = N. \tag{2.24}$$

2.3. Asymptotic Freedom

By now, we have demonstrated some important properties of the QCD Lagrangian, but we have not yet justified the validity of a perturbative approach to QCD. A perturbative treatment can only be reasonable, if the coupling of quarks and gluons is small. The observation of confinement, however, indicates that the forces between quarks and gluons have to be strong. But, the fact that QCD is based on a non-abelian gauge group accounts for one of the most astonishing features of the strong interaction: asymptotic freedom. In QCD the strength of the interaction between quarks and gluons is given by the running coupling,

$$\alpha_s(\mu_R) = \frac{g(\mu_R)^2}{4\pi}, \tag{2.25}$$

which is a function of the scale μ_R. As μ_R, which is usually chosen to be similar to the momentum transfer in a reaction, increases, the running coupling decreases. Therefore, at large momentum transfer or short distance the quarks and gluons behave as quasi-free particles and their interaction can be treated perturbatively.

The scale-dependence of the running coupling is a remnant of the renormalization procedure. In any higher-order QCD calculation one encounters singularities. To remove these singularities from physical observables one has to apply a regularization and renormalization procedure. In the following chapter, we explain in detail how to regularize and renormalize a quantum field theory. Presently, it is sufficient to know that removing the singularities inevitably introduces a scaling parameter μ_R. A physical observable f should, of course, not depend on the arbitrary value of μ_R, i.e.

$$\frac{\mathrm{d}f}{\mathrm{d}\mu_R} = 0. \tag{2.26}$$

To satisfy this condition the strong coupling α_s has to depend on μ_R in such a way that it compensates the scale dependence of the calculated matrix elements. The dependence of α_s on μ_R is then governed by the renormalization group equation,

$$\mu_R \frac{\partial}{\partial \mu_R} \alpha_s = \beta(\alpha_s), \tag{2.27}$$

where the QCD beta function $\beta(\alpha_s)$ is a power series in α_s,

$$\beta(\alpha_s) = -\frac{\beta_0}{4\pi} \alpha_s^2 - \frac{\beta_1}{(4\pi)^2} \alpha_s^3 + \dots . \tag{2.28}$$
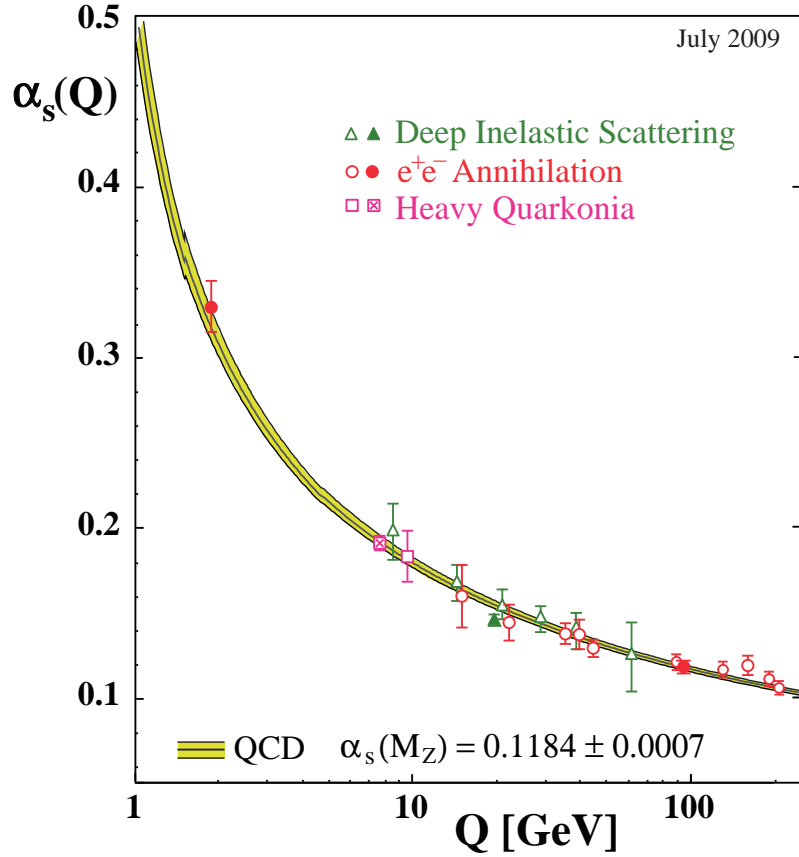
Figure 2.1.: Dependence of the running coupling α_s on the renormalization scale $\mu_R = Q$. Picture taken from Ref. [20].

The coefficients are currently known to $\mathcal{O}(\alpha_s^4)$. For our purpose, it is sufficient to know the first and second coefficient,

$$
\begin{aligned}
\beta_0 &= \frac{11}{3}C_A - \frac{2}{3}N_f, \\
\beta_1 &= \frac{34}{3}C_A^2 - \frac{10}{3}C_A N_f - 2C_F N_f,
\end{aligned}
\tag{2.29}
$$

where N_f is the number of active flavors. The coefficients β_0 and β_1 can be obtained from a perturbative one- and two-loop calculation, respectively.

The sign of the first coefficient β_0 in the beta function is crucial to the large-μ_R behavior of the theory. In QCD β_0 is positive, as long as the number of active flavors is less than $33/2 = 16.5$. Hence, the strength of the coupling decreases with increasing scale μ_R. Note that the positivity of β_0 is due to the contribution proportional to C_A, which mainly comes from non-abelian diagrams containing gluon self-interactions. In abelian quantum field theories such as QED the sign of the first coefficient is negative and, therefore, the theories are not asymptotically free.

The non-linear differential equation (2.27) is exactly solvable only at leading order. At higher orders, solutions are approximated by a series expansion. The approximate solution at two loops reads

$$
\alpha_s(\mu_R) = \frac{4\pi}{\beta_0 \ln\left(\frac{\mu_R^2}{\Lambda_{QCD}^2}\right)} \left(1 - \frac{\beta_1}{\beta_0^2} \frac{\ln \ln\left(\frac{\mu_R^2}{\Lambda_{QCD}^2}\right)}{\ln\left(\frac{\mu_R^2}{\Lambda_{QCD}^2}\right)} + \ldots \right),
\tag{2.30}
$$

where Λ_{QCD} is the low energy scale, where the running coupling diverges and perturbation theory breaks down. The value of the scale Λ_{QCD} is determined experimentally. This is done by measuring α_s at a certain mass scale, conventionally the mass of the Z boson. In Fig. 2.1 measurements of α_s in different hadronic processes, as well as, its scale dependence predicted by perturbative QCD are shown. It can clearly be seen a logarithmic decline of the strong coupling at large energy scales.

Precise measurements of α_s allow to determine the parameter Λ_{QCD} by inverting Eq. (2.30). The obtained value, of course, depends on the number of active flavors N_f and on the order of the loop calculation. Generally in this thesis, we deal with kinematics, where four active quark flavors have to be taken into account, and we use the NLO expansion of the running coupling. The corresponding value of Λ_{QCD} is approximately

$$
\Lambda_{NLO}^{(4)} \approx 250 \text{ MeV}.
\tag{2.31}
$$

By means of Eq. (2.30) we can also express the strong coupling at a scale μ_2 in terms of the coupling at scale μ_1:

$$
\alpha_s(\mu_2) = \frac{\alpha_s(\mu_1)}{1 + \frac{\beta_0}{4\pi}\alpha_s(\mu_1)\ln\frac{\mu_2^2}{\mu_1^2}} \left[1 - \frac{\beta_1}{\beta_0 4\pi} \frac{\alpha_s(\mu_1)\ln\left(1 + \frac{\beta_0}{4\pi}\alpha_s(\mu_1)\ln\frac{\mu_2^2}{\mu_1^2}\right)}{1 + \frac{\beta_0}{4\pi}\alpha_s(\mu_1)\ln\frac{\mu_2^2}{\mu_1^2}} + \ldots \right].
\tag{2.32}
$$

Despite of the fact that the strong coupling α_s vanishes at large scales or large momentum transfer, perturbation theory might not yield reasonable results. In fact, the perturbative expansion of a physical observable f in powers of α_s,

$$
f = \sum_{n=0}^{\infty} f^{(n)} \alpha_s^n,
\tag{2.33}
$$

does not uniquely define f in the limit $\alpha_s \to 0$, even if the series is summed to all orders. The reason for this ambiguity is the factorial growth of the perturbative coefficients $f^{(n)}$, i.e. they diverge as $n!$. This divergence often indicates that non-perturbative effects are non-negligible in the calculation of the observable. One of the main assumptions within perturbative QCD is therefore that the expansion in powers of α_s is *asymptotic*. A series expansion is said to be asymptotic to $f(\alpha_s)$ for $\alpha_s \to 0$, if

$$
\left| f - \sum_{n=0}^{N} f^{(n)} \alpha_s^n \right| \leq C_{N+1} \alpha_s^{N+1}
\tag{2.34}
$$

for all integer N. The perturbative expansion may then give a good approximation of the physical observable, even if the series is truncated after a few terms (of course, the observable is approximated best when the series is truncated at its minimal term). In practice only the first two (NLO) or for some specific processes three terms (NNLO) of the perturbative series have yet been calculated. However, a multitude of collider and fixed-target experiments has shown that perturbative QCD has a very good predictive power for high-energy reactions. Despite of these achievements, particularly in the fixed-target regime higher-order corrections turn out to be large and the behavior of the perturbative series is not under control. For these processes it is therefore necessary to identify the large perturbative contributions and take them into account to all orders, a procedure known as *resummation*. In Part II of this thesis we will consider the subject of resummation in great detail.

3. Regularization and Renormalization

The factorial growth and hence divergence of perturbative coefficients is not the only cumbersome problem we have to face in a higher-order perturbative-QCD calculation. In principle, we can write down an analytic expression for a matrix element $\mathcal{M}$, which governs the transition from an initial state i to a final state f, to any given order in perturbation theory by means of Feynman diagrams. At leading order the calculation is straight-forward and the results are finite and unambiguous. However, in the calculation of higher-order diagrams we encounter various divergences yielding infinite results. Obviously, physical quantities must be finite and can therefore not be directly derived from infinite matrix elements. In the following, we classify the various types of singularities emerging in loop calculations and show how they are isolated and removed from the matrix elements. This procedure then allows to calculate physical quantities to higher orders in perturbation theory.

3.1. Singularities in QCD

In massless QCD we encounter three different kinds of divergences

- soft or infrared divergences,

- collinear divergences,

- ultraviolet divergences.

Soft divergences occur in matrix elements where partons with very low energy, which are said to be *infrared*, are emitted. Since the radiation of infinitely soft partons does not 'cost' any energy, the probability of such radiation formally becomes infinitely large. However, experimentally we cannot distinguish between processes with and without soft radiation. For example, in Hilbert space a state with a single quark $|q\rangle$ and a state with a quark and an infrared gluon $|q + G\rangle$ are orthogonal although we are not able to detect the arbitrarily soft gluon. Therefore, to any given order in perturbation theory we do not only have to calculate the diagrams with soft-parton emission but also those, where no additional partons are radiated. In Fig. 3.1 the Feynman diagrams at NLO for the Drell-Yan process are shown. The third diagram, where no gluon is radiated, is often
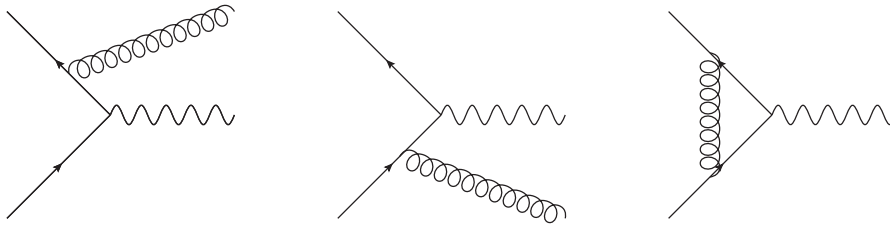
Figure 3.1.: NLO Feynman diagrams contributing to the Drell-Yan cross section.

referred to as virtual correction. The interference term of this diagram with the LO Drell-Yan diagram is of the same order in α_s as the squared matrix elements for the first two diagrams. The contributions from both real and virtual diagrams to the cross section are infrared divergent, but in the sum of all diagrams the infrared divergences cancel. This statement is true to all orders in perturbation theory and is known as Bloch-Nordsieck theorem [21] in QED and Kinoshita-Lee-Nauenberg theorem [22, 23] in QCD.

The second type of divergences occurs, when a parton is radiated collinear from another on-shell massless parton. Let us consider a massless quark with momentum p, which emits a gluon with momentum k. After the emission the propagator of the quark is given by

$$\frac{\not{p} - \not{k}}{(p-k)^2} = \frac{\not{p} - \not{k}}{-2p \cdot k} = -\frac{\not{p} - \not{k}}{2p_0 k_0 (1 - \cos\theta)}, \tag{3.1}$$

where θ is the angle between the momentum of the quark and the gluon. Again we encounter an infrared divergence for vanishing gluon energy k_0. The second singularity of Eq. (3.1) arises for $\theta = 0$ corresponding to the collinear radiation of the gluon. For infrared divergences we have argued that, since it is impossible to detect an arbitrarily soft gluon, we are not calculating a physically measurable quantity. For collinear divergences this is also the case. There is a classical example that illustrates this fact. Consider an electron that is boosted to a velocity $v \approx c$. The electromagnetic field of this very fast electron possesses exactly the same properties as a photon moving collinearly to the electron. Thus, the field can be described as a bunch of photons accompanying the electron (for details see Ref. [24]). What we observe is not the 'naked' electron, but the electron in its surrounding Coulomb cloud of photons. The same argument holds for quarks and collinear gluons. The cloud of gluons and other partons, which accompanies a quark, is absorbed into the definition of the parton distribution functions. Therefore the collinear divergences are factorized from the hard partonic scattering cross section and linked to the bare parton distribution functions. In the next chapter, we will discuss the factorization procedure in detail.

The third kind of divergences which we encounter in higher-order perturbative QCD calculations are ultraviolet divergences. They are present in most Feynman diagrams which contain a closed loop. Since we do not observe the internal loop momentum, we

have to integrate it over and find that for high momenta the loop integral is singular. We note that these ultraviolet divergences are in a way related to the incompleteness of QCD and quantum field theory in general. As a theory without gravity, QCD is not valid to arbitrarily large momentum scales. At the Planck scale $E_{Pl} \approx 10^{19}$ GeV the gravitational force is of the order of the strong interaction and can no longer be neglected. It would need a unified theory to calculate observables at such high energy scales. The standard model of particle physics is supposed to be the low-energy limit of any candidate of a unified theory.

Before the divergences can be removed from the matrix elements in a perturbative calculation, they have to be isolated and made manifest. This procedure is referred to as *regularization* and contains the introduction of an auxiliary parameter, the regulator. For divergent loop integrals the most intuitive way of regularization is to cut off the momentum integral at a scale Λ. The matrix elements for a given process then yield finite results, but they do not only depend on measurable quantities, such as the momentum transfer Q^2 in a scattering process, but also on the arbitrary scale Λ. Fortunately, for renormalizable quantum field theories like QCD and QED the cross section difference of two identical scattering processes with different momentum transfer Q^2 and Q_0^2 does not depend on the regulator Λ,

$$\sigma(Q^2, \Lambda) - \sigma(Q_0^2, \Lambda) = \Delta\sigma(Q^2, Q_0^2). \tag{3.2}$$

The divergences and hence the dependence on the arbitrary parameter Λ can be removed by redefining the bare quantities (fields, masses and coupling constants) in the Lagrangian. The procedure of absorbing the divergences into the constituents of the Lagrangian is called *renormalization*.

The simple cutoff regularization mentioned above has the advantage that it is physically transparent at first sight. However, for explicit perturbative calculations it is rather inapplicable. The generic cutoff introduces an energy scale to the theory which for a massless field theory spoils invariance under scale transformations and therefore breaks the conformal symmetry. A decent regularization procedure for QCD should respect all the fundamental properties of the theory, namely Lorentz invariance, gauge invariance and unitarity. In the following section we introduce the most often used regularization method which fulfills all these requirements: dimensional regularization.

3.2. Dimensional Regularization

The main feature of dimensional regularization is the extension of four-dimensional Minkowski space-time to d-dimensional euclidean space [25–27]. Since in a renormalizable field theory only logarithmic divergences arise, the d-dimensional integral is defined in such a way that at most logarithmic divergences give contributions and all higher divergences are set to

zero.

The first step in this procedure is the transition from four-dimensional Minkowski space to a four-dimensional euclidean space. To this end, we perform a Wick rotation of the zero component of every momentum integral to the imaginary axis. It can be shown that for a suitable choice of external momenta all poles of the calculated matrix elements lie in the second and fourth quadrant of the complex momentum space. We can therefore write

$$\int_{-\infty}^{\infty} \mathrm{d}k_0 \cdots = -\int_{i\infty}^{-i\infty} \mathrm{d}k_0 \cdots \equiv i \int_{-\infty}^{\infty} \mathrm{d}k_4^E \ldots, \tag{3.3}$$

where $k_0 = i k_4^E$. With the identifications $k_1 \equiv k_1^E$, $k_2 \equiv k_2^E$ and $k_3 \equiv k_3^E$ the square of the Minkowski four-vector k is given by

$$k^2 = -(k^E)^2 = -\left[(k_1^E)^2 + (k_2^E)^2 + (k_3^E)^2 + (k_4^E)^2\right]. \tag{3.4}$$

The four-dimensional euclidean integral is then analytically continued to d dimensions by the replacement

$$\int \frac{\mathrm{d}^4 k^E}{(2\pi)^4} \longrightarrow \int \frac{\mathrm{d}^d k^E}{(2\pi)^d}. \tag{3.5}$$

Conveniently one chooses for the number of dimensions $d = 4 - 2\epsilon$, where ϵ is arbitrary but assumed to be small. All singularities of the unregularized theory are then manifest as $1/\epsilon$ and $1/\epsilon^2$ poles. The extension of space-time to d dimensions requires to modify several quantities, which are associated with the number of dimensions. First and foremost the right hand side of the replacement in Eq. (3.5) is of energy dimension $4 - 2\epsilon$. To cancel the -2ϵ additional energy dimensions the dimensionless coupling constant g is replaced by a coupling constant $\tilde{g}$ of energy dimension ϵ,

$$g \to \tilde{g} = \mu_R^\epsilon g, \tag{3.6}$$

where μ_R is an arbitrary mass scale.

The extension of Lorentz vectors and tensors to d dimensions is straightforward, e. g. the contraction of the metric tensor yields

$$g_{\mu\nu} g^{\mu\nu} = d. \tag{3.7}$$

The algebra of the γ-matrices is extended to d dimensions such that the anti-commutation relation,

$$\{\gamma_\mu, \gamma_\nu\} = 2 g_{\mu\nu}, \tag{3.8}$$

is still valid. However, by means of Eq. (3.7) the well-known identities for the contraction

of γ-matrices are slightly modified:

$$
\begin{aligned}
\gamma^\mu \gamma_\mu &= d, \\
\gamma^\mu \gamma^\nu \gamma_\mu &= -(d-2)\gamma^\nu, \\
\gamma^\mu \gamma^\nu \gamma^\rho \gamma_\mu &= 4g^{\nu\rho} - (4-d)\gamma^\nu\gamma^\rho, \\
\gamma^\mu \gamma^\nu \gamma^\rho \gamma^\sigma \gamma_\mu &= -2\gamma^\sigma\gamma^\rho\gamma^\nu + (4-d)\gamma^\nu\gamma^\rho\gamma^\sigma.
\end{aligned}
\tag{3.9}
$$

The continuation to d dimensions is more involved for quantities which are exclusively defined in four-dimensional space-time. One of these is γ_5 defined as

$$
\gamma_5 \equiv i\gamma_0\gamma_1\gamma_2\gamma_3.
\tag{3.10}
$$

By definition it anti-commutes with the four gamma matrices. In d dimensions, however, there is no unique way to treat γ_5. One either has to give up anti-commutativity or modify the definition in Eq. (3.10). The most convenient choice for γ_5 is adopted in the so-called HVBM-scheme [25, 28]. In this scheme γ_5 anti-commutes with the gamma matrices in four dimensional space-time and commutes in the remaining $d-4$ dimensional subspace.

All the modifications, which have to be applied when going from four to d dimensional space, are of $\mathcal{O}(d-4)$ or $\mathcal{O}(2\epsilon)$. In the limit $\epsilon \to 0$ additional contribution only arise, if the corresponding terms are combined with $1/\epsilon$ poles. Singularity-free quantities such as LO cross sections are not altered by the regularization procedure. This is a key feature of any kind of regularization prescription. If this was not the case, the Lagrangian would not be renormalizable.

3.3. Renormalization

The dimensional-regularization procedure allows to identify singular terms in matrix elements as poles in $1/\epsilon$. This is only the first step to arrive at meaningful results. The second one is to remove the singularities from the cross section by a proper redefinition of the fields and coupling constants of the theory. This redefinition is equivalent to adding a finite number of terms, order by order, to the Lagrangian density. The bare quantities in the unrenormalized QCD Lagrangian are replaced by their renormalized (subscript r)
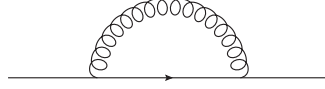
Figure 3.2.: One-loop diagram contributing to the quark self-energy.

counterpart

$$
\begin{aligned}
A_\mu^a &= Z_3^{1/2} A_{r,\mu}^a, \\
\chi^a &= \tilde{Z}_3^{1/2} \chi_r^a, \\
\Psi &= Z_2^{1/2} \Psi_r, \\
g &= Z_g g_r, \\
\xi &= Z_3 \xi_r, \\
m &= Z_m m_r,
\end{aligned}
$$

(3.11)

where Z_3, $\tilde{Z}_3$, Z_2, Z_g and Z_m are the renormalization constants for the fields, masses and coupling constants. Gauge invariance requires that the renormalization constant is the same for the gauge field A_μ^a and the gauge parameter ξ. Actually, the other constants are also not independent from each other. The gauge symmetry of QCD gives rise to so-called Slavnov-Taylor identities [29, 30], which determine relations among the renormalization constants.

In the following we exemplarily demonstrate the derivation of the renormalization constants. The quark self-energy serves as the classic example, since at one-loop order only a single diagram, which is depicted in Fig. 3.2, contributes to its matrix element. Neglecting the quark mass the full propagator for a quark with momentum p reads

$$
iS(p) = \frac{i}{\not{p} + i\eta + \Sigma(p)}
$$

(3.12)

with the self-energy $\Sigma(p)$. By means of the Feynman rules of QCD we can write down the one-loop contribution to the self-energy,

$$
\Sigma^{(1)}(p) = -g^2 \int \frac{\mathrm{d}^4 k}{(2\pi)^4} t^a \gamma_\mu \frac{\not{p} - \not{k}}{(p-k)^2 + i\eta} t^b \gamma_\nu \frac{\delta^{ab} g^{\mu\nu}}{k^2 + i\eta}.
$$

(3.13)

The color matrices are easily evaluated and yield the color factor

$$
t^a \delta^{ab} t^b = t^a t^a = C_F.
$$

(3.14)

The integral over the loop momentum k is singular, as its argument diverges in the limit $k \to \infty$. We use dimensional regularization to make the integral finite. After continuation

to d dimensions we obtain

$$\Sigma^{(1)}(p) = -C_F g^2 \mu_R^{2\epsilon} \int \frac{\mathrm{d}^d k}{(2\pi)^d} \frac{(2-d)(\not{p} - \not{k})}{(p-k)^2 k^2}, \tag{3.15}$$

where we used the modified gamma algebra in Eq. (3.9) to simplify the numerator. To cast the denominator into a more convenient form we apply a Feynman parametrization and find

$$\Sigma^{(1)}(p) = -C_F g^2 \mu_R^{2\epsilon}(2-d) \int_0^1 \mathrm{d}z \int \frac{\mathrm{d}^d k}{(2\pi)^d} \frac{(\not{p} - \not{k})}{[(1-z)k^2 + z(p-k)^2]^2}. \tag{3.16}$$

By substituting $k_\mu \rightarrow k_\mu + z p_\mu$ the integral takes the simple form

$$\Sigma^{(1)}(p) = -C_F g^2 \mu_R^{2\epsilon}(2-d) \int_0^1 \mathrm{d}z \int \frac{\mathrm{d}^d k}{(2\pi)^d} \frac{[(1-z)\not{p} - \not{k}]}{[k^2 + z(1-z)p^2]^2}. \tag{3.17}$$

It is now straightforward to perform a Wick rotation in the zeroth component of the loop momentum and evaluate the integral in $d = 4 - 2\epsilon$ dimensional euclidean space. The result reads

$$\begin{aligned}
\Sigma^{(1)}(p) &= i\not{p} C_F \frac{g^2}{(4\pi)^2} \left(\frac{4\pi\mu_R^2}{-p^2}\right)^\epsilon (1+\epsilon)\left(\frac{1}{\epsilon} - \gamma_E\right) + \mathcal{O}(\epsilon) \\
&= i\not{p} C_F \frac{g^2}{(4\pi)^2} \left(1 + \ln\frac{\mu_R^2}{-p^2} + \frac{1}{\epsilon} - \gamma_E + \ln 4\pi\right) + \mathcal{O}(\epsilon),
\end{aligned} \tag{3.18}$$

where γ_E is the Euler-Mascheroni constant. This expression diverges in the four dimensional limit $\epsilon \rightarrow 0$. As mentioned above, renormalization removes these divergences by a redefinition of the bare quantities in the Lagrangian. The renormalized quark spinor field reads $\Psi_r = Z_2^{-1/2}\Psi$. Since the quark propagator is a two-point function consisting of two quark fields, it is consistently renormalized as

$$S_r(p) = \frac{1}{Z_2} S(p) = \frac{1}{Z_2} \frac{1}{\not{p} + \Sigma(p)}. \tag{3.19}$$

Neglecting terms beyond $\mathcal{O}(\alpha_s)$ we write

$$S_r(p) = \frac{1}{\not{p} + \Sigma^{(1)}(p) - \not{p}\, \alpha_s Z_2^{(1)}} + \mathcal{O}(\alpha_s^2), \tag{3.20}$$

where we have expanded the renormalization constant Z_2 as

$$Z_2 = 1 - \alpha_s Z_2^{(1)} + \mathcal{O}(\alpha_s^2). \tag{3.21}$$

To obtain a meaningful result at one-loop order the divergent part of $\Sigma^{(1)}(p)$ must be canceled by the term $\not{p}\, \alpha_s Z_2^{(1)}$. In fact, the renormalized propagator has to be a quantity free of divergences to any given order in perturbation theory. Therefore the renormalization

constant Z_2 has to subtract the singularities from the quark self-energy Σ order by order. Of course, this requirement does not uniquely define the renormalization constants. Along with the singular terms any finite term may be subtracted from the result. The choice of this finite term defines a renormalization scheme. In the MS (*minimal subtraction*) scheme [31] the finite term is set to zero and only the poles in ϵ are subtracted from the matrix elements. However, in dimensional regularization the ϵ poles are alway accompanied by the finite terms $-\gamma_E + \ln 4\pi$. It is therefore more convenient to work in the $\overline{\text{MS}}$ (*modified minimal subtraction*) scheme [32], where the combination

$$\frac{1}{\epsilon} - \gamma_E + \ln 4\pi \tag{3.22}$$

is absorbed into the renormalization constants. In this specific scheme the one-loop coefficient of the renormalization constant Z_2 is of the form

$$Z_2^{(1)} = iC_F \frac{1}{4\pi}\left(\frac{1}{\epsilon} - \gamma_E + \ln 4\pi\right) \tag{3.23}$$

and we obtain for the renormalized quark propagator:

$$S_r(p) = \frac{1}{\not{p}}\left[1 + iC_F \frac{g^2}{(4\pi)^2}\left(1 + \ln\frac{\mu_R^2}{-p^2}\right) + \mathcal{O}(\alpha_s^2)\right]^{-1}. \tag{3.24}$$

In the same way any divergent quantity in perturbative QCD can be renormalized and is then well-defined within a specific renormalization scheme.

4. Parton Distribution Functions

In the previous chapters, we have learned that the Lagrangian of QCD contains all the information we need to describe the interaction of quarks and gluons. Although the derivation of perturbative results is very cumbersome due to the various types of singularities which we encounter in higher-order calculations, regularization and renormalization prescriptions allow to obtain meaningful and finite matrix elements for any process involving quarks and gluons. However, free partons have never been experimentally observed. Actually, the existence of free partons would be at variance with one of the most astonishing and still hardly understood findings in strong interaction physics: *confinement*. It is therefore crucial to find a framework, which allows to translate the perturbatively calculable partonic matrix elements to hadronic experimentally measurable observables.

4.1. Factorization Theorem

This brings us to another key concept of perturbative QCD: factorization. It relies on the incoherence of long-distance and short-distance effects in hadronic processes. In momentum space short distances correspond to large momentum transfers. If factorization applies, the partonic cross section of a hard process (momentum transfer $Q \gtrsim 1$ GeV) is separated from the non-perturbative soft functions involved in the process. Rigorous proofs of factorization are generally very complex and hardly worked out to all orders in perturbation theory. Sophisticated factorization theorems only exist for simple processes in strong-interaction physics, such as inclusive deep-inelastic scattering and the Drell-Yan process [33–39]. However, over the last 20 years also many arguments for the factorization of semi-inclusive and exclusive hadronic processes have been worked out (e.g. see Ref. [40]).

For example, in semi-inclusive deep inelastic scattering the hadronic cross section is schematically written as a convolution of the form

$$\sigma(Q) = \sum_{a,b} D_a^0 \otimes \hat{\sigma}_{ab}(Q, \mu_R) \otimes f_b^0 + \mathcal{O}(1/Q^2), \qquad (4.1)$$

where f_b^0 is the bare PDF of a parton b in the initial-state hadron and D_a^0 is the bare fragmentation function for a parton a fragmenting into the final-state hadron. The partonic hard-scattering cross section $\hat{\sigma}_{ab}(Q, \mu_R)$ can be calculated in perturbation theory and is a

function of the momentum transfer Q and the generic renormalization scale μ_R. It contains all deep-inelastic-scattering diagrams with a parton a in the final state and a parton b in the initial state. The sum over a and b runs over all quark and antiquark flavors and the gluon ($a, b = u, \bar{u}, d, \bar{d}, \dots, G$). Equation (4.1) is valid up to corrections suppressed by powers of the momentum transfer Q. These corrections are due to higher-twist effects in QCD.

In Ch. 3 we demonstrated how ultraviolet divergences in the partonic scattering cross section are made manifest and removed by a regularization and renormalization prescription. We have also noted that infrared divergences cancel in the sum of all diagrams to a given order in perturbation theory. However, the hard part may still involve collinear divergences stemming from the collinear emission of partons in either the initial or final state. Those divergences can be factorized from the partonic scattering cross section and be associated with the bare PDFs and fragmentation functions. To this end, we introduce two functions $C_{b'b}$ and $C'_{aa'}$ that absorb the collinear parts of $\hat{\sigma}_{ab}$ in the initial and final state, respectively. The hadronic cross section then takes the form

$$\sigma(Q) = \sum_{a,b,a',b'} D^0_a \otimes C'_{aa'}(\mu'_F) \otimes \hat{\sigma}_{a'b'}(Q, \mu_R, \mu_F, \mu'_F) \otimes C_{b'b}(\mu_F) \otimes f^0_b, \qquad (4.2)$$

where μ_F and μ'_F are two generic momentum scales referred to as factorization scales. As with the renormalization scale μ_R, the physical observable $\sigma(Q)$ should be independent of the arbitrarily introduced scales μ_F and μ'_F. However, in perturbation theory this can only be true for an all-order calculation. If the perturbative series is truncated at a given order, $\sigma(Q)$ still exhibits a factorization-scale dependence.

The factorized form of Eq. (4.2) immediately allows to couple the collinear functions $C'_{aa'}$ and $C_{b'b}$ to the bare parton densities and thereby define physical parton distribution and fragmentation functions,

$$f_{b'}(\mu_F) \equiv \sum_b C_{b'b}(\mu_F) \otimes f^0_b,$$

$$D_{a'}(\mu'_F) \equiv \sum_a C'_{aa'}(\mu'_F) \otimes D^0_a, \qquad (4.3)$$

which depend on the factorization scales μ_F and μ'_F. The collinear functions $C'_{aa'}$ and $C_{b'b}$ play a similar role as the renormalization constants in Ch. 3. Along with the collinear singularities they may contain arbitrary finite terms, which consequently have to be subtracted from the partonic cross section $\hat{\sigma}$. It is therefore necessary to specify a factorization scheme with an accurate prescription for the choice of the collinear subtraction. Most commonly employed is the $\overline{\text{MS}}$ factorization scheme. Like in the $\overline{\text{MS}}$ renormalization scheme the characteristic combination of $1/\epsilon$-poles and finite terms,

$$\frac{1}{\epsilon} - \gamma_E + \ln 4\pi, \qquad (4.4)$$

is subtracted. The ambiguity in the choice of the collinear functions implies that the definition of the physical parton densities in Eq. (4.3) is not unique. For example, in the DIS factorization scheme the collinear subtractions are chosen in such a way that the distribution function of a quark q times the square of its fractional electromagnetic charge e_q is equal to its contribution to the deep inelastic structure function F_1,

$$e_q^2 f_q^{\text{DIS}}(x, \mu_F) = F_{1,q}(x, \mu_F). \tag{4.5}$$

Note that in the previous schematic expressions we have omitted the argument x of the PDF, which corresponds to the fraction of the hadron's momentum carried by the parton.

The scheme dependence of the parton distributions makes a universal physical interpretation impossible. As an exception, at LO we do not have to specify a factorization scheme, since the partonic hard-scattering cross section is free of any divergences. In this case the PDFs can be interpreted as probability densities. The probability of finding a parton b with momentum fraction in the range $[x, x + \mathrm{d}x]$ is then given by

$$P_b(x, x + \mathrm{d}x) = f_b(x, \mu_F)\mathrm{d}x. \tag{4.6}$$

4.2. Evolution of Parton Distribution Functions

We have argued above that by virtue of factorization theorems the soft part of the hadronic cross section, namely parton distribution and fragmentation functions, can be separated from the partonic hard part. The soft functions are non-perturbative objects and can therefore not be calculated in perturbative QCD from first principles. Theory can only estimate them by means of heuristic phenomenological models on the hadron level. Nevertheless within perturbative QCD the evolution of the PDFs with the factorization scale can be computed. The evolution is governed by a set of coupled differential equations, which have been developed by Dokshitzer [41] and Altarelli and Parisi [42] independently from each other, and even earlier by Gribov and Lipatov [43] in a different context. They are therefore known as DGLAP equations and take the form

$$\mu_F \frac{\mathrm{d}\Delta_{ab}(x, \mu_F)}{\mathrm{d}\mu_F} = \frac{\alpha_s}{2\pi} \int_x^1 \frac{\mathrm{d}y}{y} P_{qq}\left(\frac{x}{y}\right) \Delta_{ab}(y, \mu_F),$$

$$\mu_F \frac{\mathrm{d}\Sigma(x, \mu_F)}{\mathrm{d}\mu_F} = \frac{\alpha_s}{2\pi} \int_x^1 \frac{\mathrm{d}y}{y} \left[P_{qq}^{NS}\left(\frac{x}{y}\right) \Sigma(y, \mu_F) + 2N_f P_{qG}\left(\frac{x}{y}\right) f_G(y, \mu_F) \right],$$

$$\mu_F \frac{\mathrm{d}f_G(x, \mu_F)}{\mathrm{d}\mu_F} = \frac{\alpha_s}{2\pi} \int_x^1 \frac{\mathrm{d}y}{y} \left[P_{Gq}\left(\frac{x}{y}\right) \Sigma(y, \mu_F) + P_{GG}\left(\frac{x}{y}\right) f_G(y, \mu_F) \right], \tag{4.7}$$

where Δ_{ab} are singlet combinations of the quark and antiquark PDFs and Σ is the non-singlet combination,

$$\Delta_{ab}(x,\mu_F) = f_a(x,\mu_F) - f_b(x,\mu_F), \quad a,b = u, \bar{u}, d, \bar{d}, \ldots$$

$$\Sigma(x,\mu_F) = \sum_{q=u,d,\ldots} \left(f_q(x,\mu_F) + f_{\bar{q}}(x,\mu_F) \right). \tag{4.8}$$

The functions $P_{ab}(x/y)$ are referred to as splitting functions. They can be calculated in perturbation theory as a series expansion in α_s,

$$P_{ab}(x/y) = P_{ab}^{(0)}(x/y) + \frac{\alpha_s}{\pi} P_{ab}^{(1)}(x/y) + \ldots \tag{4.9}$$

and are currently known up to three loops [44, 45]. In a physical picture they can be interpreted as probability for the transition from a parton b with momentum fraction y to a parton a with momentum fraction x.

A very subtle approach to solve the DGLAP equations is to make the transition to Mellin moment space. The N-th Mellin moment of a function f defined on the interval $[0,1]$ is

$$f^N \equiv \int_0^1 \mathrm{d}x \, x^{N-1} f(x). \tag{4.10}$$

Applying this transformation to both sides of Eq. (4.7) decouples the convolution integral of splitting functions and PDFs into an ordinary product of Mellin moments. In this form it is straightforward to solve the evolution equations and evolve the moments of the PDFs to any factorization scale μ_F. The distribution functions in x-space are then obtained by inverting the Mellin transform,

$$f(x) = \frac{1}{2\pi i} \int_{c-i\infty}^{c+i\infty} \mathrm{d}N \, x^{-N} f^N, \tag{4.11}$$

where c is a real number, which has to be chosen in such a way that all singularities of f^N lie to the left of the integration contour in the complex plane. Note that the Mellin transform is closely related to the Fourier transform. Actually, it can be cast into the form of a Fourier transform by substituting $x = e^{iw}$.

In Lattice QCD moments of PDFs for integer N can directly be calculated. However, as we see from Eq. (4.11) the knowledge of some integer moments is not sufficient to pin down the functional form of the PDFs in x-space. Besides, numerical calculation on the lattice are very time consuming.

As stated above, a derivation of the functional form of PDFs from first principles in QCD is not feasible. Due to the lack of reliable models of hadrons and the only limited input from lattice QCD a phenomenological analysis of experimental data is by far the most reliable approach to determine the partonic distribution in hadrons. In the context of such an analysis the DGLAP equations play a crucial role. They allow to compare

theoretical cross sections based on a set of PDFs defined at some low momentum scale with experimental data at various energy scales. To this end, the PDFs are parameterized at a fixed low momentum scale μ, the parameterization is then evolved to the desired factorization scale of the corresponding process and used to calculate the hadronic cross section in the kinematic regime relevant for the experiment. A comparison of the theoretical cross section with the experimental data allows to determine the quality of the chosen parameterization. It is measured in terms of a score function, such as χ^2. The parameterization is then optimized by repeating the procedure several times and thereby minimizing the score function.

In this way global analyses of unpolarized, i.e. spin-averaged, PDFs of the proton have been performed by a number of groups. The most commonly used parameterization are those of the CTEQ [5] and MSTW [6] groups. We note that there exist also different approaches to fitting parton distributions. For example, the NNPDF group [7] uses neural networks to generate distribution functions. The aim of this procedure is to perform a global fit of PDFs which is not biased by the initial choice of the parameterization.

In Fig. 4.1 the unpolarized NLO PDFs obtained by the three groups in the $\overline{\mathrm{MS}}$-scheme are shown at momentum scale $\mu_F^2 = 2 \ \mathrm{GeV}^2$. Also included are the uncertainty bands of the respective analyses. As can be seen, the singlet distribution, which is dominated by the valence quarks, is well-determined over the whole x-range. By contrast, the uncertainties of the gluon distribution function are rather large. Not only for small values of x but also in the valence region the gluon distribution cannot be precisely determined by current data. Concerning the strange quark densities the analyses seem not to be consistent. Although their respective uncertainty bands are rather small, the distribution functions obtained by the CTEQ and MSTW groups are at odds in the small-x region. The reason for this discrepancy is that for the most part experimental data from inclusive processes is used in these analyses. However, inclusive data has little discriminatory power with respect to the flavor of the involved partons. Therefore, the obtained strange quark content of the proton is often biased by heuristic assumptions, which are employed in the analyses, such as a vanishing strange quark distribution at some low resolution scale or a SU(3) flavor-symmetric quark sea.

So far we have only considered *unpolarized* PDFs, i.e. we have neglected the spin polarization of the partons in a hadron. Taking spin into account the unpolarized distribution function of a parton a in a hadron for instance with positive helicity can be written as

$$f_a^{H+}(x) = f_{a+}^{H+}(x) + f_{a-}^{H+}(x), \tag{4.12}$$

where $f_{a\pm}^{H+}(x)$ is the distribution function of a parton a with positive/negative helicity in a hadron H with positive helicity. This identity suggests to define polarized, or spin-
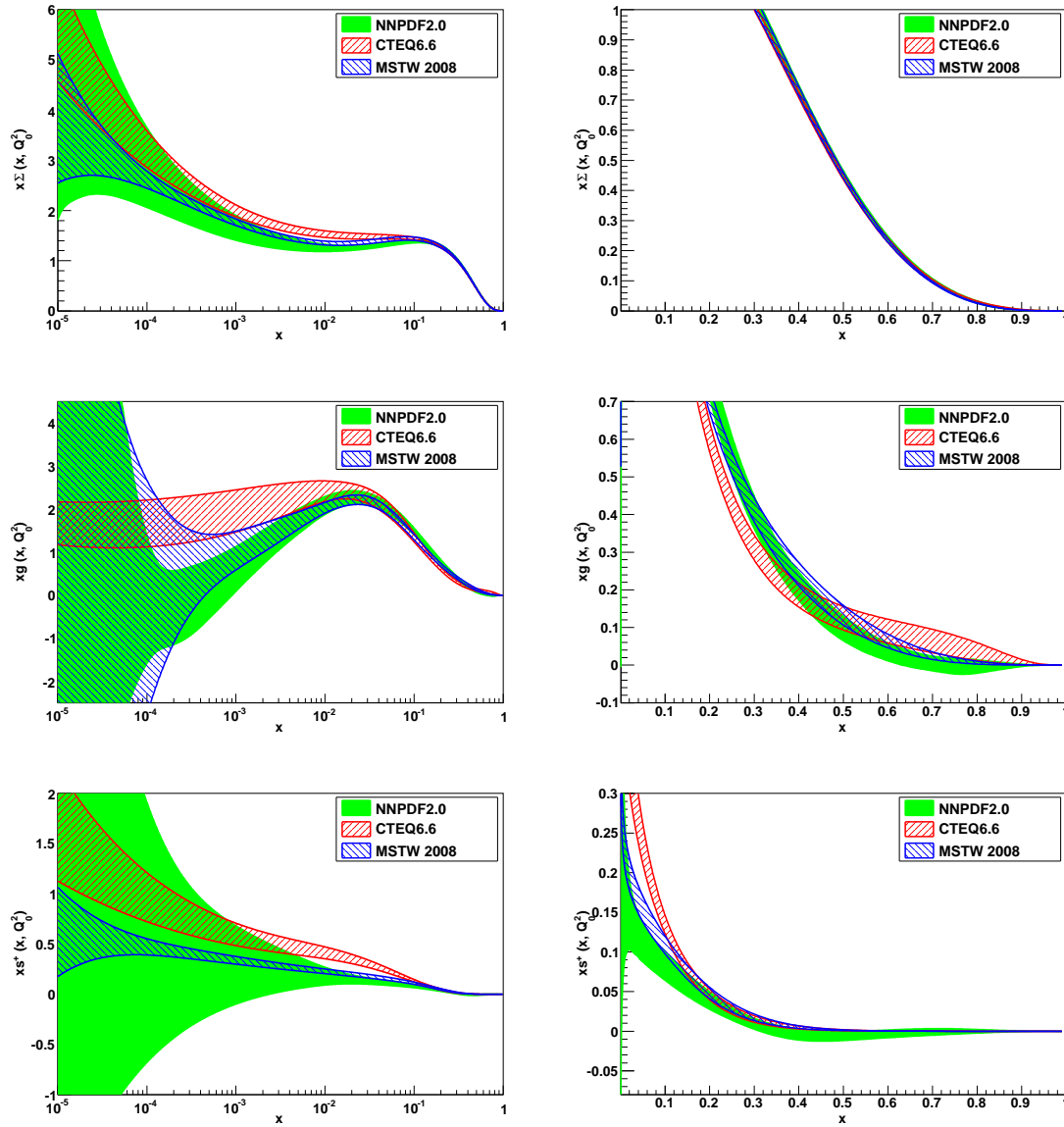
Figure 4.1.: The singlet $\Sigma(x) = \sum_q (f_q(x) + f_{\bar{q}}(x))$, gluon $g(x) = f_G(x)$ and total strangeness $s^+(x) = f_s(x) + f_{\bar{s}}(x)$ distribution functions (top-down) and their uncertainties from the NLO analyses of the CTEQ [5], MSTW [6] and NNPDF [7] groups at scale $\mu_F^2 = Q_0^2 = 2$ GeV^2. The distribution functions are plotted both on a logarithmic (left) and linear (right) scale in x. The figures are taken from Ref. [7].

dependent, PDFs as

$$\Delta f_a^{H+}(x) \equiv f_{a+}^{H+}(x) - f_{a-}^{H+}(x). \tag{4.13}$$
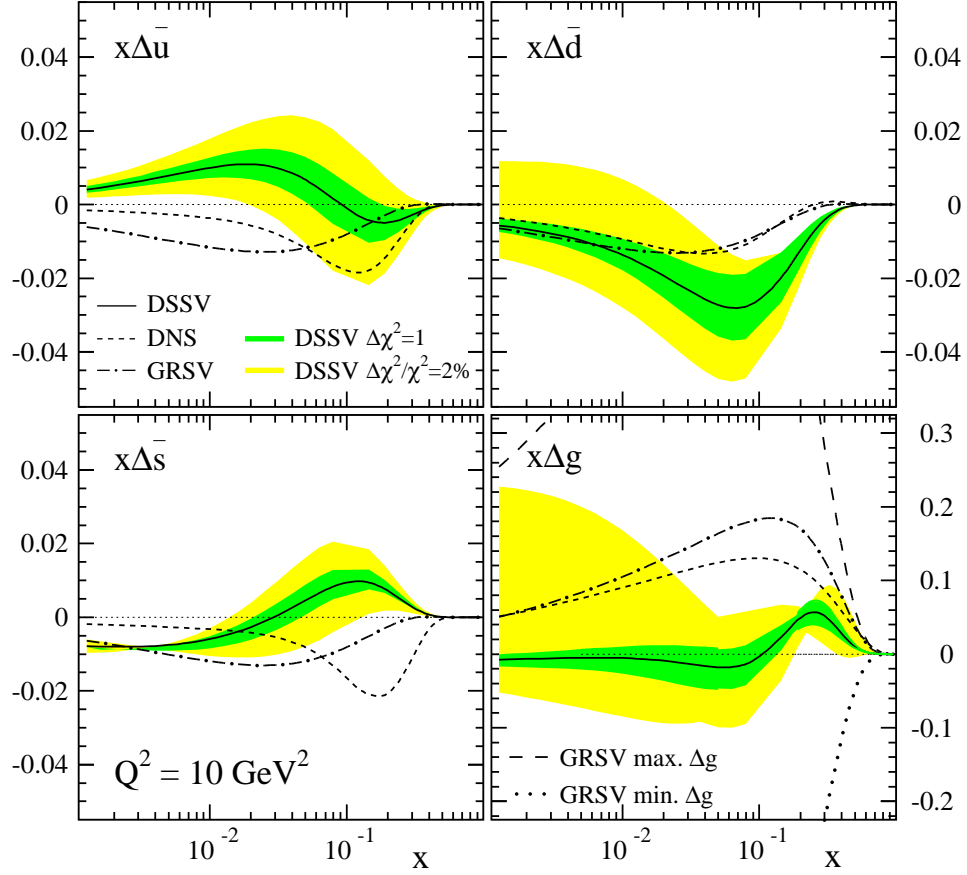
Figure 4.2.: The polarized sea and gluon distribution functions from the NLO analyses of
            DSSV [46, 47], GRSV [48] and DNS [49] at scale $\mu_F^2 = Q^2 = 10$ GeV^2. Also
            shown are uncertainty bands of the DSSV analysis. The figures are taken from
            Ref. [47].

Note that due to parity conservation distribution functions are equal for hadrons with
positive and negative helicity

$$\Delta f_{a-}^{H_-}(x) = \Delta f_{a+}^{H_+}(x), \quad f_{a+}^{H_-}(x) = \Delta f_{a-}^{H_+}(x). \tag{4.14}$$

The evolution equations in Eq. (4.7) also apply to the polarized case provided the splitting
functions P_{ab} are replaced by their spin-dependent counterparts ΔP_{ab}, which are known
to NLO [50–52]. Polarized parton distributions are generally not extracted directly from
measured cross sections. Instead one usually considers so-called *spin asymmetries*. For
example, for a process with one hadron in the initial state a longitudinal spin asymmetry

is schematically given by

$$A = \frac{d\sigma_{+\cdots} - d\sigma_{-\cdots}}{d\sigma_{+\cdots} + d\sigma_{-\cdots}}, \tag{4.15}$$

where $d\sigma_{\pm\cdots}$ denotes the differential hadronic cross section for the incoming hadron with positive/negative helicity. The dots denote spins of initial- or final-state particles, which are kept fixed in the cross section. By means of the factorization theorem the numerator of the spin asymmetry takes the form (in the following we drop the subscript a denoting the parton species)

$$\begin{aligned} d\sigma_{+\cdots} - d\sigma_{-\cdots} &= \left(f_+^{H+} \otimes d\hat{\sigma}_{+\cdots} + f_-^{H+} \otimes d\hat{\sigma}_{-\cdots} \right) - \left(f_-^{H-} \otimes d\hat{\sigma}_{-\cdots} + f_+^{H-} \otimes d\hat{\sigma}_{+\cdots} \right) \\ &= \left(f_+^{H+} - f_+^{H-} \right) \otimes d\hat{\sigma}_{+\cdots} - \left(f_-^{H-} - f_-^{H+} \right) \otimes d\hat{\sigma}_{-\cdots}, \end{aligned} \tag{4.16}$$

where $d\hat{\sigma}_{\pm\cdots}$ is the differential partonic hard-scattering cross section for the initial-state parton with positive/negative helicity. Equation (4.14) allows to simplify

$$d\sigma_{+\cdots} - d\sigma_{-\cdots} = \left(f_+^{H+} - f_-^{H+} \right) \otimes (d\hat{\sigma}_{+\cdots} - d\hat{\sigma}_{-\cdots}) = \Delta f^{H+} \otimes d\Delta\hat{\sigma}, \tag{4.17}$$

where we have defined $d\Delta\hat{\sigma} \equiv d\hat{\sigma}_{+\cdots} - d\hat{\sigma}_{-\cdots}$. The numerator of the spin asymmetry is expressed as convolution of polarized PDFs and perturbatively calculable partonic hard-scattering cross sections. This factorized form allows to extract polarized PDFs from experimental data similar to the global analysis of unpolarized PDFs. However, since it is experimentally much more involved to produce a polarized beam (or target) than an unpolarized one and since spin asymmetries are usually very small ($A \ll 1$), there is fewer accurate data to be analyzed. A comprehensive analysis of the available data was done by the DSSV group [46, 47]. Figure 4.2 shows their fitted polarized PDFs for sea quarks and the gluon compared to previous analyses by the groups GRSV [48] and DNS [49]. Also included are uncertainty bands corresponding to $\Delta\chi^2 = 1$ and $\Delta\chi^2/\chi^2 = 2\%$. In the figure a usual convention for labeling PDFs is applied, namely $(\Delta)f_q(x, \mu_F) \equiv (\Delta)q(x, \mu_F)$, $(\Delta)f_{\bar{q}}(x, \mu_F) \equiv (\Delta)\bar{q}(x, \mu_F)$ with $q \equiv u, d, s, \ldots$ and $(\Delta)f_G(x, \mu_F) \equiv (\Delta)g(x, \mu_F)$. As can be seen, the parameterizations of the sea and gluon distributions obtained in the three analyses do not agree with each other and exhibit large uncertainties. This is a clear indicator for a lack of sound data in the small-x region, where the sea quark and gluon distribution functions dominate.

This insufficient determination is all the more regrettable since polarized PDFs play an important role in the composition of the proton's spin. The spin sum rule states that the spin of the proton, which is well-known to be 1/2, is built up from the spin and the orbital angular momentum of it constituents,

$$S_z^p = \frac{1}{2}\Delta\Sigma(\mu) + \Delta G(\mu) + L^q(\mu) + L^{\bar{q}}(\mu) + L^G(\mu) = \frac{1}{2}, \tag{4.18}$$

where L^q, $L^{\bar{q}}$ and L^G denote the orbital angular momentum of quarks, antiquarks and gluons, respectively, and

$$\Delta\Sigma(\mu) = \int_0^1 \mathrm{d}x \sum_{q=u,d,s,\dots} \left[\Delta q(x,\mu) + \Delta\bar{q}(x,\mu)\right], \quad \Delta G(\mu) = \int_0^1 \mathrm{d}x \Delta g(x,\mu). \tag{4.19}$$

Summing up the first moments of the DSSV polarized PDFs one finds that $\Delta\Sigma \lesssim 0.2$ and $\Delta G \sim 0$ which implies that huge contributions to the total spin have to be due to the orbital angular momentum of the partons. Therefore, it is an important challenge in strong-interaction physics to not only determine the distribution of longitudinal momentum among the partons but also resolve the spatial structure of nucleons. A promising approach to this issue is the on-going development of *generalized parton distributions*, which contain the distribution of partons in the plane transverse to the nucleon's momentum. Information on their functional form can experimentally be obtained from appropriate exclusive scattering processes [53, 54]. On the theoretical side Lattice-QCD calculations [55, 56] help to gain valuable insight. However, it is beyond the scope of this thesis to go into more detail on generalized parton distributions.

4.3. Parton Distribution Functions of the Pion

The exploration of the internal structure of hadrons is not limited to the nucleons. There have also been various approaches to determine the partonic content of mesons. Special significance is assigned to the pion, which is one of the most important particles in strong-interaction physics. It exhibits a dual role in this context, since it is not only the lightest quark-antiquark bound state but also serves as the Nambu-Goldstone boson of the dynamical chiral symmetry breaking in QCD. However, our knowledge about its internal quark and gluon partonic structure is still rather poor.

On the experimental side, most of the available information comes from Drell-Yan dimuon production. The Fermilab E615 [8] and CERN NA10 [57] experiments provide Drell-Yan data for charged pions incident on a nuclear fixed target. These data primarily constrain the distribution of the valence quarks in the pion,

$$v^\pi \equiv u_v^{\pi^+} = \bar{d}_v^{\pi^+} = d_v^{\pi^-} = \bar{u}_v^{\pi^-}. \tag{4.20}$$

The equality holds, if we assume that the three pions (π^+, π^- and π^0) form an ideal isospin triplet. In the small-x region some data from prompt-photon production with incident pions exist [58], but not enough to gain reliable information on the sea and gluon distributions in the pion. Nevertheless, several NLO analyses of the Drell-Yan and prompt-photon data have been performed to extract pionic PDFs [9–11]. A striking feature has been that the resulting valence distribution $v^\pi(x, \mu_F)$ turned out to be rather hard at high
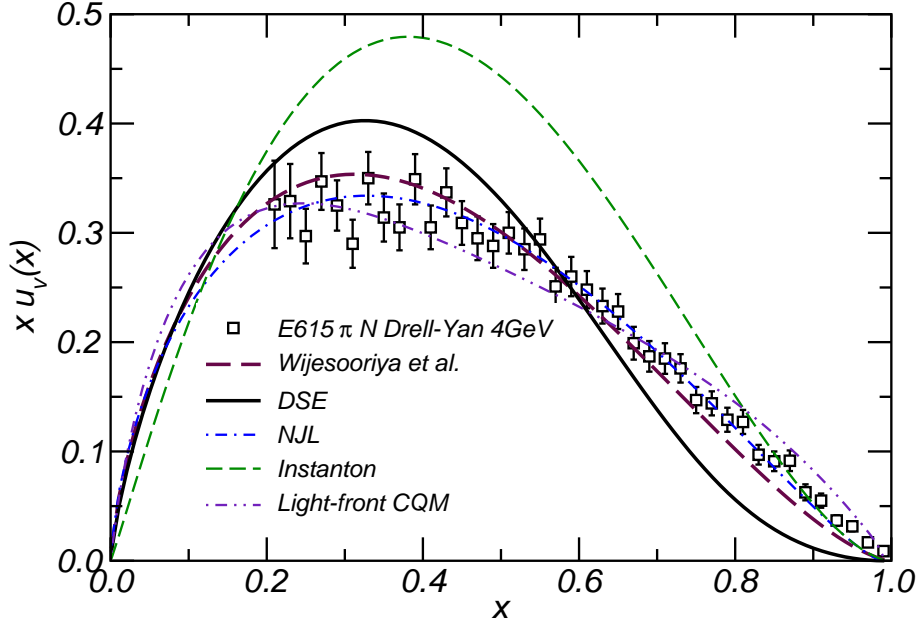
Figure 4.3.: Compilation of valence quark distributions of the pion at scale $\mu_F = 4$ GeV
(top-down in key): LO extraction of Fermilab Drell-Yan data [8], NLO analysis
of Drell-Yan data (Wijesooriya *et al.*) [11], Dyson-Schwinger equation study
(DSE) [63], Nambu-Jona-Lasinio model (NJL) [12, 65], instanton model [66],
light-front constituent-quark model (CQM) [67]. The figure is taken from Ref.
[12].

momentum fraction x, typically showing a linear or slightly faster falloff, i.e. $v^\pi \sim (1-x)^1$
at high x.

Indeed, this finding is at variance with theoretical predictions (For a review see Ref.
[12]). Calculations based on the parton model and perturbative QCD find a much faster
falloff $\sim (1-x)^2$ [59–62]. This soft high-x behavior is also predicted by recent non-
perturbative calculations using Dyson-Schwinger equations [63, 64]. On the other hand,
some low-energy models of hadronic structure favor a linear behavior of the pionic valence
distribution. In Fig. 4.3 several model predictions are compared to valence distributions
obtained by LO and NLO analyses of pionic Drell-Yan data.

This discrepancy between theoretical predictions and analyses of experimental data
concerning the high-x behavior of v^π is widely regarded to be an important problem in
strong-interaction physics. Part II of this thesis is dedicated to solving this problem. It
turns out that fixed-order analyses of data from low-energy fixed-target experiments are
not sufficient to determine pionic PDFs at large x. Higher-order contributions to the
cross section are sizable in this specific kinematic regime and hence have to be taken into

account to all orders in perturbation theory. We do so by resumming threshold logarithms and find a much softer pionic valence distribution well in line with expectations based on perturbative-QCD counting rules and Dyson-Schwinger equations.

4.4. Fragmentation Functions

Finally, we consider the last non-perturbative object in the factorized cross section in Eq. (4.1), the fragmentation function. At leading order it can be interpreted as probability density for the collinear fragmentation of a parton a into a hadron H. It is a function of the factorization scale μ'_F and the fraction z of the parton's momentum that is carried by the produced hadron. As in the case of PDFs, the dependence on the factorization scale is governed by evolution equations similar to DGLAP, whose splitting functions are currently known to NLO [68]. The extraction of fragmentation functions from experimental data is also similar to global PDF analyses. However, to determine fragmentation functions hadrons in the final state have to be identified which turns out to be a challenging task for high-energy experiments.

Analyses of fragmentation functions mainly focus on data from e^+e^- collider experiments with the advantage that the results are not biased by the choice of a PDF set for hadrons in the initial state. On the other hand, it is very hard to separate contributions from the fragmentation of the light quark flavors u, d and s in e^+e^- annihilation. Therefore also semi-inclusive data from e.g. lepton-hadron scattering have to be included in the analyses. The knowledge of the partonic content of the initial state hadron makes it easier to determine the dominating fragmenting quark flavors in the respective reaction. LO and NLO fits of fragmentation functions have been performed by several groups [69–72]. Figure 4.4 shows parameterizations for charged pions from the most recent analysis by the group DSS [73, 74].
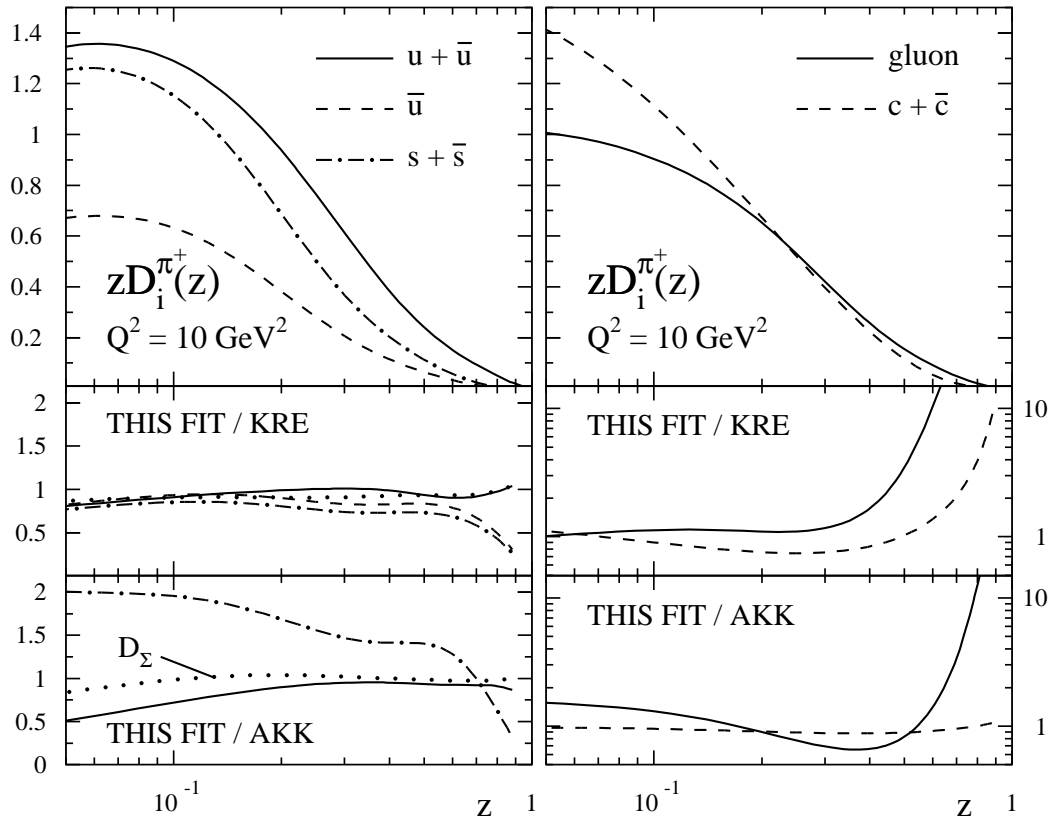
Figure 4.4.: The upper panels show the DSS fragmentation functions [73] for positively charged pions at scale $\mu_F'^2 = Q^2 = 10\ \text{GeV}^2$. The middle and lower panels show ratios of the DSS fragmentation functions to the ones of Kretzer [69] and the group AKK [70]. The figure is taken from Ref. [73].

Part II.

Threshold Resummation and the Valence PDF of the Pion

5. Fixed-Order Cross Sections for the Drell-Yan Process

In this chapter we introduce a fundamental and very important process in strong interaction physics, the Drell-Yan process [75]. At lowest order in perturbation theory, it is the annihilation of a quark and antiquark into a virtual photon, which subsequently creates a pair of leptons. Its properties have been extensively studied since the emergence of high-energy physics for good reasons. First, it is relatively easy to detect pairs of leptons and thereby reconstruct the momentum of the parent virtual photons. Secondly, since photons and leptons only interact via the electromagnetic force, final-state interactions can be neglected and we obtain a clear probe of the involved initial-state quark antiquark pair. The Drell-Yan process is therefore well-suited to investigate the internal structure of the participating hadrons. To this end, it is necessary to compute the perturbatively calculable partonic cross section to a good accuracy.

We rederive the LO and NLO partonic cross sections for the Drell-Yan process in the following two sections and identify contributions to the fixed-order result that may become large in certain kinematic regimes.

5.1. Drell-Yan Cross Section at LO

On the parton level the Drell-Yan process can schematically be written as

$$q(p_1) + \bar{q}(p_2) \to (l^+ + l^-)(q) + X, \tag{5.1}$$

where p_1 and p_2 denote the momenta of the quark and antiquark, respectively, and q is the total momentum of the lepton pair. As we have mentioned above the lepton pair and its parent virtual photon do not interact strongly. Since higher-order QED corrections are negligible, it is sufficient to calculate the leading squared matrix element for the splitting of a virtual photon into a pair of leptons and only consider the partonic cross section for the production of a virtual photon to higher orders. The partonic Drell-Yan cross section then takes the form

$$\frac{\mathrm{d}\hat{\sigma}}{\mathrm{d}Q^2}(q + \bar{q} \to l^+ + l^- + \dots) = \frac{\mathrm{d}\hat{\sigma}_\gamma}{\mathrm{d}Q^2}(q + \bar{q} \to \gamma^*)\frac{\alpha}{3\pi Q^2}, \tag{5.2}$$
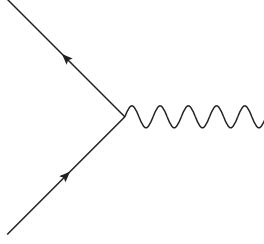
Figure 5.1.: LO Feynman diagram contributing to the Drell-Yan process.

where Q^2 denotes the squared invariant mass of the lepton pair. At LO we have to consider only one Feynman diagram in the calculation of $\mathrm{d}\hat{\sigma}$, which is depicted in Fig. 5.1. By means of the Feynman rules in Appendix A.1 it is trivial to write down the corresponding matrix element,

$$\mathcal{M}^{(0)} = \bar{v}(p_2, s_2)(-ie_q e\gamma^\mu)u(p_1, s_1)\epsilon^*_\mu(q), \tag{5.3}$$

 with the momentum and spin of the incoming quark, p_1 and s_1, and the momentum and spin of the incoming antiquark, p_2 and s_2. The quark's fractional electromagnetic charge is denoted by e_q and the polarization vector of the outgoing virtual photon by ϵ_μ. Squaring the matrix element and averaging over spins and colors of the incoming quark and antiquark we obtain

$$\frac{1}{9}\frac{1}{4}\sum_{s_1,s_2}|\mathcal{M}^{(0)}|^2 = \frac{e_q^2 e^2}{12}\,\mathrm{Tr}(-\not{p}_2\gamma^\mu\not{p}_1\gamma_\mu) = \frac{e_q^2 e^2 \hat{s}}{3}, \tag{5.4}$$

where $\hat{s} = (p_1 + p_2)^2$ is the partonic center-of-mass energy. The partonic differential cross section for the production of a virtual photon to LO is then given by

$$\mathrm{d}\hat{\sigma}^{(0)}_\gamma(q + \bar{q} \to \gamma^*) = \frac{1}{F}\frac{e_q^2 e^2 \hat{s}}{3}\mathrm{d}\mathcal{P} \tag{5.5}$$

with the invariant flux factor, $F = 2\hat{s}$, for massless quarks and the differential phase space,

$$\mathrm{d}\mathcal{P} = \frac{\mathrm{d}^4 q}{(2\pi)^3}(2\pi)^4\delta^{(4)}(p_1 + p_2 - q), \tag{5.6}$$

The delta function assures momentum conservation at the quark-photon vertex. Since we are only interested in the mass of the virtual photon, we integrate over its momentum to obtain

$$\frac{\mathrm{d}\hat{\sigma}^{(0)}_\gamma}{\mathrm{d}Q^2}(q + \bar{q} \to \gamma^*) = \frac{e_q^2 e^2}{6}\int\frac{\mathrm{d}^4 q}{(2\pi)^3}(2\pi)^4\delta^{(4)}(p_1 + p_2 - q)\delta(q^2 - Q^2)\theta(q_0)$$

$$= \frac{e_q^2 e^2 \pi}{3}\delta(\hat{s} - Q^2) = \frac{4\pi^2\alpha e_q^2}{3}\delta(\hat{s} - Q^2). \tag{5.7}$$

Equation (5.2) now allows to write down the partonic Drell-Yan cross section to LO accuracy,

$$
\begin{aligned}
\frac{\mathrm{d}\hat{\sigma}^{(0)}}{\mathrm{d}Q^2} &= \frac{\mathrm{d}\hat{\sigma}_\gamma^{(0)}}{\mathrm{d}Q^2}(q + \bar{q} \to \gamma^*)\frac{\alpha}{3\pi Q^2} \\
&= \frac{4\pi\alpha^2 e_q^2}{9Q^2}\delta(\hat{s} - Q^2).
\end{aligned}
\tag{5.8}
$$

The factorization theorem for the Drell-Yan process now allows to make the transition from the partonic cross section to the hadronic one. In the naive collinear parton model we neglect transverse motion of partons in a fast moving hadron. Therefore the momentum of the quark and antiquark can be written as fraction of the parent hadron's momentum,

$$
p_1 = x_1 P_1, \quad p_2 = x_2 P_2.
\tag{5.9}
$$

The probability of finding a parton a with momentum fraction x in the hadron H is given by the parton distribution $f_a^H(x)$. Hence, the cross section at the hadron level is of the form

$$
\begin{aligned}
\frac{\mathrm{d}\sigma^{(0)}}{\mathrm{d}Q^2} &= \int_0^1 \mathrm{d}x_1 \int_0^1 \mathrm{d}x_2 \sum_q \frac{\mathrm{d}\hat{\sigma}^{(0)}}{\mathrm{d}Q^2}\left[f_q^{H_1}(x_1)f_{\bar{q}}^{H_2}(x_2) + f_{\bar{q}}^{H_1}(x_1)f_q^{H_2}(x_2)\right] \\
&= \frac{4\pi\alpha^2}{9Q^2 S}\int_0^1 \frac{\mathrm{d}x_1}{x_1} \int_0^1 \frac{\mathrm{d}x_2}{x_2} \sum_q e_q^2 \left[f_q^{H_1}(x_1)f_{\bar{q}}^{H_2}(x_2) + f_{\bar{q}}^{H_1}(x_1)f_q^{H_2}(x_2)\right]\delta\left(1 - \frac{\tau}{x_1 x_2}\right)
\end{aligned}
\tag{5.10}
$$

with $\tau = Q^2/S$ and $S = (P_1 + P_2)^2$ being the hadronic center-of-mass energy squared, i.e. $x_1 x_2 S = \hat{s}$. This is the full LO result for the hadronic Drell-Yan cross section.

As we will see in the next section, to higher orders in perturbation theory $q\bar{q}$ annihilation is not the only partonic channel to produce a massive photon. In NLO contributions arise also from qG and $\bar{q}G$ scattering. Beyond that the partonic channels qq, $\bar{q}\bar{q}$ and GG contribute at the NNLO level. The hadronic Drell-Yan cross section to arbitrary order in perturbation theory is therefore more conveniently written as a sum over parton flavors a and b,

$$
\frac{\mathrm{d}\sigma}{\mathrm{d}Q^2} = \sigma_0 \sum_{a,b} \int_0^1 \frac{\mathrm{d}x_1}{x_1} \int_0^1 \frac{\mathrm{d}x_2}{x_2} f_a^{H_1}(x_1,\mu^2)e_{ab}\omega_{ab}\left(\frac{\tau}{x_1 x_2}, \frac{Q}{\mu}\right)f_b^{H_2}(x_2,\mu^2),
\tag{5.11}
$$

where $\sigma_0 = 4\pi\alpha^2/9Q^2 S$ is the so-called Born cross section. The coupling e_{ab} equals e_q^2 for the $q\bar{q}$ and qG, $\bar{q}G$ scattering processes which we are interested in. The factorization and renormalization scales are collectively denoted by μ. Scale dependence emerges at NLO. The hard-scattering functions ω_{ab} are perturbatively calculable as a series in α_s,

$$
\omega_{ab} = \omega_{ab}^{(0)} + \frac{\alpha_s}{\pi}\omega_{ab}^{(1)} + \left(\frac{\alpha_s}{\pi}\right)^2 \omega_{ab}^{(2)} + \dots.
\tag{5.12}
$$

So far we have calculated the zeroth order term in the Drell-Yan cross section. To this order the $q\bar{q}$ channel gives the only non-vanishing contribution to ω_{ab}. Comparing Eq. (5.11) with Eq. (5.10) we can identify

$$\omega_{q\bar{q}}^{(0)} = \omega_{\bar{q}q}^{(0)} = \delta(1-z) \tag{5.13}$$

with $z = Q^2/\hat{s} = \tau/x_1 x_2$.

Equation (5.11) gives the Drell-Yan cross section differential in the invariant mass of the lepton pair. However, to obtain more information on the momentum fractions of the participating partons it is useful to additionally consider the rapidity of the virtual photon with respect to the beam axis. Similar to Eq. (5.11) the factorized form of the rapidity-differential cross section can be written as

$$\frac{\mathrm{d}\sigma}{\mathrm{d}Q^2\mathrm{d}\eta} = \sigma_0 \sum_{a,b} \int_{x_1^0}^1 \frac{\mathrm{d}x_1}{x_1} \int_{x_2^0}^1 \frac{\mathrm{d}x_2}{x_2} f_a^{H_1}(x_1, \mu^2) e_{ab}\bar{\omega}_{ab}\left(x_1, x_1^0, x_2, x_2^0, \frac{Q}{\mu}\right) f_b^{H_2}(x_2, \mu^2),$$
$$\tag{5.14}$$

where $x_{1,2}^0$ are given in terms of the rapidity η by

$$x_{1,2}^0 = \sqrt{\tau}\, e^{\pm\eta}. \tag{5.15}$$

The bounds of the integrals in Eq. (5.14) immediately imply that the cross section at large forward rapidities is built up by contributions from high x_1 and at large backward rapidities (i.e. $\eta < 0$) from high x_2. Drell-Yan experiments at large rapidities are therefore well-suited to investigate the high-x behavior of PDFs. The calculation of the rapidity-differential hard-scattering functions $\bar{\omega}_{ab}$ is analogue to the derivation of ω_{ab}. The only difference is that in Eq. (5.7) the longitudinal momentum of the photon $q_\parallel$ is not integrated over but substituted by the rapidity

$$\eta = \frac{1}{2}\ln\left(\frac{q_0 + q_\parallel}{q_0 - q_\parallel}\right). \tag{5.16}$$

At lowest order one then obtains

$$\bar{\omega}_{q\bar{q}}^{(0)} = \bar{\omega}_{\bar{q}q}^{(0)} = x_1 x_2 \delta(x_1 - x_1^0)\delta(x_2 - x_2^0). \tag{5.17}$$

5.2. Drell-Yan Cross Section at NLO

Let us now go beyond the lowest-order approximation and calculate the $\mathcal{O}(\alpha_s)$ correction to the Drell-Yan cross section. Due to the emergence of different types of singularities the NLO calculation is much more involved than the lowest-order calculation. To regularize the divergences we work in $d = 4 - 2\epsilon$ dimensions throughout. We note that the sign of
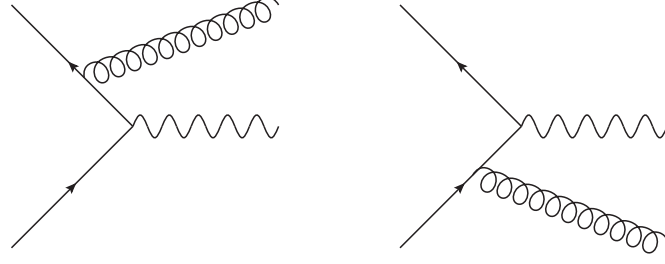
Figure 5.2.: Real gluon-emission diagrams for the Drell-Yan process at NLO.

ϵ is different for the regularization of infrared/collinear ($\epsilon < 0$) and ultraviolet ($\epsilon > 0$) divergences. Subtraction of singularities is performed in the $\overline{\text{MS}}$ scheme. In this scheme the NLO corrections to the Drell-Yan process were fist derived by Altarelli *et al.* [76] in the late 70s.

In the following we will discriminate between *real* and *virtual* corrections to the cross section. In this context, *real* refers to contributions from Feynman diagrams, which do not contain undetermined loop momenta. I.e. each added gluon or fermion line has to have one external end and is therefore on mass shell. By contrast *virtual* diagrams originate from adding a gluon or fermion line attached to two internal vertices. The virtual particle's mass is then undefined and has to be integrated over.

At NLO we encounter two real diagrams, which originate from radiating an additional gluon from the external quark and antiquark lines of the LO diagram. These diagrams are depicted in Fig. 5.2. By means of the Feynman rules of QCD, it is straightforward to evaluate the corresponding matrix element. Taking the modulus squared of the matrix element and averaging over spin and color of the incoming particles we find

$$\frac{1}{9}\frac{1}{4}\sum_{s_1,s_2}|\mathcal{M}_{q\bar{q}\to\gamma^*G}|^2 = \frac{2}{3}e^2g^2e_q^2\mu_R^{2\epsilon}C_F(1-\epsilon)\left\{(1-\epsilon)\left(\frac{\hat{u}}{\hat{t}}+\frac{\hat{t}}{\hat{u}}\right)+\frac{2Q^2\hat{s}}{\hat{u}\hat{t}}-2\epsilon\right\}, \quad (5.18)$$

where $\hat{u}$, $\hat{t}$ and $\hat{s}$ are the partonic Mandelstam variables defined as

$$\begin{aligned}
\hat{u} &= (p_1-k)^2 = (p_2-q)^2,\\
\hat{t} &= (p_1-q)^2 = (p_2-k)^2,\\
\hat{s} &= (p_1+p_2)^2 = (q+k)^2,
\end{aligned} \quad (5.19)$$

where k is the momentum of the gluon. The factors proportional to ϵ stem from the modified gamma algebra in d dimensions.

The contribution of the real NLO diagrams to the partonic Drell-Yan cross section is given by their modulus-squared matrix element multiplied by the flux factor, the factor

for the production of a lepton pair and the differential phase space

$$\frac{\mathrm{d}\hat{\sigma}^{(1)}}{\mathrm{d}Q^2} = \frac{1}{2\hat{s}} \int \frac{\alpha}{3\pi Q^2} \frac{1}{9} \frac{1}{4} \sum_{s_1,s_2} |\mathcal{M}_{q\bar{q}\rightarrow\gamma^*G}|^2 \mathrm{d}\mathcal{P}. \tag{5.20}$$

In this case the evaluation of the phase-space integrals is more involved since we have two particles, namely the massless gluon with momentum k and the massive virtual photon with momentum q and mass Q, in the final state:

$$\mathrm{d}\mathcal{P} = \frac{\mathrm{d}^d k}{(2\pi)^{d-1}} \frac{\mathrm{d}^d q}{(2\pi)^{d-1}} (2\pi)^d \delta^{(4)}(p_1 + p_2 - q - k) \delta(k^2)\theta(k_0)\delta(q^2 - Q^2)\theta(q_0)$$

$$= \frac{\mathrm{d}^{d-1}\vec{k}}{(2\pi)^{d-2} 2k_0} \delta\left((p_1 + p_2 - k)^2 - Q^2\right) \theta\left[(p_1)_0 + (p_2)_0 - k_0\right]. \tag{5.21}$$

In the partonic center-of-mass system, where we can write $p_1^\mu = (p,0,0,p)$, $p_2^\mu = (p,0,0,-p)$, the phase space is of the form

$$\mathrm{d}\mathcal{P} = \frac{\mathrm{d}^{d-1}\vec{k}}{(2\pi)^{d-2} 2k_0} \delta\left(\hat{s} - 2|\vec{k}|\sqrt{\hat{s}} - Q^2\right), \tag{5.22}$$

where we have dropped the theta function $\theta\left[(p_1)_0 + (p_2)_0 - k_0\right] = \theta(\sqrt{\hat{s}} - |\vec{k}|)$ because the argument of the delta function does not have a root for $|\vec{k}| > \sqrt{\hat{s}}$. The matrix element only depends on the absolute value of the gluon momentum $|\vec{k}|$ and the angle between the beam axis and the emitted gluon $\theta = \angle(\vec{p},\vec{k})$. The d-dimensional momentum of the gluon can then be written as

$$k^\mu = (|\vec{k}|,\ldots,|\vec{k}|\cos\theta). \tag{5.23}$$

The dots indicate $d - 2$ unspecified momenta, which can be integrated over in spherical coordinates,

$$\mathrm{d}^{d-1}\vec{k} = \frac{2\pi^{\frac{d-2}{2}}}{\Gamma\left(\frac{d-2}{2}\right)} |\vec{k}|^{d-2}(1 - \cos^2\theta)^{d/2-2}\mathrm{d}(\cos\theta)\mathrm{d}|\vec{k}|$$

$$= \frac{2\pi^{1-\epsilon}}{\Gamma(1-\epsilon)} |\vec{k}|^{2-2\epsilon}(1 - \cos^2\theta)^{-\epsilon}\mathrm{d}(\cos\theta)\mathrm{d}|\vec{k}|, \tag{5.24}$$

where Γ denotes the gamma function. Let us now introduce the dimensionless variable $y = \frac{1}{2}(1 + \cos\theta)$, which has values in the interval $[0,1]$. After coordinate transformation the phase-space factor takes the form

$$\mathrm{d}\mathcal{P} = \frac{(4\pi)^\epsilon}{4\pi\Gamma(1-\epsilon)} 2^{1-2\epsilon}|\vec{k}|^{1-2\epsilon}\mathrm{d}|\vec{k}|(y(1-y))^{-\epsilon}\mathrm{d}y \, \delta\left(\hat{s} - 2|\vec{k}|\sqrt{\hat{s}} - Q^2\right)$$

$$= \frac{(4\pi)^\epsilon}{4\pi\Gamma(1-\epsilon)} 2^{1-2\epsilon} \frac{1}{2\sqrt{\hat{s}}} \left(\frac{\hat{s} - Q^2}{2\sqrt{\hat{s}}}\right)^{1-2\epsilon} (y(1-y))^{-\epsilon}\mathrm{d}y$$

$$= \frac{1}{8\pi} \left(\frac{4\pi}{Q^2}\right)^\epsilon \frac{1}{\Gamma(1-\epsilon)} z^\epsilon(1-z)^{1-2\epsilon}(y(1-y))^{-\epsilon}\mathrm{d}y. \tag{5.25}$$

To this point, we have simplified the phase-space integrals of the massive photon and the massless gluon such that the multi-dimensional momentum integrals in Eq. (5.20) are reduced to a single integral over a dimensionless quantity. The partonic Mandelstam variables defined in Eq. (5.19) can be expressed in terms of the dimensionless variables y and z and the invariant mass of the lepton pair Q as

$$\hat{s} = \frac{Q^2}{z}, \quad \hat{t} = -\frac{Q^2}{z}(1-z)(1-y), \quad \hat{u} = -\frac{Q^2}{z}(1-z)y. \tag{5.26}$$

With these identities we can combine the squared matrix element and the phase-space factor to obtain the contribution of the real NLO diagrams to the partonic Drell-Yan cross section in Eq. (5.20)

$$
\begin{aligned}
\frac{\mathrm{d}\hat{\sigma}^{(1)}}{\mathrm{d}Q^2} &= \frac{2\alpha^2 \alpha_s e_q^2 C_F}{9\hat{s}Q^2} \left(\frac{4\pi\mu_R^2}{Q^2}\right)^\epsilon \frac{1-\epsilon}{\Gamma(1-\epsilon)} z^\epsilon (1-z)^{1-2\epsilon} \\
&\quad \times \int_0^1 \mathrm{d}y\, y^{-\epsilon}(1-y)^{-\epsilon} \left[(1-\epsilon)\left(\frac{1-y}{y} + \frac{y}{1-y}\right) + \frac{2z}{(1-z)^2 y(1-y)} - 2\epsilon\right] \\
&= \frac{\sigma_0}{x_1 x_2} e_q^2 \frac{\alpha_s}{2\pi} C_F \left(\frac{4\pi\mu_R^2}{Q^2}\right)^\epsilon \frac{1}{\Gamma(1-\epsilon)} z^\epsilon (1-z)^{1-2\epsilon} \\
&\quad \times \int_0^1 \mathrm{d}y\, y^{-\epsilon}(1-y)^{-\epsilon} \left[(1-\epsilon)\left(\frac{1-y}{y} + \frac{y}{1-y}\right) + \frac{2z}{(1-z)^2 y(1-y)} - 2\epsilon\right] \\
&\equiv \frac{\sigma_0 e_q^2}{x_1 x_2} \frac{\alpha_s}{\pi} \omega_{q\bar{q}}^{(1)}|_{\text{real}},
\end{aligned}
\tag{5.27}
$$

where

$$\sigma_0 = \frac{4\pi\alpha^2}{9SQ^2}(1-\epsilon) \tag{5.28}$$

is the Born cross section in $d = 4 - 2\epsilon$ dimensions. We have defined $\omega_{q\bar{q}}^{(1)}$ according to Eqs. (5.11) and (5.12). We perform the integral over y, where we use

$$\int_0^1 \mathrm{d}y\, y^a (1-y)^b = \frac{\Gamma(a+1)\Gamma(b+1)}{\Gamma(2+a+b)}, \tag{5.29}$$

and apply the recurrence relation of the gammma function, $\Gamma(x+1) = x\Gamma(x)$, several times to find

$$\frac{\alpha_s}{\pi} \omega_{q\bar{q}}^{(1)}|_{\text{real}} = C_F \frac{\alpha_s}{2\pi} \left(\frac{4\pi\mu_R^2}{Q^2}\right)^\epsilon \frac{\Gamma(1-\epsilon)}{\Gamma(1-2\epsilon)} \left\{-\frac{2}{\epsilon}\left[(1-z)^{1-2\epsilon} z^\epsilon + 2z^{1+\epsilon}(1-z)^{-1-2\epsilon}\right]\right\}. \tag{5.30}$$

In this expression we encounter singularities as $\epsilon \to 0$. We can make these singularities manifest by introducing so-called *plus prescriptions*. Through these prescriptions distributions are defined which have finite integrals in the limit $\epsilon \to 0$. A plus distribution $g(z)_+$ has the well-known property when convoluted with a smooth function $f(x)$,

$$\int_0^1 \mathrm{d}z\, f(z) g(z)_+ = \int_0^1 \mathrm{d}z\, (f(z) - f(1)) g(z). \tag{5.31}$$
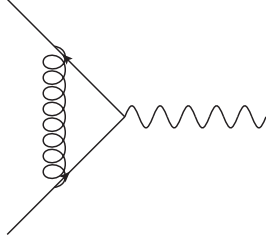
Figure 5.3.: Virtual diagram contributing to the Drell-Yan cross section at NLO.

By means of these particular distributions the singular terms in Eq. (5.30) can be expanded in powers of ϵ [77], for example

$$(1-z)^{-1-2\epsilon} = -\frac{1}{2\epsilon}\delta(1-z) + \frac{1}{(1-z)_+} - \epsilon\left(\frac{\ln(1-z)}{1-z}\right)_+ + \mathcal{O}(\epsilon^2). \qquad (5.32)$$

The singularities are then manifest as poles in $1/\epsilon$. After expansion, we finally obtain the contribution of the real diagrams to the NLO hard-scattering function,

$$\begin{aligned}
\frac{\alpha_s}{\pi}\omega_{q\bar{q}}^{(1)}|_{\text{real}} =&\, C_F\frac{\alpha_s}{2\pi}\left(\frac{4\pi\mu_R^2}{Q^2}\right)^\epsilon\frac{\Gamma(1-\epsilon)}{\Gamma(1-2\epsilon)} \\
&\times\left[\frac{2}{\epsilon^2}\delta(1-z) - \frac{2}{\epsilon}\frac{1+z^2}{(1-z)_+} + 4(1+z^2)\left(\frac{\ln(1-z)}{1-z}\right)_+ - 2\frac{1+z^2}{1-z}\ln z\right].
\end{aligned}$$
$$(5.33)$$

The term proportional to $1/\epsilon^2$ is singular as $z \to 1$. It is an infrared divergence due to the emission of an arbitrarily soft gluon from the quark or antiquark. As discussed in Ch. 3 infrared singularities cancel in the sum of all diagrams to a given order in perturbation theory. In our case this is the sum of real and virtual diagrams.

The only virtual diagram contributing at NLO is depicted in Fig. 5.3. Actually, there are two more virtual diagrams at this order in perturbation theory, namely the one-loop self-energy diagrams for the quark and antiquark lines. However, we see from Eq. (3.18) that the contributions from the self-energy diagrams vanish, if the quark (antiquark) is massless and $\epsilon < 0$. We note that in Landau gauge, where $\xi \to 0$ in the gauge-fixing term in the Lagrangian (see Eq. (2.6)), self-energy diagrams do not contribute regardless of the mass of the fermions. The virtual contribution to the $\mathcal{O}(\alpha_s)$ cross section is calculated from the interference of the diagram in Fig. 5.3 with the LO diagram. Its derivation is similar to the derivation of the contribution from the real diagrams. We therefore do not show the entire calculation and simply state the result,

$$\frac{\alpha_s}{\pi}\omega_{q\bar{q}}^{(1)}|_{\text{virtual}} = C_F\frac{\alpha_s}{2\pi}\left(\frac{4\pi\mu_R^2}{Q^2}\right)^\epsilon\frac{\Gamma(1-\epsilon)}{\Gamma(1-2\epsilon)}\left[-\frac{2}{\epsilon^2} - \frac{3}{\epsilon} - 8 + \frac{2}{3}\pi^2\right]\delta(1-z). \qquad (5.34)$$

Adding the real and virtual contributions we obtain the full expression for the hard-scattering function $\omega_{q\bar{q}}$ at NLO,

$$
\begin{aligned}
\omega_{q\bar{q}}^{(1)} =&\omega_{q\bar{q}}^{(1)}|_{\text{real}} + \omega_{q\bar{q}}^{(1)}|_{\text{virtual}} \\
=&\frac{C_F}{2}\left(\frac{4\pi\mu_R^2}{Q^2}\right)^{\epsilon}\frac{\Gamma(1-\epsilon)}{\Gamma(1-2\epsilon)}\left[-\frac{2}{\epsilon}\frac{1+z^2}{(1-z)_+} - \frac{3}{\epsilon}\delta(1-z) - 2\frac{1+z^2}{1-z}\ln(z)\right. \\
&\left. +4(1+z^2)\left(\frac{\ln(1-z)}{1-z}\right)_+ + \left(-8+\frac{2}{3}\pi^2\right)\delta(1-z)\right].
\end{aligned}
\tag{5.35}
$$

Indeed, the infrared pole cancels in the sum of both contributions. However, the expression still exhibits a collinear divergence proportional to $1/\epsilon$ corresponding to the emission of the real gluon collinear to either the incoming quark or antiquark. These divergences are 'renormalized' by a collinear subtraction. To this end, let us first expand the prefactors according to

$$
\begin{aligned}
\left(\frac{4\pi\mu_R^2}{Q^2}\right)^{\epsilon} &= 1 + \epsilon\ln\frac{\mu_R^2}{Q^2} + \epsilon\ln 4\pi + \mathcal{O}(\epsilon^2), \\
\frac{\Gamma(1-\epsilon)}{\Gamma(1-2\epsilon)} &= 1 - \gamma_E\epsilon + O(\epsilon^2)
\end{aligned}
\tag{5.36}
$$

to find

$$
\begin{aligned}
\omega_{q\bar{q}}^{(1)} =&P_{qq}(z)\left(\ln\frac{Q^2}{\mu_R^2} - \frac{1}{\epsilon} + \gamma_E - \ln 4\pi\right) + C_F\left[2(1+z^2)\left(\frac{\ln(1-z)}{1-z}\right)_+\right. \\
&\left. -\frac{1+z^2}{1-z}\ln(z) + \left(-4+\frac{1}{3}\pi^2\right)\delta(1-z)\right],
\end{aligned}
\tag{5.37}
$$

where

$$
P_{qq}(z) = C_F\left(\frac{1+z^2}{(1-z)_+} + \frac{3}{2}\delta(1-z)\right) = C_F\left(\frac{1+z^2}{1-z}\right)_+
\tag{5.38}
$$

is the lowest-order quark-quark splitting function. In the $\overline{\text{MS}}$-scheme the collinear subtraction reads

$$
\omega_{q\bar{q}}^{(1)}|_{coll} = \frac{1}{\epsilon\Gamma(1-\epsilon)}\left(\frac{4\pi\mu_R^2}{\mu_F^2}\right)^{\epsilon}P_{qq}(z),
\tag{5.39}
$$

where μ_F denotes the factorization scale. Subtracting this term we do not only remove the $1/\epsilon$ pole, but also the terms proportional to $\ln(4\pi)-\gamma_E$ from the hard-scattering function. The final result in the $\overline{\text{MS}}$-scheme reads

$$
\begin{aligned}
\omega_{q\bar{q}}^{\overline{\text{MS}}(1)} =&C_F\left[2(1+z^2)\left(\frac{\ln(1-z)}{1-z}\right)_+ - \frac{1+z^2}{1-z}\ln(z) + \left(-4+\frac{1}{3}\pi^2\right)\delta(1-z)\right] \\
&+ P_{qq}(z)\ln\frac{Q^2}{\mu_F^2}.
\end{aligned}
\tag{5.40}
$$

When we calculate the hadronic cross section, we integrate over the momentum fractions x_1 and x_2 of the initial state partons. With the relation $z = Q^2/x_1 x_2 S$ one of the
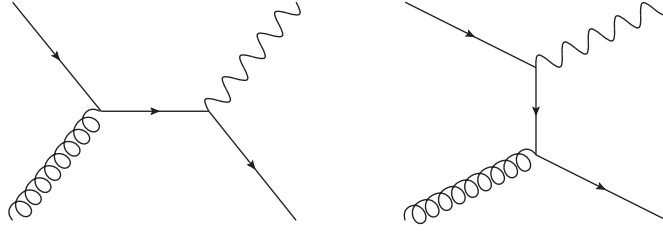
Figure 5.4.: Leading diagrams for the QCD Compton process $q + G \rightarrow \gamma^* + q$.

integrals may be transformed into an integral over z. The lower bound of this integral then corresponds to $x_1 = x_2 = 1$ or $z_{min} = Q^2/S = \tau$. If the ratio Q^2/S is relatively large, which is particularly the case in the fixed-target regime, the integral over z is restricted to the threshold region, where $z \lesssim 1$. As z increases towards unity, little phase space for the emission of real gluons remains, since most of the initial partonic energy is used to produce the virtual photon. This suppression of real-gluon radiation leads to an imbalance of the infrared cancellation of real and virtual contributions and hence the hard-scattering function in Eq. (5.40) receives large logarithmic contributions from the term proportional to

$$\frac{\alpha_s}{\pi} \left(\frac{\ln(1-z)}{1-z} \right)_+ , \tag{5.41}$$

which is referred to as threshold logarithm. Such large logarithms are present to any order in perturbation theory. In kth order the logarithmic term is of the form

$$\left(\frac{\alpha_s}{\pi} \right)^k \left(\frac{\ln^{2k-1}(1-z)}{1-z} \right)_+ . \tag{5.42}$$

Since for values of z near the partonic threshold the logarithms compensate the smallness of α_s, fixed-order calculations do not sufficiently approximate the perturbative series. Instead, the large logarithmic corrections have to be taken into account to all orders to obtain reliable results. The technique to resum these logarithms is known as *threshold resummation* or *soft-gluon resummation*. In the next chapter, we elucidate this procedure in detail.

Before we do so, let us complete the calculation of the NLO partonic Drell-Yan cross section. So far we have only considered the $\mathcal{O}(\alpha_s)$ correction to the $q\bar{q}$ annihilation process, but to this order in perturbation theory also the process

$$q(\bar{q}) + G \rightarrow \gamma^* + q(\bar{q}) \tag{5.43}$$

referred to as QCD Compton scattering contributes to the cross section. The respective Feynman diagrams are depicted in Fig. 5.4. Their derivation can be found in Ref. [76],

we simply state the result in the $\overline{\text{MS}}$-scheme,

$$\omega_{qG}^{\overline{\text{MS}}(1)} = \frac{1}{4}\left[(z^2 + (1-z)^2)\ln\frac{(1-z)^2}{z} - \frac{3}{2}z^2 + z + \frac{3}{2}\right] + \frac{1}{2}P_{qG}(z)\ln\frac{Q^2}{\mu_F^2}, \qquad (5.44)$$

where

$$P_{qG}(z) = \frac{1}{2}\left[(1-z)^2 + z^2\right] \qquad (5.45)$$

is the lowest-order gluon-quark splitting function.

In the previous section, we also introduced the rapidity-differential cross section (see Eq. (5.14)). The $\mathcal{O}(\alpha_s)$ corrections to this quantity were first derived by Kubar et $al.$ [78] in the DIS factorization scheme. For completeness, we present their full NLO result adapted to the $\overline{\text{MS}}$-scheme in Appendix A.2.

6. Exponentiation of Eikonal Cross Sections

The previous chapter dealt with fixed-order calculations of the Drell-Yan cross section. In the NLO hard-scattering functions we identified large logarithmic corrections, which are due to the radiation of soft gluons from the quark lines and which dominate the cross section in the threshold region, i.e. $z \to 1$. These logarithms turn out to give large contributions to the cross section to any order in perturbation theory. A reliable theoretical study of the Drell-Yan cross section should therefore take into account these large corrections to all orders. However, since it is impossible to calculate all-order observables in the full theory of QCD, certain approximations have to be applied which allow for the resummation of large logarithms in the perturbative series.

This was first done a long time ago for soft-photon radiation in QED [79]. The proof of resummation makes use of the *eikonal approximation*, which we will consider below in detail. By means of this approximation a cross section X, which incorporates multiple soft-photon radiation to all orders in perturbation theory, can be written as the exponential of the cross section for the emission of one soft photon Y,

$$X = \exp(Y). \tag{6.1}$$

The proof of this equation, however, does not directly apply to QCD. It makes use of the factorization of matrix elements for multiple photon emission. Since QCD is a non-abelian gauge theory, the gauge bosons interact with each other and therefore do not posses the same simple abelian factorization property as photons. Nevertheless, Sterman [80] observed 30 years ago that exponentiation in the eikonal approximation is also applicable in non-abelian QCD. A formal proof was little later provided by Gatheral [81] and Frenkel and Taylor [82]. They showed that the exponential of a special subset of diagrams contains contributions from the emission and interaction of soft gluons to all perturbative orders. In the procedure of exponentiation the diagrams included in the subset are dressed with a modified color factor.

The first section of this chapter deals with the soft-photon exponentiation in QED. Following the discussion in Ref. [83], we rederive the resummed formula in the eikonal approximation. In Sec. 6.2 we outline the proof of exponentiation of eikonal diagrams in non-abelian gauge theories, which allows to resum large logarithmic corrections due to soft-gluon radiation in QCD.
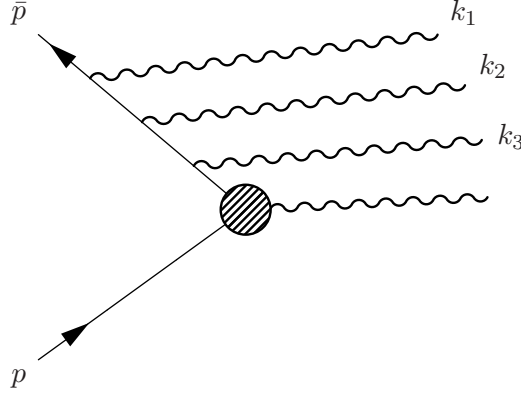
Figure 6.1.: Outgoing electron in a hard process emits three photons with momenta k_1, k_2 and k_3.

6.1. Soft-Photon Exponentiation in QED

Let us consider an arbitrary hard process, which involves an outgoing lepton line. For simplicity we assume the lepton to be an electron and neglect its rest mass. The outgoing electron with momentum $\bar{p}$ emits n photons with momenta $k_1, \ldots, k_n$. The corresponding QED Feynman diagram is depicted in Fig. 6.1 for $n = 3$. The blob denotes the hard process. We do not yet specify whether the emitted photons are on mass shell (real) or not (virtual). The matrix element is then of the form

$$\bar{u}(\bar{p})(-ie\gamma^{\mu_1})\frac{i(\bar{\slashed{p}} + \slashed{k}_1)}{(\bar{p} + k_1)^2}(-ie\gamma^{\mu_2})\frac{i(\bar{\slashed{p}} + \slashed{k}_1 + \slashed{k}_2)}{(\bar{p} + k_1 + k_2)^2}\cdots(-ie\gamma^{\mu_n})\frac{i(\bar{\slashed{p}} + \slashed{k}_1 + \cdots + \slashed{k}_n)}{(\bar{p} + k_1 + \cdots + k_n)^2}(i\mathcal{M}_{\text{hard}})\cdots,$$
$$(6.2)$$

where we omit the polarization vectors of the emitted photons. The matrix element of the hard-scattering process is denoted by $\mathcal{M}_{\text{hard}}$. In $\mathcal{M}_{\text{hard}}$ all interactions, which involve high momenta, are contained. Therefore, we allow only soft radiation from the external fermion line. In this limit of soft radiation it is useful to apply the eikonal approximation to the matrix element. In our case the approximation involves the following two simplifications:

1. Neglect k_i^{μ} compared to $\bar{p}^{\mu}$ in the numerator.

2. Neglect k_i^2 compared to $\bar{p} \cdot k_i$ in the denominator.

By means of the anti-commutation relation of the gamma matrices, we bring all the factors of $\bar{\slashed{p}}$ to the left of the gamma matrices and use the massless Dirac equation, $\bar{u}(\bar{p})\bar{\slashed{p}} = 0$, to remove them from the matrix element. Equation (6.2) then becomes

$$\bar{u}(\bar{p})\left(e\frac{\bar{p}^{\mu_1}}{\bar{p} \cdot k_1}\right)\left(e\frac{\bar{p}^{\mu_2}}{\bar{p} \cdot (k_1 + k_2)}\right)\cdots\left(e\frac{\bar{p}^{\mu_n}}{\bar{p} \cdot (k_1 + \cdots + k_n)}\right)(i\mathcal{M}_{\text{hard}})\cdots. \qquad (6.3)$$

Since it is experimentally impossible to determine, in which ordering the photons with momenta $k_1, \ldots, k_n$ are emitted from the electron, we have to sum over all possible permutations of the photon momenta. The sum over permutations looks very cumbersome at first sight. Let us therefore fist consider the trivial case of the emission of two photons, where the sum consists of only two terms and is easily simplified to

$$\frac{1}{\bar{p} \cdot k_1} \frac{1}{\bar{p} \cdot (k_1 + k_2)} + \frac{1}{\bar{p} \cdot k_2} \frac{1}{\bar{p} \cdot (k_2 + k_1)} = \frac{1}{\bar{p} \cdot k_1} \frac{1}{\bar{p} \cdot k_2}. \tag{6.4}$$

By mathematical induction the argument can be generalized to the emission of n photons [83],

$$\sum_\pi \frac{1}{\bar{p} \cdot k_{\pi(1)}} \frac{1}{\bar{p} \cdot (k_{\pi(1)} + k_{\pi(2)})} \cdots \frac{1}{\bar{p} \cdot (k_{\pi(1)} + \cdots + k_{\pi(n)})} = \frac{1}{\bar{p} \cdot k_1} \cdots \frac{1}{\bar{p} \cdot k_n}, \tag{6.5}$$

where π denotes a permutation of the n photon lines. Equation (6.5) is usually referred to as generalized eikonal identity. With this identity we find for the matrix element of multiple soft-photon emission

$$\bar{u}(\bar{p}) \left(e \frac{\bar{p}^{\mu_1}}{\bar{p} \cdot k_1} \right) \left(e \frac{\bar{p}^{\mu_2}}{\bar{p} \cdot k_2} \right) \cdots \left(e \frac{\bar{p}^{\mu_n}}{\bar{p} \cdot k_n} \right) (i\mathcal{M}_{\text{hard}}) \cdots . \tag{6.6}$$

QED (as well as QCD) conserves the lepton number in any reaction. Therefore, in our arbitrary hard process each outgoing electron is either accompanied by an incoming electron or equivalently an outgoing positron. Let us assume the hard process includes an incoming electron line with momentum p. Now that we have worked out the matrix element for the emission of n soft photons from an outgoing electron line, it is straightforward to apply the same method to the emission of m photons from an incoming electron. The only difference in the calculation is that the photon momenta, which we denote by $k_{n+1}, \ldots, k_{n+m}$, are subtracted from the electron's momentum p, which results in a negative sign for each photon-emission factor. In analogy to Eq. (6.6) we can write for the matrix element of the emission of m soft photons from an incoming electron line

$$\cdots (i\mathcal{M}_{\text{hard}}) \left(-e \frac{p^{\mu_{n+1}}}{p \cdot k_{n+1}} \right) \left(-e \frac{p^{\mu_{n+2}}}{p \cdot k_{n+2}} \right) \cdots \left(-e \frac{p^{\mu_{n+m}}}{p \cdot k_{n+m}} \right) u(p). \tag{6.7}$$

We have mentioned above that the ordering of the external photon momenta cannot be determined experimentally. For the same reason, we cannot distinguish whether a soft photon is emitted from the incoming or outgoing electron, i.e. we have to sum over all possible diagrams with a total number of $l = n + m$ soft photons in the final state. Let us again first consider the simple case of two photons with momenta $k_1^{\mu_1}$ and $k_2^{\mu_2}$ in the final state. We can immediately write down the corresponding matrix element,

$$\bar{u}(\bar{p}) i\mathcal{M}_{\text{hard}} u(p) e^2 \left[\frac{\bar{p}^{\mu_1}}{\bar{p} \cdot k_1} \frac{\bar{p}^{\mu_2}}{\bar{p} \cdot k_2} - \frac{\bar{p}^{\mu_1}}{\bar{p} \cdot k_1} \frac{p^{\mu_2}}{p \cdot k_2} - \frac{p^{\mu_1}}{p \cdot k_1} \frac{\bar{p}^{\mu_2}}{\bar{p} \cdot k_2} + \frac{p^{\mu_1}}{p \cdot k_1} \frac{p^{\mu_2}}{p \cdot k_2} \right]$$

$$= \bar{u}(\bar{p}) i\mathcal{M}_{\text{hard}} u(p) e^2 \left(\frac{\bar{p}^{\mu_1}}{\bar{p} \cdot k_1} - \frac{p^{\mu_1}}{p \cdot k_1} \right) \left(\frac{\bar{p}^{\mu_2}}{\bar{p} \cdot k_2} - \frac{p^{\mu_2}}{p \cdot k_2} \right). \tag{6.8}$$

It is easily proven by induction that for a number of l soft photons the sum over all diagrams yields

$$\bar{u}(\bar{p})i\mathcal{M}_{\text{hard}}u(p)e^l\left(\frac{\bar{p}^{\mu_1}}{\bar{p}\cdot k_1}-\frac{p^{\mu_1}}{p\cdot k_1}\right)\left(\frac{\bar{p}^{\mu_2}}{\bar{p}\cdot k_2}-\frac{p^{\mu_2}}{p\cdot k_2}\right)\cdots\left(\frac{\bar{p}^{\mu_l}}{\bar{p}\cdot k_l}-\frac{p^{\mu_l}}{p\cdot k_l}\right). \qquad (6.9)$$

The virtue of this formula is that the matrix element completely factorizes into the hard-scattering part and l identical factors for the emission of soft photons. This factorized expression is of course only true in the eikonal approximation. An exact analysis in the full theory would yield additional terms proportional to combinations of the photon momenta k_i.

So far in our derivation, we have not specified whether the emitted photons are real or virtual. Let us first consider the case of n real photons. To this end, we multiply the matrix element by the polarization vector $\epsilon_i^{\mu_i}$ for each radiated photon. Subsequently we take the absolute square of the matrix element, sum over polarizations and integrate over the photon phase space. What we obtain are n factors of the form,

$$\int\frac{\text{d}^3\vec{k}}{(2\pi)^3 2k_0}e^2(-g_{\mu\nu})\left(\frac{\bar{p}^\mu}{\bar{p}\cdot k}-\frac{p^\mu}{p\cdot k}\right)\left(\frac{\bar{p}^\nu}{\bar{p}\cdot k}-\frac{p^\nu}{p\cdot k}\right)\equiv Y_{\text{real}}. \qquad (6.10)$$

Hence, our considered cross section has n identical bosons in the final state, where by 'identical' we mean that they carry the same amount of energy, which is zero. Speaking in the language of quantum mechanics, the n bosons occupy the same energy level. Statistical physics now tells us that there are $n!$ ways of realizing this specific state and therefore an observable corresponding to that state has to be divided by the symmetry factor $n!$. The cross section of the hard process including the emission of n additional soft gluons is then given by

$$\sigma(e^-+\cdots\to e^-+n\gamma+\dots)=\sigma(e^-+\cdots\to e^-+\dots)\cdot\frac{Y_{\text{real}}^n}{n!}, \qquad (6.11)$$

where $\sigma(e^-+\cdots\to e^-+\dots)$ denotes the cross section without emission of soft photons.

Next, we address the emission and absorption of virtual photons. We obtain a virtual photon by connecting two photon lines. In our derivation this is done by multiplying Eq. (6.9) by a photon propagator and integrating over the virtual photon's momentum. Besides, to prevent counting virtual graphs twice we divide each virtual contribution by a factor 2. For m virtual photons we get m factors in the matrix element of the form (note that we have not yet taken the absolute square),

$$\frac{1}{2}\int\frac{\text{d}^4k}{(2\pi)^4}e^2\frac{-ig_{\mu\nu}}{k^2+i\eta}\left(\frac{\bar{p}^\mu}{\bar{p}\cdot k}-\frac{p^\mu}{p\cdot k}\right)\left(\frac{\bar{p}^\nu}{-\bar{p}\cdot k}-\frac{p^\nu}{-p\cdot k}\right)\equiv Y_{\text{virt}}. \qquad (6.12)$$

As interchanging the m virtual photons with each other does not alter the diagram, we again have to multiply by a symmetry factor of $1/m!$ when calculating the cross section.

Since we are interested in the corrections due to soft-photon emission to all orders in perturbation theory, we sum over the number of real and virtual photons when calculating

the cross section. Suppose two external electron (respectively positron) lines are attached to the hard process, the cross section is then given by

$$
\begin{aligned}
\sigma_{\text{all orders}} &= \sum_{n,m=0}^{\infty} \sigma(e^- + \cdots \to e^- + n\gamma + \dots) \\
&= \sigma(e^- + \cdots \to e^- + \dots) \cdot \sum_{n=0}^{\infty} \frac{Y_{\text{real}}^n}{n!} \cdot \left(\sum_{m=0}^{\infty} \frac{Y_{\text{virt}}^m}{m!} \right)^2 \\
&= \sigma(e^- + \cdots \to e^- + \dots) \cdot \exp(Y_{\text{real}}) \cdot \exp(2Y_{\text{virt}}).
\end{aligned}
\tag{6.13}
$$

This expression shows that the emission of soft photons, as well as, the virtual corrections exponentiate in the eikonal approximation and are, consequently, resummed to all orders. We did not address the fact that both the expression for Y_{real} and Y_{virt} are infrared divergent. It turns out, however, that these divergences cancel in the sum $Y_{\text{real}} + 2Y_{\text{virt}}$ order by order. In the context of exponentiation of soft real and virtual contributions, this cancellation of infrared divergences to all orders was proven by Yennie, Frautschi and Suura [79].

6.2. Eikonal Exponentiation in Non-Abelian Gauge Theories

The exponentiation of soft-emission diagrams is by far more difficult in QCD due to the non-abelian character of the theory. Nevertheless, an exponentiation theorem for non-abelian gauge theories was developed and proven [81, 82]. It states that similar to QED a cross section X with two external colored fermion lines can schematically be written as

$$
X = \exp(Y),
\tag{6.14}
$$

where Y has the properties [82]:

1. Y is calculated as a perturbative series of terms, each of which corresponds to a Feynman diagram.

2. The diagrams in Y are a subset of the diagrams contributing to X.

3. Each diagram in Y is dressed with a modified color factor, which is in general different from the one in X.

4. The phase space is symmetric in the real gluon momenta.

In the following we outline the proof developed by Gatheral, Frenkel and Taylor [81, 82]. The proof relies on two theorems: the first one is the generalized eikonal identity in Eq. (6.5). In the previous section we have already shown how the eikonal identity factorizes the Feynman integrals associated with soft momenta. The second theorem, which is presented

in the following subsection, deals with the color factors of the diagrams in Y. At the heart of the approach lies that Feynman diagrams can be decomposed into a product of a Feynman integral and a color factor (however, this is not completely true for a Feynman diagram which contains a four-gluon vertex. Such a diagram can only be decomposed into a sum of products of Feynman integrals and color factors.). To visualize the calculation of the color factors we use color diagrams. The color diagram for an arbitrary cut Feynman graph is given by closing the fermion lines and keeping the order of the attached gluons to the lines. For example,
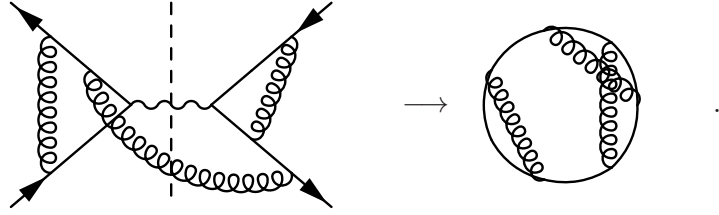
We can neglect photon lines, when we draw color diagrams, since photons do neither interact with each other nor with gluons. All soft-gluon lines have to be drawn inside the fermion loop. The rules for the evaluation of the color diagrams follow directly from the color part of the QCD Feynman rules. Consequently a quark-gluon vertex is associated with the generator t_{ij}^a, where i,j are the matrix indices. A three-gluon vertex is associated with if^{abc}, a quark line with δ_{ij} and a gluon line with δ^{ab}. With these rules it is straightforward to evaluate fundamental color diagrams, such as

$$\frac{1}{N}\left(\text{\includegraphics{}}\right) \equiv C\left(\text{\includegraphics{}}\right) = C_F,$$

$$\frac{1}{N}\left(\text{\includegraphics{}}\right) \equiv C\left(\text{\includegraphics{}}\right) = -\frac{1}{2}C_F C_A. \tag{6.15}$$

6.2.1. Decomposition of Color Diagrams

Considering more involved diagrams it is useful to classify different types of topologies. We adopt the definitions in Refs. [81] and [82], where a *web* is defined as a set of gluon lines, which cannot be partitioned without cutting at least one of its lines. More strictly a *connected web* ('c-web') is defined as a connected set of gluon lines. Since crossed gluon lines are not counted as being connected, a c-web must not contain crossed lines. Some examples are illustrated in Fig. 6.2. The color factor of a c-web W is in general not equal to the color factor $C(D[W])$ of the corresponding Feynman diagram $D[W]$. We therefore denote the color factor of a c-web by $\tilde{C}(W)$.
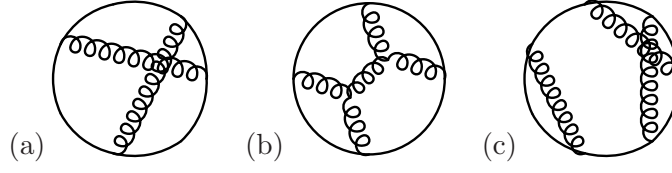
Figure 6.2.: The diagram (a) is a web, (b) is a c-web and (c) is not a web at all.
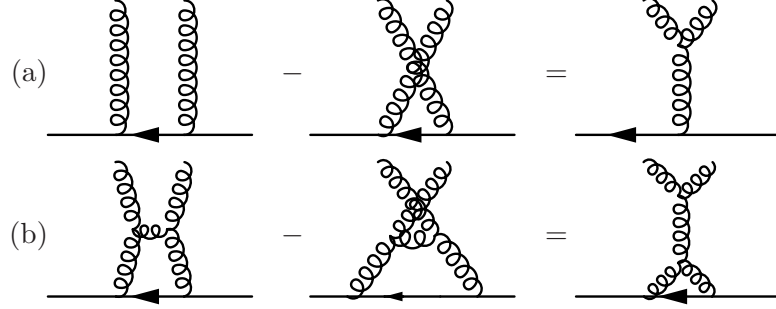

Figure 6.3.: The commutation relation a) and the Jacobi identity b) in the language of color diagrams.

The major theorem we need for the exponentiation in non-abelian field theory is that each color diagram can be decomposed into a sum of products of c-webs by using the commutation relation in Eq. (2.16) and the Jacobi identity in Eq. (2.18). Both identities are visualized in terms of color diagrams in Fig. 6.3. For the color factor C of a Feynman diagram D the theorem states

$$C(D) = \sum_k C^{(k)}, \tag{6.16}$$

where $C^{(k)}$ itself is a sum of terms containing exactly k factor c-webs. Each $C^{(k)}$ is uniquely determined by $C(D)$. Fig. 6.4 illustrates the theorem. Its proof can be found in the appendix of Ref. [82]. Each term in the sum in Eq. (6.16) is called a decomposition. The color factor $C(d)$ of a decomposition d into $n(d)$ c-webs is the product of the color factors of the c-webs W_i in d,

$$C(d) = \prod_{i=1}^{n(d)} \tilde{C}(W_i). \tag{6.17}$$

The set of decompositions of a web W is denoted by $Dec(W)$. Furthermore we denote the subset of decompositions, which only contains non-trivial decompositions of the web, by $Dec'(W)$. If the web W is a c-web, the trivial decomposition is the web itself and its color factor corresponds to the term $C^{(1)}$ in Eq. (6.16). Hence a non-trivial decomposition is characterized by the property that it contains more than one c-web. It follows from
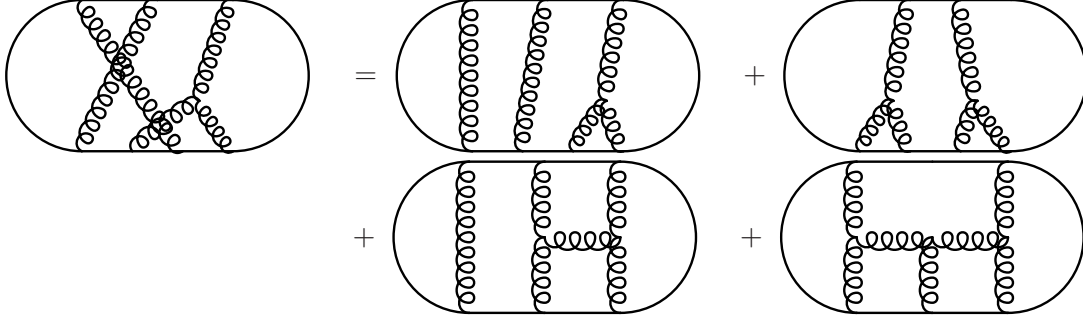
Figure 6.4.: Decomposition of a color diagram into a sum of products of c-webs.

these definitions that the color factor of a web W is the color factor of the diagram $D(W)$ minus the sum over the color factors of all non-trivial decompositions of W,

$$\tilde{C}(W) = C(D[W]) - \sum_{d\in Dec'(W)} \prod_{i=1}^{n(d)} \tilde{C}(W_i), \qquad (6.18)$$

or equivalently,

$$C(D[W]) = \sum_{d\in Dec(W)} \prod_{i=1}^{n(d)} \tilde{C}(W_i). \qquad (6.19)$$

Equation (6.18) is a recursive definition of the color factor of a web. Comparing Eq. (6.18) with Eq. (6.16) one can identify the color factor of a web $\tilde{C}$ with the term $C^{(1)}$. As we will see in the following, the factor $\tilde{C}(W)$ is the modified color factor which multiplies the corresponding Feynman integral in the resummed exponent. From this observation we can immediately state that only diagrams which consist of a single web are exponentiated, otherwise $C^{(1)} = 0$ and thus $\tilde{C} = 0$.

6.2.2. Generalized Eikonal Identity

As mentioned earlier, the second key ingredient next to the decomposition of color diagrams is the factorization of the 'Feynman part' in the eikonal approximation. We denote the Feynman integral of the diagram corresponding to a web W by $\mathcal{F}(W)$. In $\mathcal{F}$ it is understood that the absolute square of the matrix element is taken and the phase space integral is included. What we need is the non-abelian analogue of the eikonal identity in Eq. (6.5). By contrast to QED, quarks do not only radiate single independent gluons but also bundles of gluons, which are woven together in a web due to the gluonic self-interaction. Hence, we cannot find an eikonal identity, which allows to factorize the emission of individual

Figure 6.5.: Example for the reordering of the sum in equation (6.21) to order α_s^2 for two eikonal lines.

gluons but instead the emission of gluonic webs. This generalized identity reads [81]: If S_d is a set of Feynman diagrams F, whose color diagrams have decompositions d into $n(d)$ webs and if $\mathcal{F}(W_i)$ is the Feynman integral in the eikonal approximation corresponding to a given web W_i, then

$$\sum_{F \in S_d} F = \prod_{i=1}^{n(d)} \mathcal{F}(W_i). \tag{6.20}$$

The left hand side is nothing but the sum over all permutations of the gluon lines, where the order of the gluon lines within a web is kept fixed. The proof is basically the same as in QED, the only difference is that you must not permute the gluon lines within the webs. It can be found in Ref. [81].

6.2.3. Proof of Exponentiation

The decomposition of color diagrams into a sum over products of c-webs in Eq. (6.19) and the generalized eikonal identity in Eq. (6.20) provide the framework for the proof of exponentiation of eikonal cross sections in non-abelian gauge theories. We define $X^{(m)}$ as the sum of squared matrix elements for any process with two eikonal lines to order α_s^m. The set of Feynman diagrams contributing to $X^{(m)}$ is denoted by $G(m)$. By means of the two identities in Eq. (6.19) and Eq. (6.20), $X^{(m)}$ can be written as

$$
\begin{aligned}
X^{(m)} &= \sum_{F \in G(m)} C(F)F \\
&= \sum_{F \in G(m)} \sum_{d \in Dec(D[F])} \prod_{i=1}^{n(d)} \tilde{C}(W_i)F \\
&= \sum_{d \in Dec(G(m))} \prod_{i=1}^{n(d)} \tilde{C}(W_i) \sum_{F \in S_d} F \\
&= \sum_{d \in Dec(G(m))} \prod_{i=1}^{n(d)} \tilde{C}(W_i) \prod_{i=1}^{n(d)} \mathcal{F}(W_i) \\
&= \sum_{d \in Dec(G(m))} \prod_{i=1}^{n(d)} \tilde{C}(W_i)\mathcal{F}(W_i).
\end{aligned}
\tag{6.21}
$$

The sum over Feynman diagrams with their corresponding color factor is cast into a sum over decompositions. Each decomposition is a product of diagrams multiplied by the color factor of the corresponding c-web. Since this reordering is far from trivial, we show the procedure step by step for the contributions of $\mathcal{O}(\alpha_s^2)$ in QCD in Fig. 6.5. In case the phase space integration measure is symmetric in the real gluon momenta, the combinatorial factor of $1/2!$ in the last line of the figure has to be included to prevent overcounting of identical diagrams. A systematical treatment of combinatorial factors in Eq. (6.21) can be employed by arranging webs of the same order in α_s. Following the discussion and notation in Ref. [84] we split up the sum over decompositions into two sums of the form,

$$
X^{(m)} = \sum_{\{n_i\}, \sum i n_i = m} \prod_i \frac{1}{n_i!} \left(\sum_{\text{webs of order } i} \tilde{C}(W)\mathcal{F}(W) \right)^{n_i},
\tag{6.22}
$$

where i denotes the order of the c-web in α_s and $\{n_i\}$ are sets of integers with the constraint $\sum_i i n_i = m$. The factor of $1/n_i!$ is the combinatorial factor due to the symmetry of the n_i real gluon momenta in phase space. Comparing Eq. (6.22) with our example in Fig. 6.5 we find that to order α_s^2 the sum over $\{n_i\}$ consists of two terms, namely $\{2, 0, \dots\}$ and $\{0, 1, 0, \dots\}$ corresponding to $n_1 = 2$ c-webs of order 1 and $n_2 = 1$ c-web of order 2, respectively.

To obtain the cross section to all order in perturbation theory we resum the perturbative series in powers of α_s^m. The sum over m removes the constraint $\sum_i i n_i = m$ on the first sum in Eq. (6.22) and we obtain

$$
\begin{aligned}
X &= \sum_{m=0}^{\infty} X^{(m)} \\
&= \sum_{\{n_i\}} \prod_i \frac{1}{n_i!} \left(\sum_{\text{webs of order } i} \tilde{C}(W)\mathcal{F}(W) \right)^{n_i} \\
&= \prod_{i=1}^{\infty} \left\{ \sum_{n_i=0}^{\infty} \frac{1}{n_i!} \left(\sum_{\text{webs of order } i} \tilde{C}(W)\mathcal{F}(W) \right)^{n_i} \right\} \\
&= \prod_{i=1}^{\infty} \exp \left(\sum_{\text{webs of order } i} \tilde{C}(W)\mathcal{F}(W) \right) \\
&= \exp \left(\sum_{i=1}^{\infty} \sum_{\text{webs of order } i} \tilde{C}(W)\mathcal{F}(W) \right) \equiv \exp(Y).
\end{aligned}
\tag{6.23}
$$

The exponent Y is given by the infinitesimal sum

$$
Y = \sum_{i=1}^{\infty} \sum_{\text{webs of order } i} \tilde{C}(W)\mathcal{F}(W).
\tag{6.24}
$$

This completes the proof of Eq. (6.14) for processes with two eikonal lines with Y fulfilling the properties 1 through 4 stated at the beginning of this section.

As in the case of exponentiation of soft photon emission in QED, infrared divergences of the eikonal diagrams emerge in the exponent. However, those divergences cancel order by order, which was shown by Gatheral, Frenkel and Taylor. We refrain from presenting the proof here but refer to their original work in Ref. [85]. We note that exponentiation in non-abelian gauge theories was also performed beyond the eikonal approximation ('next-to-eikonal' exponentiation) [86, 87]. Besides, in recent years other approaches to the resummation of large logarithmic corrections have been worked out. Most notable are the renormalization group approach [88] and the resummation in soft-collinear effective theory (SCET) [89–91].

7. Resummed Cross Section for the Drell-Yan Process

The formal proof of exponentiation of eikonal diagrams, which we outlined in the previous chapter, laid the ground for the resummation of soft-gluon radiation in QCD. In their seminal papers Sterman [13] and Catani and Trentadue [14] derived the resummed exponents for the Drell-Yan process and deep-inelastic scattering. The techniques developed in these papers have since then been successfully applied to the resummation of large contributions associated with soft radiation in many hard QCD processes.

For the Drell-Yan process the eikonal approximation corresponds to taking the partonic-threshold limit, i.e. $z = Q^2/\hat{s} \to 1$. As we have observed in Ch. 5, soft-gluon radiation leads to logarithmic corrections of the form

$$\left(\frac{\alpha_s}{\pi}\right)^k \left(\frac{\ln^{2k-1}(1-z)}{1-z}\right)_+ \tag{7.1}$$

in kth order of perturbation theory, which are particularly large near the partonic threshold. The exponentiation of these logarithms is therefore referred to as *threshold resummation*. Beside the leading logarithms (LL) in Eq. (7.1) subleading terms, which are down by powers of the logarithm and are referred to as next-to-leading logarithms (NLL) and so forth, emerge in the calculation of the cross section. These subleading logarithms may also be exponentiated to improve the validity of the resummed formula. For the Drell-Yan process threshold resummation is currently worked out to NNLL accuracy [92]. However, in the following we will consider soft-gluon resummation only to NLL order.

We present threshold-resummed formulae for both the rapidity-integrated and rapidity-differential Drell-Yan cross section in the $\overline{\text{MS}}$-scheme.

7.1. Phase Space Factorization in Mellin-Moment Space

In the previous chapter, we presented the proof of exponentiation in non-abelian gauge theories and in Eq. (6.24) we gave a general formula for the resummed exponent. Nevertheless, this expression is only formal since we have not at all considered the underlying hard process. Although the phase space is symmetric in the momenta of the emitted real

gluons, the phase-space integral of particles involved in the hard process may still couple the gluons' momenta and spoil the factorization of multiple soft-gluon emission.

This is the case for the Drell-Yan cross section $d\sigma/dQ^2$. Considering the emission of n soft gluons, the differential phase space is of the form

$$
\begin{aligned}
d\mathcal{P} &= (2\pi^4)\,\delta^{(4)}\left(p_1 + p_2 - q - \sum_i k_i\right)\delta(q^2 - Q^2)\theta(q_0)\frac{d^4q}{(2\pi)^3}\prod_{i=1}^{n}\frac{d^3\vec{k}_i}{(2\pi)^3 2(k_i)_0} \\
&= 2\pi\,\delta\left(\left[p_1 + p_2 - \sum_i k_i\right]^2 - Q^2\right)\prod_{i=1}^{n}\frac{d^3\vec{k}_i}{(2\pi)^3 2(k_i)_0} \\
&\approx 2\pi\,\delta\left(\hat{s} - \sum_i 2(k_i)_0\sqrt{\hat{s}} - Q^2\right)\prod_{i=1}^{n}\frac{d^3\vec{k}_i}{(2\pi)^3 2(k_i)_0} \\
&= \frac{2\pi}{\hat{s}}\,\delta\left(1 - z - \sum_i z_{k_i}\right)\prod_{i=1}^{n}\frac{d^3\vec{k}_i}{(2\pi)^3 2(k_i)_0},
\end{aligned}
\tag{7.2}
$$

where $z_{k_i} = 2(k_i)_0/\sqrt{\hat{s}}$ denotes the energy fraction of the ith gluon. The momenta of the n real gluons are denoted by k_i and q is the momentum of the virtual photon of mass Q. Due to the delta function the gluon-momentum integrals are not independent from each other and cannot readily be exponentiated. However, in the threshold region the phase space can still be factorized. To this end, we express the delta function by its inverse Laplace transform,

$$
\delta\left(1 - z - \sum_i z_{k_i}\right) = \frac{1}{2\pi i}\int_{c-i\infty}^{c+i\infty}dN\,e^{N\left(1 - z - \sum_i z_{k_i}\right)},
\tag{7.3}
$$

with c an arbitrary real number. In the limit $z \to 1$, it holds $e^{N(1-z)} \approx e^{-N\ln z} = z^{-N}$. Therefore, in the significant region of the phase space the delta function can be expressed in terms of an inverse Mellin transform,

$$
\delta\left(1 - z - \sum_i z_{k_i}\right) = \frac{1}{2\pi i}\int_{c-i\infty}^{c+i\infty}dN\,z^{-N}\prod_i e^{-N z_{k_i}}.
\tag{7.4}
$$

Consequently, we find for the Mellin transform of the differential phase space

$$
\int_0^1 dz\,z^{N-1}d\mathcal{P} \approx \frac{2\pi}{\hat{s}}\prod_{i=1}^{n}\frac{d^3\vec{k}_i}{(2\pi)^3 2(k_i)_0}e^{-N z_{k_i}},
\tag{7.5}
$$

which indicates that in Mellin moment space the phase space for multiple soft-gluon emission completely factorizes and can hence be exponentiated.

The transition to Mellin moment space is already made on the hadron level. As mentioned in Ch. 5 the hadronic rapidity-integrated Drell-Yan cross section is of the form,

$$
\frac{d\sigma}{dQ^2} = \sigma_0\sum_{a,b}\int_0^1\frac{dx_1}{x_1}\int_0^1\frac{dx_2}{x_2}f_a^{H_1}(x_1,\mu^2)e_{ab}\omega_{ab}\left(\frac{\tau}{x_1 x_2},\frac{Q}{\mu}\right)f_b^{H_2}(x_2,\mu^2),
\tag{7.6}
$$

with the perturbative hard-scattering cross sections ω_{ab} and the non-perturbative PDFs $f_a^{H_1}$ and $f_b^{H_2}$. Applying a Mellin transform in the variable $\tau = Q^2/S = x_1 x_2 z$ to the cross section,

$$\frac{\mathrm{d}\sigma^N}{\mathrm{d}Q^2} \equiv \int_0^1 \mathrm{d}\tau \tau^{N-1} \frac{\mathrm{d}\sigma}{\mathrm{d}Q^2}, \tag{7.7}$$

the convolution integrals in Eq. (7.6) algebraically decouple into ordinary products. Defining the moments of the PDFs,

$$f^N(\mu^2) \equiv \int_0^1 \mathrm{d}x x^{N-1} f(x, \mu^2), \tag{7.8}$$

and introducing the corresponding transform of the hard-scattering cross sections,

$$\omega_{ab}^N \equiv \int_0^1 \mathrm{d}z z^{N-1} \omega_{ab}, \tag{7.9}$$

one finds

$$\frac{\mathrm{d}\sigma^N}{\mathrm{d}Q^2} = \sigma_0 \sum_{a,b} f_a^{H_1,N}(\mu^2) f_b^{H_2,N}(\mu^2) e_{ab} \omega_{ab}^N(Q/\mu). \tag{7.10}$$

As mentioned earlier, the dominating partonic channel in the Drell-Yan process is quark-antiquark annihilation corresponding to the hard-scattering function $\omega_{q\bar{q}}^N$. In Mellin moment space large logarithmic corrections due to the emission of soft gluons in $\omega_{q\bar{q}}^N$ can now be resummed to all orders.

7.2. NLL Resummation for the Cross Section $\mathrm{d}\sigma/\mathrm{d}Q^2$

For the rapidity-integrated Drell-Yan process the threshold-resummed cross section is in the $\overline{\mathrm{MS}}$-scheme given by [13] [14]

$$\ln \omega_{q\bar{q}}^N(Q/\mu) = C_q\left(\frac{Q^2}{\mu^2}, \alpha_s(\mu)\right) + 2 \int_0^1 \mathrm{d}\zeta \frac{\zeta^{N-1}-1}{1-\zeta} \int_{\mu^2}^{(1-\zeta)^2 Q^2} \frac{\mathrm{d}k_\perp^2}{k_\perp^2} A_q(\alpha_s(k_\perp)), \tag{7.11}$$

where $A_q(\alpha_s)$ is a perturbative series. The terms of the expansion correspond to those of the series of diagrams in Eq. (6.24). For resummation to NLL accuracy the first two orders are sufficient [13, 14]:

$$A_q(\alpha_s) = \frac{\alpha_s}{\pi} A_q^{(1)} + \left(\frac{\alpha_s}{\pi}\right)^2 A_q^{(2)} + \dots, \tag{7.12}$$

with [93]

$$A_q^{(1)} = C_F, \quad A_q^{(2)} = \frac{1}{2} C_F \left[C_A \left(\frac{67}{18} - \frac{\pi^2}{6} \right) - \frac{5}{9} N_f \right]. \tag{7.13}$$

The first term in Eq. (7.11) does not originate from soft-gluon emission but instead mostly contains hard virtual corrections. It is also a perturbative series in α_s, and we need only its first-order term:

$$C_q = \frac{\alpha_s}{\pi} C_F \left(-4 + \frac{2\pi^2}{3} + \frac{3}{2} \ln \frac{Q^2}{\mu^2} \right) + \mathcal{O}(\alpha_s^2), \tag{7.14}$$

whose exponentiated form is given in Ref. [94].

Since the running coupling $\alpha_s(k_\perp)$ diverges at $k_\perp = \lambda_{\text{QCD}}$, Eq. (7.11) is ill-defined for arbitrary values of N. However, the singularities turn out to be subleading in the invariant mass Q [95]. To NLL, Eq. (7.11) can therefore be simplified and brought into an infrared safe form. To this end, we use that to NLL accuracy it holds [14]

$$\zeta^{N-1} - 1 \simeq -\theta\left(1 - \zeta - \frac{1}{\bar{N}}\right), \tag{7.15}$$

where $\bar{N} = N e^{\gamma_E}$. The two integrals in the resummed formula can easily be interchanged,

$$\int_0^1 d\zeta \int_{\mu^2}^{(1-\zeta)^2 Q^2} dk_\perp^2 \ldots \longrightarrow \int_{\mu^2}^{Q^2} dk_\perp^2 \int_0^1 d\zeta \ldots$$

$$- \int_0^{Q^2} dk_\perp^2 \int_{1-\sqrt{\frac{k_\perp^2}{Q^2}}}^1 d\zeta \ldots, \tag{7.16}$$

and after performing the trivial ζ integral one finds for the second term in Eq. (7.11)

$$2 \int_{Q^2/\bar{N}^2}^{Q^2} \frac{dk_\perp^2}{k_\perp^2} A_q(\alpha_s(k_\perp)) \ln \frac{\bar{N} k_\perp}{Q} + 2 \int_{Q^2}^{\mu^2} \frac{dk_\perp^2}{k_\perp^2} A_q(\alpha_s(k_\perp)) \ln \bar{N}. \tag{7.17}$$

The remaining integral in $k_\perp$ can be performed analytically by making use of the two-loop expansion of the running coupling $\alpha_s(k_\perp)$ in terms of the running coupling at momentum scale μ (c.f. Eq. (2.32)),

$$\alpha_s(k_\perp) = \frac{\alpha_s(\mu)}{1 + b_0 \alpha_s(\mu) \ln \frac{k_\perp^2}{\mu^2}} \left[1 - \frac{b_1}{b_0} \frac{\alpha_s(\mu) \ln\left(1 + b_0 \alpha_s(\mu) \ln \frac{k_\perp^2}{\mu^2}\right)}{1 + b_0 \alpha_s(\mu) \ln \frac{k_\perp^2}{\mu^2}} + \ldots\right], \tag{7.18}$$

where the coefficients b_0 and b_1 are

$$b_0 = \frac{\beta_0}{4\pi} = \frac{1}{12\pi}(11 C_A - 2 N_f), \quad b_1 = \frac{\beta_1}{(4\pi)^2} = \frac{1}{24\pi^2}(17 C_A^2 - 5 C_A N_f - 3 C_F N_f). \tag{7.19}$$

The entire resummed exponent can then be brought into the form [96, 97],

$$\ln \omega_{q\bar{q}}^N = C_q + 2 h^{(1)}(\lambda) \ln \bar{N} + 2 h^{(2)}\left(\lambda, \frac{Q^2}{\mu^2}\right), \tag{7.20}$$

where

$$\lambda = b_0 \alpha_s(\mu) \ln \bar{N}. \tag{7.21}$$

The functions $h^{(1)}$, $h^{(2)}$ collect all LL and NLL terms in the exponent, which are of the form $\alpha_s^k \ln^{k+1} \bar{N}$ and $\alpha_s^k \ln^k \bar{N}$, respectively. They read

$$h^{(1)}(\lambda) = \frac{A_q^{(1)}}{2\pi b_0 \lambda}\left[2\lambda + (1 - 2\lambda)\ln(1 - 2\lambda)\right], \tag{7.22}$$

$$h^{(2)}\left(\lambda, \frac{Q^2}{\mu^2}\right) = -\frac{A_q^{(2)}}{2\pi^2 b_0^2}\left[2\lambda + \ln(1 - 2\lambda)\right] + \frac{A_q^{(1)} b_1}{2\pi b_0^3}\left[2\lambda + \ln(1 - 2\lambda) + \frac{1}{2}\ln^2(1 - 2\lambda)\right]$$

$$+ \frac{A_q^{(1)}}{2\pi b_0}\left[2\lambda + \ln(1 - 2\lambda)\right]\ln \frac{Q^2}{\mu^2} - \frac{A_q^{(1)} \alpha_s(\mu)}{\pi}\ln(\bar{N})\ln \frac{Q^2}{\mu^2}. \tag{7.23}$$

The last term of the function $h^{(2)}$ depends on the factorization scale and compensates the evolution of the PDFs. The scale dependence of the second-to-last term results from the running of the strong coupling constant. Since scale evolution exponentiates and is therefore taken into account to all orders, one expects a significant decrease in the scale dependence of the resummed cross section compared to a fixed order cross section (For example, see Refs. [98–102]).

The scale dependence can even further be reduced by taking into account certain subleading terms in the resummation [103–105]. Let us first rewrite Eqs. (7.20)-(7.23) as

$$
\ln \omega_{q\bar{q}}^N = \frac{1}{\pi b_0} \left[2\lambda + \ln(1 - 2\lambda)\right] \left(\frac{A_q^{(1)}}{b_0 \alpha_s(\mu)} - \frac{A_q^{(2)}}{\pi b_0} + \frac{A_q^{(1)} b_1}{b_0^2} + A_q^{(1)} \ln \frac{Q^2}{\mu^2} \right)
$$
$$
+ \frac{\alpha_s(\mu)}{\pi} C_F \left(-4 + \frac{2\pi^2}{3} \right) + \frac{A_q^{(1)} b_1}{2\pi b_0^3} \ln^2(1 - 2\lambda) + B_q^{(1)} \frac{\ln(1 - 2\lambda)}{\pi b_0}
$$
$$
+ \left[-2 A_q^{(1)} \ln \bar{N} - B_q^{(1)} \right] \left(\frac{\alpha_s(\mu)}{\pi} \ln \frac{Q^2}{\mu^2} + \frac{\ln(1 - 2\lambda)}{\pi b_0} \right), \tag{7.24}
$$

where $B_q^{(1)} = -3 C_F/2$. The last term in Eq. (7.24) can be identified as the LL expansion of the integral

$$
\int_{\mu^2}^{Q^2/\bar{N}^2} \frac{\mathrm{d}k_\perp^2}{k_\perp^2} \frac{\alpha_s(k_\perp)}{\pi} [-2 A_q^{(1)} \ln \bar{N} - B_q^{(1)}]. \tag{7.25}
$$

The term in square brackets is the leading term in the large-N limit of the anomalous dimension of the one-loop diagonal ($q \to q$) splitting function P_{qq}^N, i.e. it governs the evolution of the parton distributions between scales μ and $Q/\bar{N}$. To improve the scale dependence of the resummed formula we replace it by the full flavor nonsinglet LO splitting function [103, 104]

$$
[-2 A_q^{(1)} \ln \bar{N} - B_q^{(1)}] \to C_F \left[\frac{3}{2} - 2 S_1(N) + \frac{1}{N(N + 1)} \right], \tag{7.26}
$$

which entirely reproduces the diagonal part of the quark and antiquark evolution. We could also include a non-diagonal contribution from $g \to q$ splitting, corresponding to singlet mixing. However, this contribution turns out to be numerically unimportant for the Drell-Yan process in fixed-target kinematics.

The resummed exponent to NLL in Eq. (7.20) still exhibits singularities due to the terms proportional to $\ln(1 - 2\lambda)$. The singularity at

$$
N = \exp\left(\frac{1}{2 b_0 \alpha_s} - \gamma_E \right) \equiv N_L \tag{7.27}
$$

is referred to as Landau pole. When performing the Mellin inversion, special care has to be taken of this pole and the associated branch cut on the real axis for $N > N_L$. However, before we turn to the inverse transformation of the cross section, let us first consider resummation of the rapidity distribution of the Drell-Yan process.

7.3. NLL Resummation for the rapidity-differential Cross Section $\mathrm{d}\sigma/\mathrm{d}Q^2\mathrm{d}\eta$

For rapidity-differential cross sections it is more involved to derive resummed formulae. The reason for that is the additional degree of freedom, which is not integrated over in the phase-space integral and leaves us with one more delta function in Eq. (7.2). While in the rapidity-integrated case a Mellin transform is sufficient to factorize the phase-space integrals for multiple soft-gluon emission, an additional Fourier transform has to be applied for the rapidity-differential cross section.[1] This method of doubly transforming the hadronic cross section was developed and applied in Ref. [107] to the resummation of large logarithms in prompt-photon production. Later the method was successfully adopted to the production of W-bosons [108], which is in large part equivalent to Drell-Yan lepton pair production.

Let us first recall the hadronic rapidity-differential cross section for the Drell-Yan process from Eq. (5.14)

$$\frac{\mathrm{d}\sigma}{\mathrm{d}Q^2\mathrm{d}\eta} = \sigma_0 \sum_{a,b} \int_{x_1^0}^1 \frac{\mathrm{d}x_1}{x_1} \int_{x_2^0}^1 \frac{\mathrm{d}x_2}{x_2} f_a^{H_1}(x_1,\mu^2) e_{ab}\bar{\omega}_{ab}\left(x_1,x_1^0,x_2,x_2^0,\frac{Q}{\mu}\right) f_b^{H_2}(x_2,\mu^2).$$

(7.28)

As mentioned above, to factorize the multiple-gluon phase space, we apply a Mellin transform in τ and, additionally, a Fourier transform in the rapidity η to the hadronic cross section [108],

$$\sigma(N,M) \equiv \int_0^1 \mathrm{d}\tau\,\tau^{N-1} \int_{-\ln\frac{1}{\sqrt{\tau}}}^{\ln\frac{1}{\sqrt{\tau}}} \mathrm{d}\eta\, e^{iM\eta} \frac{\mathrm{d}\sigma}{\mathrm{d}Q^2\mathrm{d}\eta}.$$

(7.29)

We define the double transform of the partonic hard-scattering functions as

$$\tilde{\omega}_{ab}(N,M) \equiv \int_0^1 \mathrm{d}z\,z^{N-1} \int_{-\ln\frac{1}{\sqrt{z}}}^{\ln\frac{1}{\sqrt{z}}} \mathrm{d}\hat{\eta}\, e^{iM\hat{\eta}} \bar{\omega}_{ab},$$

(7.30)

where $\hat{\eta} = \eta - \frac{1}{2}\ln(x_1/x_2)$ is the partonic center-of-mass rapidity, and find in analogy to Eq. (7.10) that the hadronic cross section factorizes in Mellin and Fourier space:

$$\sigma(N,M) = \sigma_0 \sum_{a,b} f_a^{H_1,N+i\frac{M}{2}} f_b^{H_2,N-i\frac{M}{2}} e_{ab}\tilde{\omega}_{ab}(N,M).$$

(7.31)

We note that by contrast to Eq. (7.10) the Mellin moments of the PDFs are shifted by $\pm iM/2$.

By means of the Fourier transform, the rapidity dependence of the partonic hard-scattering functions is translated to a dependence on the Fourier 'frequency' M. Let

---

[1] Alternatively, instead of the Fourier transform a second Mellin transform can be used [106].

us explicitly calculate the M-dependence of the partonic cross section to lowest order. To this end, we transform the lowest order contribution to $\bar\omega_{ab}$, namely

$$\bar\omega_{q\bar q}^{(0)} = x_1 x_2 \delta(x_1 - x_1^0)\delta(x_2 - x_2^0). \tag{7.32}$$

By making use of the relations

$$\frac{x_1^0}{x_1} = \sqrt{z}e^{\hat\eta}, \quad \frac{x_2^0}{x_2} = \sqrt{z}e^{-\hat\eta}, \tag{7.33}$$

the Fourier transform of $\bar\omega_{q\bar q}^{(0)}$ is easily calculated:

$$
\begin{aligned}
&\int_{-\ln(1/\sqrt{z})}^{\ln(1/\sqrt{z})} d\hat\eta\, e^{iM\hat\eta} x_1 x_2 \delta(x_1 - x_1^0)\delta(x_2 - x_2^0) \\
&= \int_{-\ln(1/\sqrt{z})}^{\ln(1/\sqrt{z})} d\hat\eta\, e^{iM\hat\eta} \delta(1 - \sqrt{z}e^{\hat\eta})\delta(1 - \sqrt{z}e^{-\hat\eta}) \\
&= \frac{1}{2}\left(e^{iM\ln(1/\sqrt{z})} + e^{-iM\ln(1/\sqrt{z})}\right)\delta(1 - z) \\
&= \cos\left(M\ln(1/\sqrt{z})\right)\delta(1 - z),
\end{aligned} \tag{7.34}
$$

where we appropriately averaged over the two possible solutions for the integral in the second line. The emerging factor $\delta(1-z)$ is just the lowest-order hard-scattering contribution $\omega_{q\bar q}^{(0)}$ in Eq. (5.10) to the rapidity-*integrated* Drell-Yan cross section. Hence, the Fourier transform of the LO rapidity-differential partonic cross section is equal to the LO rapidity-integrated partonic cross section times $\cos\left(M\ln(1/\sqrt{z})\right)$ [108]. The rapidity-dependence is therefore fully contained in the cosine factor.

However, since soft-gluon resummation is achieved near the partonic threshold, we are only interested in the limit $z \to 1$. In this limit the cosine factor is subleading due to the expansion

$$\cos\left(M\ln(1/\sqrt{z})\right) = 1 - \frac{(1-z)^2 M^2}{8} + O((1-z)^4 M^4). \tag{7.35}$$

We can therefore neglect the cosine and state that near the partonic threshold the rapidity dependence of the hard-scattering function vanishes. I.e. the double moment of the LO rapidity-differential hard-scattering function $\bar\omega_{q\bar q}^{(0)}$ is equal to the Mellin transform of its rapidity-integrated counterpart $\omega_{q\bar q}^{(0)}$

$$\tilde\omega_{q\bar q}^{(0)}(N, M) \simeq \omega_{q\bar q}^{(0)N}. \tag{7.36}$$

As was discussed in Refs. [108–110], even at higher orders in perturbation theory the dependence of the double moments of the rapidity-dependent partonic cross section $\tilde\omega_{ab=q\bar q}(N, M)$ on M becomes subleading near threshold, whereas the N-dependence is

identical to that of the rapidity-integrated cross section $\omega_{q\bar{q}}^N$. Therefore the resummed expression for $\tilde{\omega}_{q\bar{q}}(N, M)$ is given by

$$\tilde{\omega}_{q\bar{q}}(N, M) \simeq \omega_{q\bar{q}}^N, \tag{7.37}$$

where $\omega_{q\bar{q}}^N$ is the threshold-resummed expression from Eq. (7.24) for the rapidity-integrated Drell-Yan cross section. Owing to this approximation the partonic hard-scattering function does not at all depend on the rapidity. The hadronic cross section then solely exhibits its dependence on the rapidity through the shifting of the Mellin moments of the PDFs by $\pm iM/2$ in Eq. (7.31).

However, as was shown in Ref. [108], keeping the cosine term in Eq. (7.34) to all orders in $\tilde{\omega}_{q\bar{q}}(N, M)$ slightly more faithfully reproduces the rapidity dependence of the cross section. The resummed cross section may then be written as

$$\tilde{\omega}_{q\bar{q}}(N, M) \simeq \int_0^1 \mathrm{d}z z^{N-1} \cos\left(M \ln(1/\sqrt{z})\right) \omega_{q\bar{q}} = \int_0^1 \mathrm{d}z z^{N-1} \frac{1}{2}\left(z^{iM/2} + z^{-iM/2}\right) \omega_{q\bar{q}}$$
$$= \frac{1}{2}\omega_{q\bar{q}}^{N+iM/2} + \frac{1}{2}\omega_{q\bar{q}}^{N-iM/2}. \tag{7.38}$$

7.4. Inverse Transform

In the previous two sections, we presented threshold-resummed formulae for the Drell-Yan cross section. To this end, we had to make the transition to Mellin moment space and, in case of the rapidity-differential cross section, we additionally applied a Fourier transform. The final step in obtaining a physically measurable cross section on the hadron level is to invert the Mellin and if necessary the Fourier transform. (From now on we only consider the inverse transform of the rapidity-differential cross section. The inversion of the total (rapidity-integrated) cross section is simply obtained by disregarding the integral in M and letting $M = 0$ in the following formula.)

The corresponding inversion of the doubly transformed cross section in Eq. (7.31) is given by

$$\frac{\mathrm{d}\sigma}{\mathrm{d}Q^2 \mathrm{d}\eta} = \int_{-\infty}^{\infty} \frac{\mathrm{d}M}{2\pi} e^{-iM\eta} \int_{C-i\infty}^{C+i\infty} \frac{\mathrm{d}N}{2\pi i} \tau^{-N} \sigma(N, M). \tag{7.39}$$

Since the cross section $\sigma(N, M)$ contains various singularities and branch cuts in the complex plain, special care has to be taken in the choice of the contour in complex Mellin moment space. Usually, the parameter C for the Mellin inversion has to be chosen in such a way that all singularities of the integrand lie to the left of the integration contour. However, the partonic resummed cross section has a Landau singularity at $N = N_L = \exp\left(1/2b_0\alpha_s - \gamma_E\right)$, as a result of the divergence of the running coupling α_s in Eq. (7.11) for $k_\perp \to \Lambda_{\mathrm{QCD}}$. Associated with this pole is a branch cut along the real axis for $N > N_L$. Choosing the integration contour to the right of the Landau pole would therefore
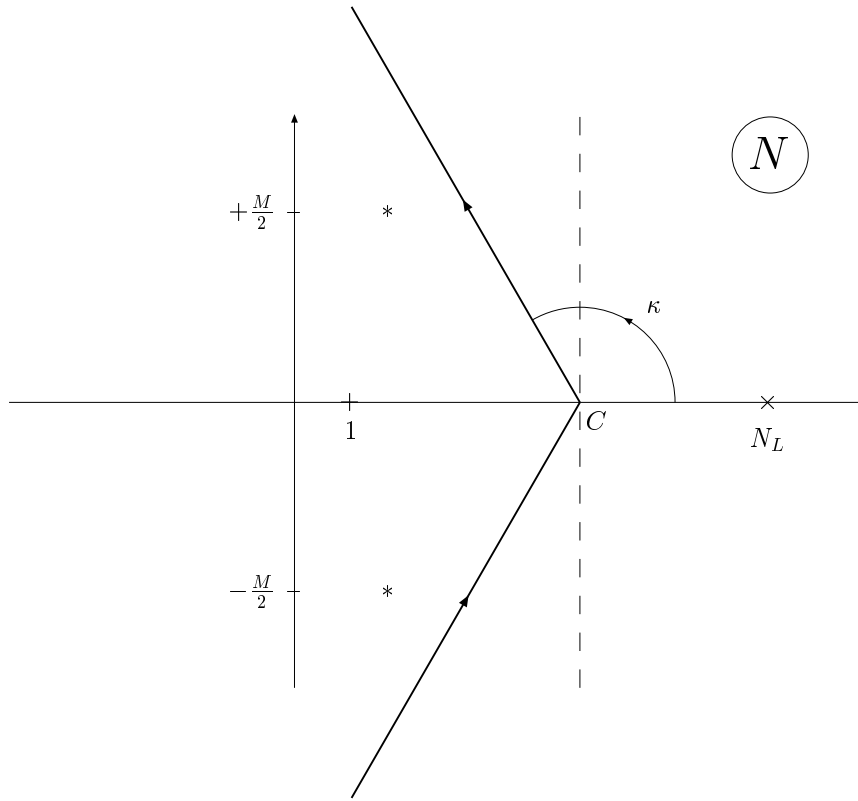
Figure 7.1.: Integration contour for the Mellin inversion in Eq. (7.39). The position of the Landau pole is denoted by N_L and the asterisks denote the positions of the rightmost singularities of the PDFs shifted by $\pm iM/2$. The picture is taken from Ref. [107].

result in passing through the branch cut. Instead, we adopt the *minimal prescription* developed in Ref. [96]. For this prescription the contour is chosen to lie to the *left* of the Landau singularity. In Ref. [96] it is shown that the inverse transform of the perturbative expansion of the resummed cross section converges asymptotically to the minimal prescription formula.[2]

Above and below the real axis, the contour is tilted into the half-plane with negative real part. This improves the convergence of the integration, since contributions with negative real part are exponentially suppressed by the factor τ^{-N} in Eq. (7.39). The distribution functions exhibit moment-space singularities for values of N smaller than $N_P \approx 1$. As

---

[2]We note that an alternative possibility for dealing with the Landau singularity is to perform the resummation directly in z-space [91].

mentioned earlier, these singularities are shifted by $\pm iM/2$ from the real axis due to the Fourier transform. To prevent the tilted contour from passing below or through the PDF singularities we use the parameterization developed in Ref. [107]:

$$N = C + ye^{\pm i\kappa}, \quad 0 \le y < \infty,$$
$$\kappa = \pi - \arctan\left(\frac{C - 1 + M/2}{C - 1}\right). \tag{7.40}$$

The corresponding contour is depicted in Fig. 7.1.

8. Extraction of the Valence PDF of the Pion from Drell-Yan Data

Now that we have presented all the necessary formulae to calculate threshold-resummed Drell-Yan cross sections on the hadron level, we are able to perform a consistent analysis of Drell-Yan data to NLL accuracy. Our focus lies on the determination of the valence PDF of the pion. As already discussed in Sec. 4.3, pionic PDFs mainly extracted from Drell-Yan data seem to be at odds with theoretical predictions. Several fixed-order analyses found a rather hard valence distribution at high momentum fraction x, approximately showing a linear falloff $\sim (1-x)^1$. By contrast, perturbative-QCD counting rules and nonperturbative Dyson-Schwinger equation approaches predict a much faster falloff $\sim (1-x)^2$.

In this chapter, we reanalyze the pionic Drell-Yan data and thereby determine a new valence PDF of the pion. We find that including NLL threshold-resummation effects results in a much softer valence distribution at high momentum fraction x than that found in an NLO analysis. Indeed, our pionic valence PDF agrees very well with the predictions based on perturbative QCD and Dyson-Schwinger equations. The results presented in this chapter were published in Physical Review Letters [111].

8.1. NLL Threshold Resummation vs. Fixed-Order Calculations

Before we present the results of our analysis, let us examine the size of the threshold effects in the kinematic regime of the considered Drell-Yan experiments and discuss to what extend resummation affects the shape of the cross section. To this end, we calculate the Drell-Yan cross section for the generic process

$$\pi^- + p \to \mu^+ + \mu^- + X \tag{8.1}$$

at $\sqrt{S} = 20$ GeV, which is a typical kinematic set-up for a fixed-target experiment. We use the NLO ($\overline{\text{MS}}$-scheme) GRS [10] parton distributions for the negatively charged pion and the NLO ($\overline{\text{MS}}$-scheme) CTEQ6M [5] parton distributions for the proton. We choose the renormalization and factorization scales as equal and set $\mu = Q$. We calculate the rapidity-differential Drell-Yan cross section at fixed-order (LO and NLO), as well as for the NLL-resummed case.
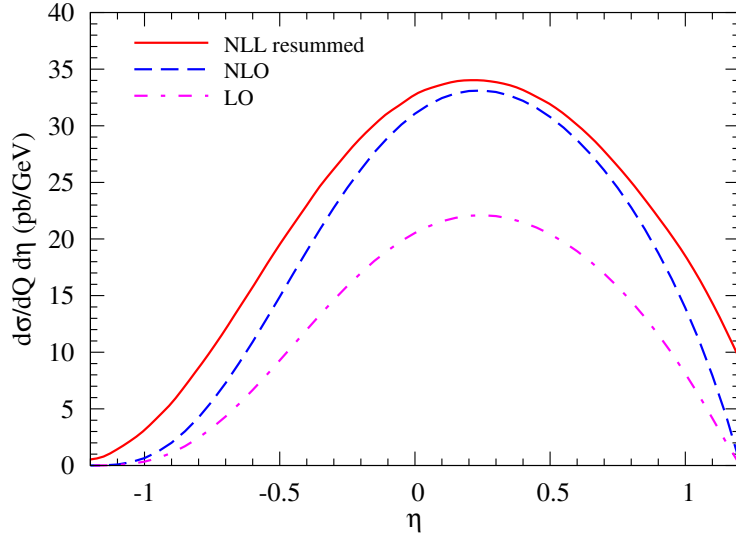
Figure 8.1.: Rapidity-differential Drell-Yan cross section $d\sigma/dQd\eta$ for $\pi^- p$ scattering at $\sqrt{S} = 20$ GeV and $\sqrt{\tau} = 0.3$. The LO, NLO and NLL-resummed cross sections are shown. We use NLO GRS [10] parton distributions for the pion.

When calculating the resummed cross section we want to take into account the full information from the NLO result. For this purpose we match the resummed cross section to the NLO one by subtracting the $\mathcal{O}(\alpha_s)$ expansion of the resummed expression and adding the full NLO cross section [108]. This 'matched' cross section consequently not only resums the large threshold logarithms to all orders, but also contains the full NLO results for the $q\bar{q}$ and qG channels.

In Fig. 8.1 we show the cross section $d\sigma/dQd\eta$ for $\sqrt{\tau} = 0.3$ at LO, NLO and NLL-resummed. At this rather small value of τ the overall enhancement due to resummation compared to NLO seems to be under control. However, the shape of the cross section is still significantly altered. To examine this further we show the ratios

$$K_{\text{res}} = \frac{\left(\dfrac{d\sigma_{\text{res}}}{dQd\eta}\right)}{\left(\dfrac{d\sigma_{\text{LO}}}{dQd\eta}\right)}, \quad K_{\text{NLO}} = \frac{\left(\dfrac{d\sigma_{\text{NLO}}}{dQd\eta}\right)}{\left(\dfrac{d\sigma_{\text{LO}}}{dQd\eta}\right)} \tag{8.2}$$

in Fig. 8.2 as function of the pair rapidity. One can see that K_{res} becomes very large towards the boundaries of the η interval. The resummed cross section particularly shows a sizable enhancement above the NLO one at high rapidities. This enhancement is due to the fact that at fixed τ the limit $\eta \to \eta_{\text{max}}$ corresponds to the limit $z \to 1$ at parton level. In this limit threshold logarithms become large regardless of the value of τ.

Since high rapidities in the fixed-target regime probe high momentum fractions x in the PDFs, including threshold resummation in the analysis of parton distributions has
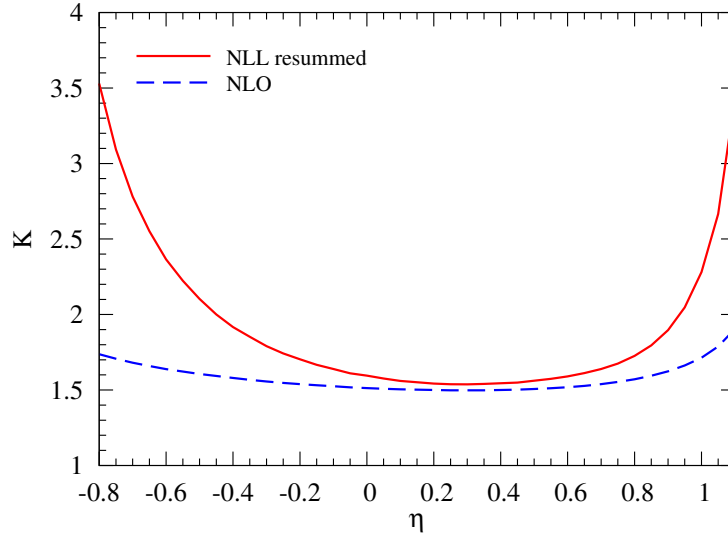
Figure 8.2.: Ratios K_{res} and K_{NLO} as defined in Eq. (8.2) at $\sqrt{S} = 20$ GeV and $\sqrt{\tau} = 0.3$, as function of the rapidity η of the dimuon pair. We use NLO GRS [10] parton distributions for the pion.

significant effects on their extracted high-x behavior. This was recently also examined in the context of deep-inelastic lepton scattering off a proton target [112]. However, in DIS there is only a minor enhancement of the cross section by soft-gluon resummation and therefore the effects on the high-x behavior of the PDFs are not as striking as in case of the Drell-Yan process.

8.2. Fit to Pion Drell-Yan Data

In the following, we outline our fitting procedure for the pionic PDFs. The fixed-target pion Drell-Yan data from the Fermilab E615 experiment [8], which we want to analyze, are in a kinematic regime where the probed partons' momentum fractions are relatively large ($x \gtrsim 0.3$). In this regime we expect contributions from the valence quarks to strongly dominate the cross section. Besides, contributions from the gluon distribution enter the Drell-Yan cross section only at NLO and are consequently suppressed by a factor $\alpha_s/2\pi$. The sensitivity of the data is therefore restricted to the pion's valence distribution v^π.

We follow the NLO GRS analysis [10] and choose the initial scale $Q_0 = 0.63$ GeV for the evolution of the PDFs. At this low initial scale we parameterize the valence distribution as

$$xv^\pi(x, Q_0^2) = N_v x^\alpha (1-x)^\beta (1 + \gamma x^\delta), \tag{8.3}$$

where the normalization factor N_v is determined through the valence quark sum rule,

$$\int_0^1 v^\pi(x, Q_0^2)\mathrm{d}x = 1. \tag{8.4}$$

Since the Drell-Yan data hardly constrain the gluon and sea-quark distributions, we adopt their parameterizations from the NLO GRS analysis and do not vary them during the fit:

$$xG^\pi(x, Q_0^2) = 5.90x^{1.270}(1 - 2.074\sqrt{x} + 1.824x)(1 - x)^{1.290},$$
$$x\bar{q}^\pi(x, Q_0^2) = N_{\bar{q}}x^{0.207}(1 - 2.466\sqrt{x} + 3.855x)(1 - x)^{4.454}, \tag{8.5}$$

where it is assumed that the light pion sea is SU(2) flavor-symmetric and the strange quark distribution vanishes at the low input scale Q_0, i.e. $\bar{q}^\pi = u^{\pi^-} = \bar{u}^{\pi^+} = d^{\pi^+} = \bar{d}^{\pi^-}$ and $s^\pi = \bar{s}^\pi = 0$. When we vary the free parameters in Eq. (8.3), the sea-quark normalization factor $N_{\bar{q}}$ is adjusted in such a way that the momentum sum rule is always fulfilled:

$$\int_0^1 x(2v^\pi(x, Q_0^2) + 4\bar{q}^\pi(x, Q_0^2) + G^\pi(x, Q_0^2))\mathrm{d}x = 1. \tag{8.6}$$

All distributions are evolved to the factorization scale, which we again choose as $\mu = Q$, using NLO QCD evolution kernels. The resummed hadronic cross section is then calculated as in Eq. (7.39), matched to the full NLO cross section, and compared to the experimental data.

The E615 data were obtained by using a 252 GeV π^- beam on a tungsten target. The probed partons either stem from a proton or a neutron in a tungsten nucleus. We use isospin symmetry to express the parton content in the neutron in terms of the proton's PDFs,

$$d^n(x) = u^p(x), \quad u^n(x) = d^p(x), \quad s^n(x) = s^p(x),\ldots. \tag{8.7}$$

We take into account the nuclear effects in this heavy target by using the nuclear PDFs from the global analysis in Ref. [113]. The distribution function $f_a^{p,A}$ of a proton bound in a nucleus of mass number A is then related to the PDF of a free proton f_a^p by

$$f_a^{p,A}(x, \mu^2) = R_a(x, \mu^2, A)f_a^p(x, \mu^2), \tag{8.8}$$

where $R_a(x, Q^2, A)$ is a multiplicative nuclear correction factor. Consequently, the average distribution of a parton a per nucleon in a nucleus N with mass number A and proton number Z is given by

$$f_a^N(x, \mu^2) = \frac{Z}{A}R_a(x, \mu^2, A)f_a^p(x, \mu^2) + \left(1 - \frac{Z}{A}\right)R_a(x, \mu^2, A)f_a^n(x, \mu^2). \tag{8.9}$$

We use the average distribution f_a^W for tungsten to calculate the Drell-Yan cross section per nucleon in the target.

Table 8.1.: Results for our NLL threshold-resummed fits to the Fermilab E615 Drell-Yan data [8].

Fit	$2\langle xv^\pi\rangle$	α	β	γ	K	χ^2 (no. of points)
1	0.55	0.15 ± 0.04	1.75 ± 0.04	89.4	0.999 ± 0.011	82.8 (70)
2	0.60	0.44 ± 0.07	1.93 ± 0.03	25.5	0.968 ± 0.011	80.9 (70)
3	0.65	0.70 ± 0.07	2.03 ± 0.06	13.8	0.919 ± 0.009	80.1 (70)
4	0.7	1.06 ± 0.05	2.12 ± 0.06	6.7	0.868 ± 0.009	81.0 (70)

We consider data points with lepton pair mass in the range $4.03 \text{ GeV} \leq Q \leq 8.53 \text{ GeV}$, between the J/Ψ and Υ resonances. This corresponds to $0.185 < \sqrt{\tau} < 0.392$. Due to possible reinteraction effects we reject data points with $x_F < 0$ (see Ref. [9]). Here, x_F is the Feynman variable. Besides, we discard bins with $x_F > 0.8$ resulting in a total number of 70 bins considered in our fit. As the data in the Fermilab E615 experiment was binned in terms of the Feynman variable x_F, we accordingly have to transform the rapidity-differential cross section. Soft-gluon resummation primarily addresses the near-threshold region $z \to 1$. In this particular region the kinematics are very similar to LO, where $z = 1$. We can therefore use lowest-order kinematics to determine the relation between x_F and η,

$$x_F = x_1^0 - x_2^0 = \frac{Q}{\sqrt{S}} \left(e^\eta - e^{-\eta} \right) = 2\sqrt{\tau} \sinh(\eta), \tag{8.10}$$

which yields for the cross section

$$\frac{\mathrm{d}\sigma}{\mathrm{d}Q^2 \mathrm{d}x_F} = \frac{\mathrm{d}\sigma}{\mathrm{d}Q^2 \mathrm{d}\eta} \frac{1}{\sqrt{4\tau + x_F^2}}. \tag{8.11}$$

Since the E615 data have a nominal overall systematic error of 16%, we introduce a normalization factor K that multiplies the theoretical cross section. In fixed-order analyses such a K-factor is usually introduced to account for higher-order QCD corrections. Leading-order studies find for the E615 Drell-Yan data $K \lesssim 2$ [8, 11, 114]. At NLO the K-factor is substantially reduced but usually still larger than one [9, 11]. By means of threshold resummation, we take into account dominant higher order corrections to all orders in perturbation theory. We therefore expect that the K-factor in our analysis only corrects for the overall systematic uncertainty of the data and not for higher-order QCD effects.

We now choose some initial values for the parameters in Eq. (8.3) evolve the PDFs and evaluate the resummed cross section. To compare the theoretical cross section σ^{theo} with the measured cross section σ^{data} and estimate the quality of the parameterization we calculate

$$\chi^2 = \sum_{i=1}^{70} \left(\frac{K\sigma_i^{\text{theo}} - \sigma_i^{\text{data}}}{\Delta\sigma_i^{\text{data}}} \right)^2, \tag{8.12}$$
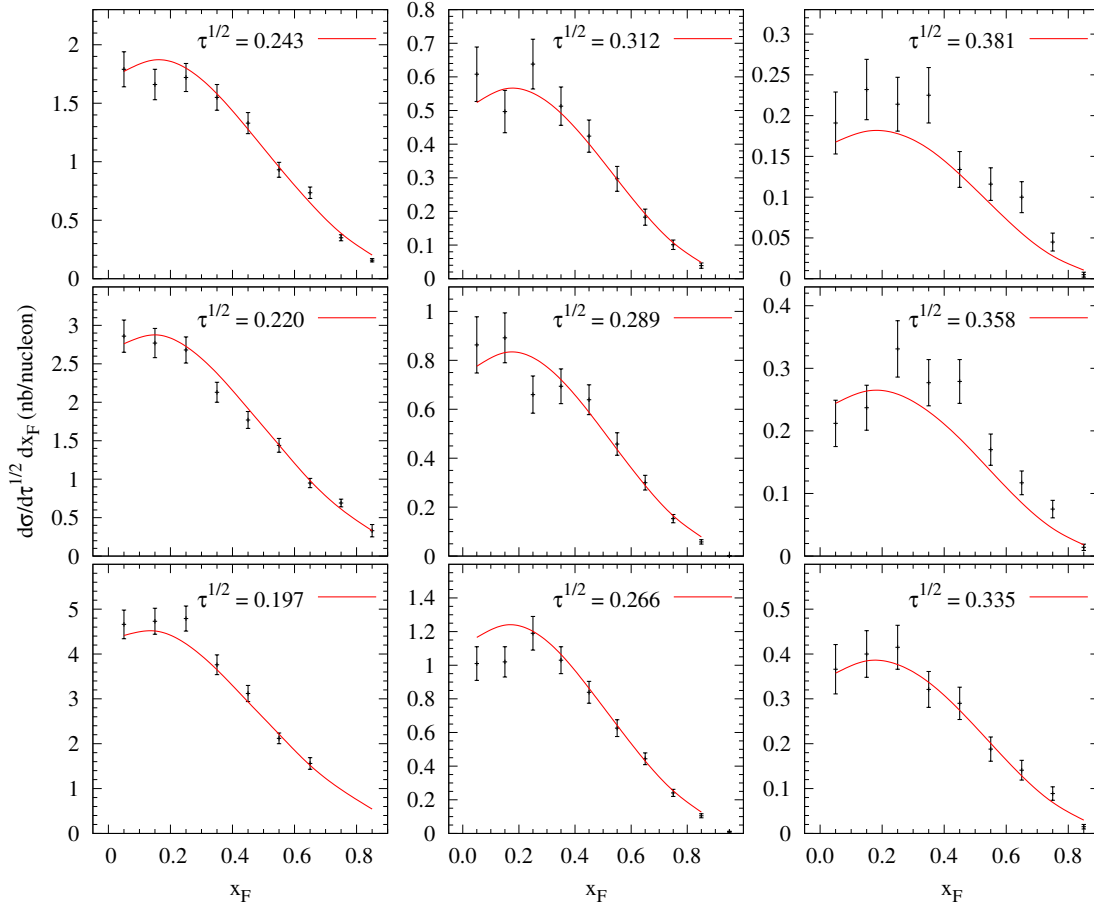
Figure 8.3.: Comparison of our NLL-resummed Drell-Yan cross section based on fit 3 to
the E615 Drell-Yan data.

where the sum runs over all considered data bins and $\Delta\sigma_i^{\text{data}}$ denotes the statistical error of
the respective bin. By repeating this procedure several times and thereby minimizing χ^2,
we find an optimized set of parameters for the valence distribution of the pion. However,
in our analysis it turns out that the experimental data is not equally sensitive to all
parameters in Eq. (8.3). Particularly the parameter δ is not well determined within the
range $1.5 \leq \delta \leq 2.5$. Allowing δ to freely vary has only marginal effects on the obtained
minimal value of χ^2. Hence, we fix it to $\delta = 2$, a value roughly preferred by the fit.
According to the overall systematic error of 16% of the E615 data we allow the K-factor
to vary between $0.84 < K < 1.16$. However, we find that the value of the K-factor is
strongly correlated with the second moment of the pionic valence distribution, i.e. its
total momentum fraction,

$$\langle xv^\pi \rangle = \int_0^1 xv^\pi(x, Q_0^2)\mathrm{d}x. \tag{8.13}$$
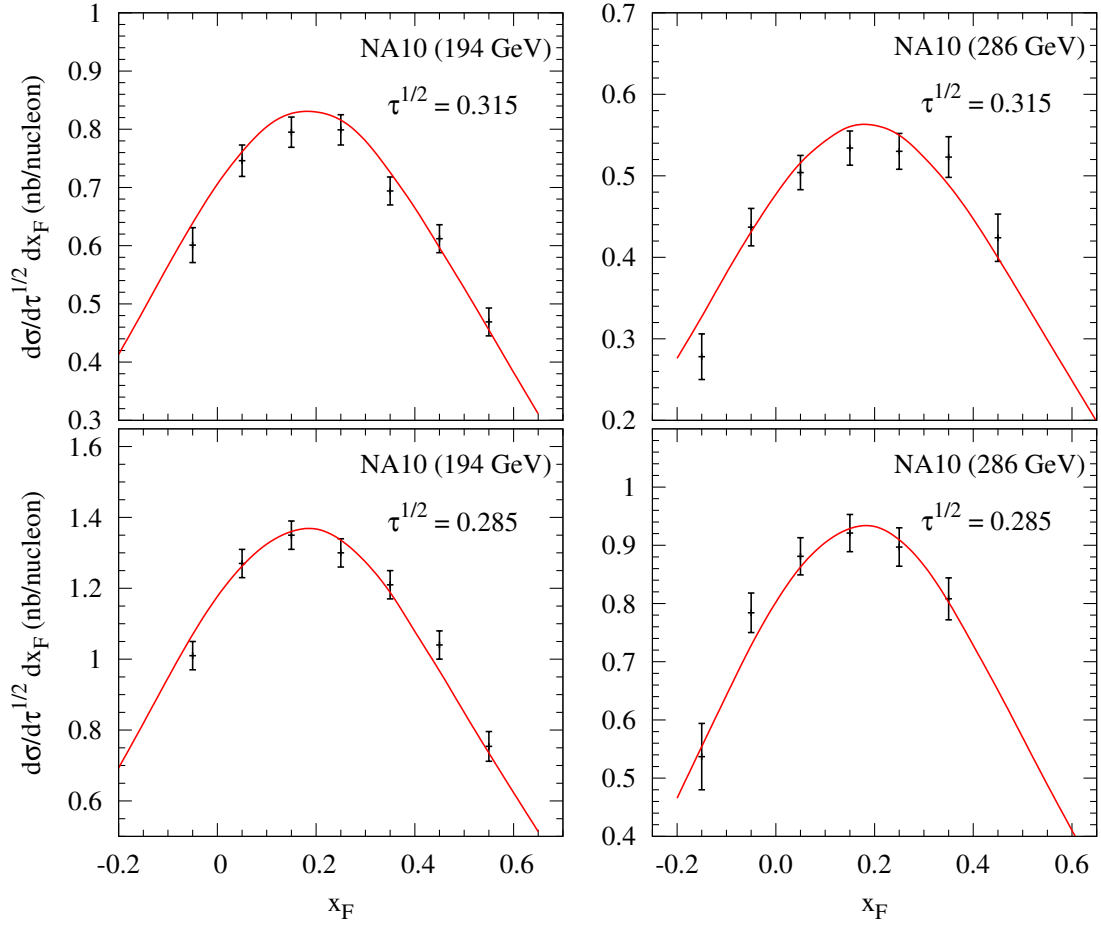
Figure 8.4.: Comparison of our resummed cross section for fit 3 to some of the CERN NA10 $\pi^- W$ data [57] at pion beam energy 194 GeV (left) and 286 GeV (right). The theoretical cross sections are multiplied by normalization factors $K_{194} = 1.045$ (left) and $K_{286} = 1.108$ (right).

We therefore perform several fits for different fixed values of $\langle xv^\pi \rangle$. Fixing the total momentum fraction of the valence distribution makes one parameter in Eq. (8.3) redundant, which we choose to be γ.

The remaining three parameters α, β and K are fitted to the 70 data points. The results are shown in Table 8.1, for four different values of the total valence quark momentum fraction $2\langle xv^\pi \rangle$. One observes that fit 3 for which the valence distribution carries 65% of the pion's momentum is preferred. Fit 2 and fit 4 with slightly higher and lower values of $2\langle xv^\pi \rangle$ are also well acceptable with an increase of the minimal χ^2 by only one unit. The most important result of our analysis is that all fits show a clear preference for a falloff much softer than linear, with fits 2, 3, and 4 having a value of β very close to 2. The values of the K-factor vary from $K = 0.999$ to $K = 0.868$ and lie well within the
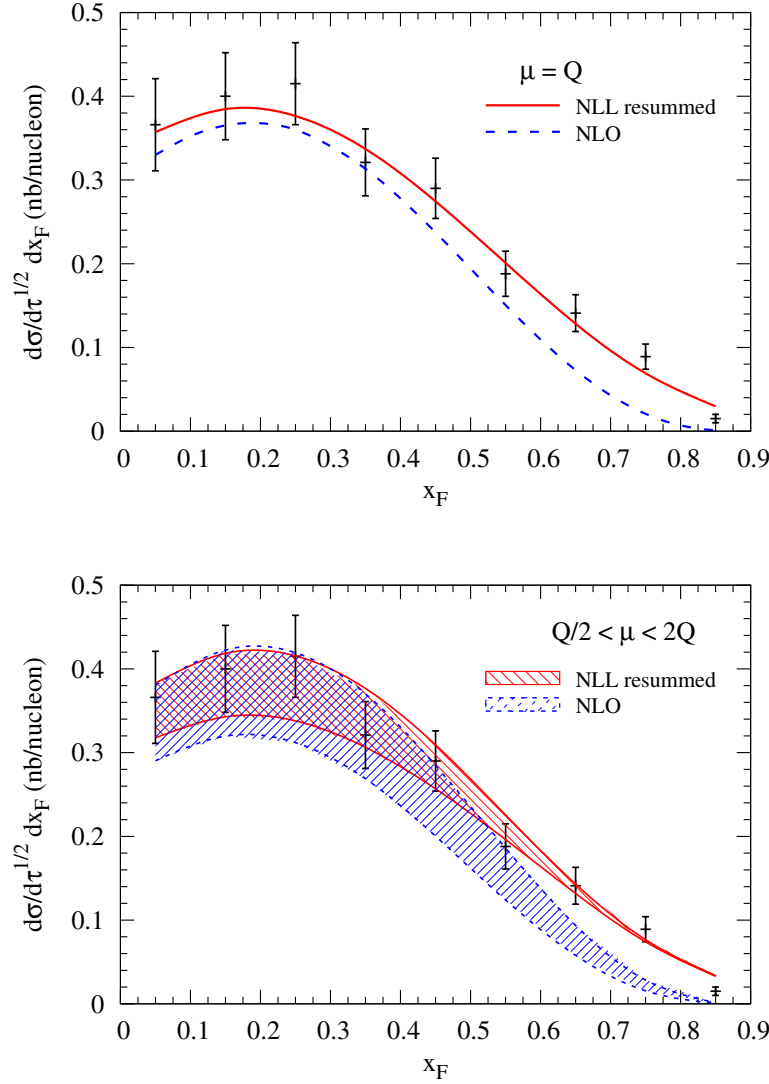
Figure 8.5.: NLL-resummed and NLO cross sections based on fit 3 compared to some of
           the E615 Drell-Yan data at $\sqrt{\tau} = 0.335$. The upper plot shows the cross
           sections with renormalization and factorization scale $\mu = Q$. The lower plot
           shows the uncertainty bands when varying the scale between $Q/2$ and $2Q$.

systematic normalization uncertainty of the data. We compare the NLL-resummed cross
section for fit 3 to the E615 data in Fig. 8.3. The theoretical cross section is multiplied
by the factor $K = 0.919$ obtained from the fit. To check our analysis for consistency with
Drell-Yan data, which were not included in our fit, we compare our resummed cross section
based on fit 3 to some of the CERN NA10 [57] $\pi^- W$ Drell-Yan data in Fig. 8.4. Again
owing to the overall systematic error of the data we have multiplied the cross section by a
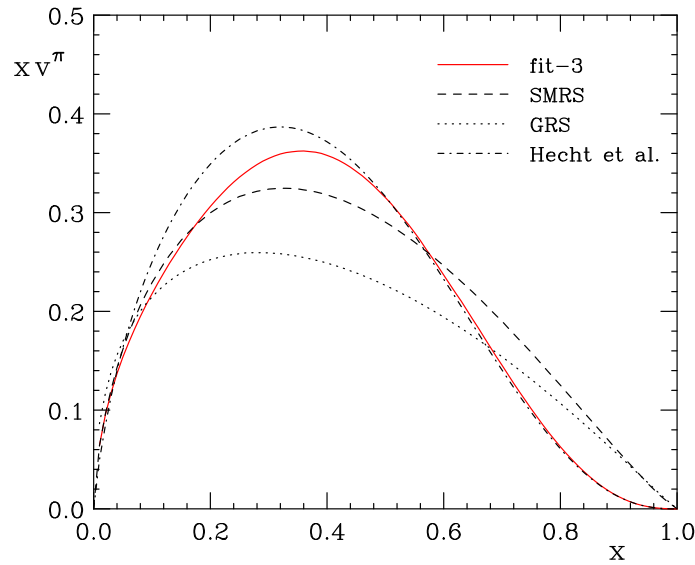
Figure 8.6.: The pionic valence (v^π) distribution obtained from our fit 3 to the E615 Drell-Yan data at $\mu = 4$ GeV, compared to the NLO parameterizations of [9] (SMRS) and [10] (GRS) and to the distribution obtained from Dyson-Schwinger equations [63] (Hecht et al.).

normalization factor. As one can see, the data are very well described for both pion beam energies used in the NA10 experiment.

The main theoretical uncertainty in our analysis comes from the dependence of the calculated cross section on the renormalization and factorization scale. However, inclusion of higher-order QCD corrections to the cross section reduces this scale ambiguity. We make this clear in Fig. 8.5, where we show NLL-resummed cross sections and NLO cross sections at $\mu = Q$ and the corresponding uncertainty bands when varying the scale between $\mu = Q/2$ and $\mu = 2Q$. The cross sections are evaluated at $\sqrt{\tau} = 0.335$ using the pion PDFs from fit 3. Also shown are the corresponding E615 Drell-Yan data. Since, as discussed earlier, at moderate values of τ threshold resummation particularly enhances the cross section at high rapidities and hence high x_F, the NLO cross section falls off too rapidly to describe the data. As one can see the scale uncertainty is significantly reduced after resummation and becomes smaller than the statistical uncertainty of the experimental data. In fact, at high x_F the scale dependence almost vanishes. This implies that our findings for the pion's valence distribution are stable with respect to the main theoretical uncertainty in the calculation. In the next section on phenomenological predictions for the COMPASS Drell-Yan experiment at CERN, we will come back to this point and examine the scale dependence of the resummed cross section over the whole range of τ.

Let us now compare our results for the pionic parton distributions to those from earlier
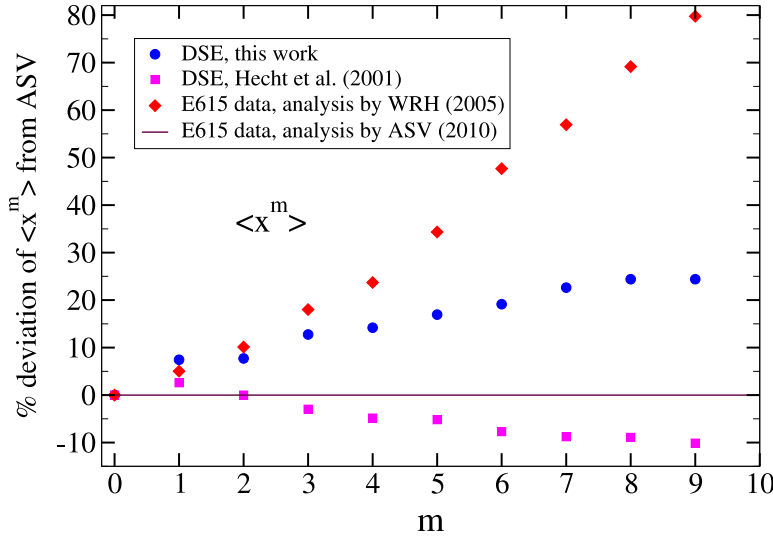
Figure 8.7.: Moments of pion valence distributions v^π at scale $\mu = 5.2$ GeV as deviation from results for our preferred fit (ASV). Included are the valence distributions from the calculations based on Dyson-Schwinger equations by Nguyen *et al.* ('DSE', circles) and Hecht *et al.* [63] ('DSE', squares) as well as the NLO analysis in Ref. [11] ('WRH', diamonds). The figure is taken from Ref. [64].

analyses. We therefore show the valence distribution xv^π for our best fit 3 in Fig. 8.6, evolved to $\mu = 4$ GeV. At this momentum scale it behaves as $(1-x)^{2.34}$ at high x. Valence distributions obtained from previous NLO analyses [9, 10], which have a roughly linear behavior at high x, and from calculations using Dyson-Schwinger equations [63], for which $v^\pi \sim (1-x)^{2.4}$, are also shown. Apparently our analysis yields a considerably softer valence distribution at high momentum fraction x than previous NLO analyses. Indeed, it agrees very well with the result from Dyson-Schwinger equations. Although not shown in the figure, the high-x behavior of our valence distribution is also in line with predictions from perturbative QCD, for which the falloff is expected to be $\sim (1-x)^{2+\gamma}$ with $\gamma \gtrsim 0$. Recently a new analysis of pion and kaon valence PDFs based on a rainbow-ladder truncation of Dyson-Schwinger equations was performed by Nguyen *et al.* [64]. Their obtained valence distribution for the pion is also in very good agreement with our preferred fit. Beside the functional form they also considered moments of the pion valence distributions, which are compared to our results in Fig. 8.7. As one can see the moments of our preferred valence distribution lie between the results from the two different Dyson-Schwinger equation approaches by Hecht *et al.* and Nguyen *et al.*.

To summarize, we find that a valence distribution with a fall-off $\sim (1-x)^2$ predicted by perturbative QCD and Dyson-Schwinger equation approaches is in fact well consistent with the Drell-Yan data, if large logarithmic contributions near the partonic threshold are resummed to all orders. Resummation also significantly reduces the main theoretical uncertainty, namely the dependence of the cross section on the renormalization and factorization scale. Indeed, the uncertainty due to the scale ambiguity in our NLL-resummed analysis is even smaller than the statistical error of the considered Drell-Yan data. However, as can be seen in Table 8.1 the available pionic Drell-Yan data are not able to completely determine the valence parton distribution of the pion. The data are almost equally well described by fits 2, 3 and 4 with a valence distribution that carries 60 %, 65 % and 70 % of the pion's momentum at the input scale $Q_0 = 0.63$ GeV, respectively. The quality of the three fits only differs by about one unit in χ^2. This uncertainty in the valence momentum is also manifest in earlier NLO analyses of the E615 and NA10 data. For example, at $Q = 2$ GeV the valence parton distribution of SMRS [9] carries 46 % of the pion's momentum, whereas the valence distribution of GRS [10] carries only 40 %, although both distributions describe the same data sets equally well. We find that the value of the total valence quark momentum fraction $2\langle xv^\pi \rangle$ is strongly correlated with the K-factor which multiplies the theoretical cross section and accounts for the large overall systematic uncertainties of the Drell-Yan data. Pion Drell-Yan data with a well understood normalization could make the inclusion of a K-factor in the analysis redundant and enable us to really pin down the pion's valence distribution. We hope that the upcoming fixed-target πN Drell-Yan experiment at COMPASS [115] will provide such urgently needed data and will resolve this issue. In the following section, we will therefore make predictions for the Drell-Yan cross section at COMPASS and study the significance of threshold-resummation effects in the kinematic regime of that experiment.

8.3. Phenomenological Predictions for COMPASS Kinematics

We present a detailed phenomenological study of both the rapidity-integrated and rapidity-differential Drell-Yan cross section for the kinematics relevant at COMPASS. In the light of our analysis of fixed-target Drell-Yan data in the previous section, we expect that the resummation of threshold logarithms also plays a significant role for the Drell-Yan cross section at COMPASS. The significance of threshold resummation in the Drell-Yan process has also been examined in numerous earlier phenomenological applications [91, 108, 110, 116–119], both for fixed-target and for collider energies. Our results, which we present in the following, were published in Ref. [120].

The π^- beam foreseen at COMPASS has an energy of 190 GeV. The pions are scattered off a proton target at rest, so that the resulting center-of-mass energy of the system is
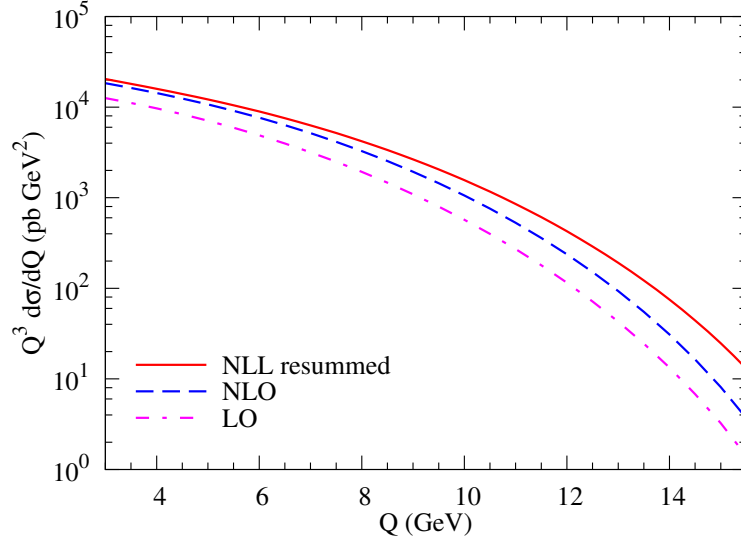
Figure 8.8.: Rapidity-integrated Drell-Yan cross section $Q^3 \mathrm{d}\sigma/\mathrm{d}Q$ for $\pi^- \, p$ scattering at $\sqrt{S} = 19$ GeV, at LO, NLO and NLL-resummed, as a function of the invariant mass Q of the lepton pair.

$\sqrt{S} \approx 19$ GeV. For the pionic PDFs we use the ones for the preferred fit in the previous section ('fit 3'). For the proton target we use the NLO ($\overline{\mathrm{MS}}$ scheme) CTEQ6M [5] parton distributions. The cross section is calculated at renormalization and factorization scale $\mu = Q$ unless stated otherwise. Again, we match the resummed cross section to the NLO one to take into account the full information from the NLO result. We will occasionally also consider a resummed cross section that has not been matched to the NLO one. We will refer to such a cross section as 'unmatched'.

We first consider the cross section $\mathrm{d}\sigma/\mathrm{d}Q$ integrated over all rapidities. We do so to show the relevance and the validity of the resummation effects over the whole range of the invariant mass Q. Here, we ignore for simplicity charmonium and bottomonium resonances in the lepton pair spectrum, whose contributions are dominant for resonant invariant masses, and calculate only the smooth (continuum) part of the cross section. Figure 8.8 shows the cross section $Q^3 \mathrm{d}\sigma/\mathrm{d}Q$ at $\sqrt{S} = 19$ GeV at fixed order (LO and NLO), as well as for the NLL-resummed case. It can be seen that the enhancement of the resummed cross section over LO increases strongly with invariant mass Q. This becomes even more apparent in Fig. 8.9, where we show the ratio of the cross section to the LO one:

$$K = \frac{\mathrm{d}\sigma/\mathrm{d}Q}{\mathrm{d}\sigma^{\mathrm{LO}}/\mathrm{d}Q}. \tag{8.14}$$

The ratio is plotted for the NLO and the NLL-resummed result. At high invariant mass Q the resummed cross section exceeds the LO one by an order of magnitude. We also
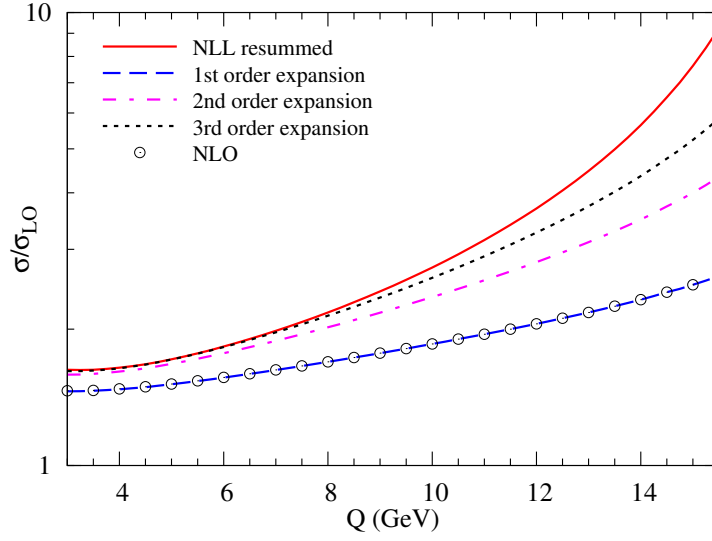
Figure 8.9.: Ratio as defined in Eq. (8.14) at $\sqrt{S} = 19$ GeV as functions of the lepton pair mass Q, at NLO (symbols) and for the NLL-resummed case. Also shown are the expansions of the resummed cross section to first, second and third order in the strong coupling.

expand the unmatched resummed cross section in powers of α_s and show the first, second and third order expansion in Fig. 8.9. One can see that in the fixed-target regime higher orders (beyond NLO) still make significant contributions to the cross section, especially at high invariant mass Q. This confirms that at high Q and hence large $\tau = Q^2/S$ the threshold logarithms indeed compensate the smallness of α_s in the perturbative series. This finding is in line with that in the earlier study in Ref. [116] for $\bar{p}p$-scattering. We also observe that the exact NLO cross section agrees extremely well with the first order expansion of the unmatched resummed result. This demonstrates that the logarithmic contributions from soft-gluon radiation give by far the most important contribution to the cross section, not only very close to threshold as $\tau \to 1$, but also for rather moderate values of τ.

Next, we present the results for the rapidity distributions $d\sigma/dQd\eta$. As mentioned above, charmonium and bottomonium resonances complicate the calculation of Drell-Yan cross sections. Therefore usually only lepton pairs with invariant mass Q between the J/Ψ and Υ resonances and above the Υ are considered. Since the Drell-Yan event rate decreases rapidly with $\sqrt{\tau}$, it may not be possible to measure it accurately above the Υ resonance in the medium-energy fixed-target regime accessed by the COMPASS experiment. We therefore make predictions for $\sqrt{\tau} = 0.3$ and $\sqrt{\tau} = 0.45$, corresponding to $Q = 5.7$ GeV and $Q = 8.6$ GeV, respectively. Our results are presented in Figs. 8.10 and 8.11. Again
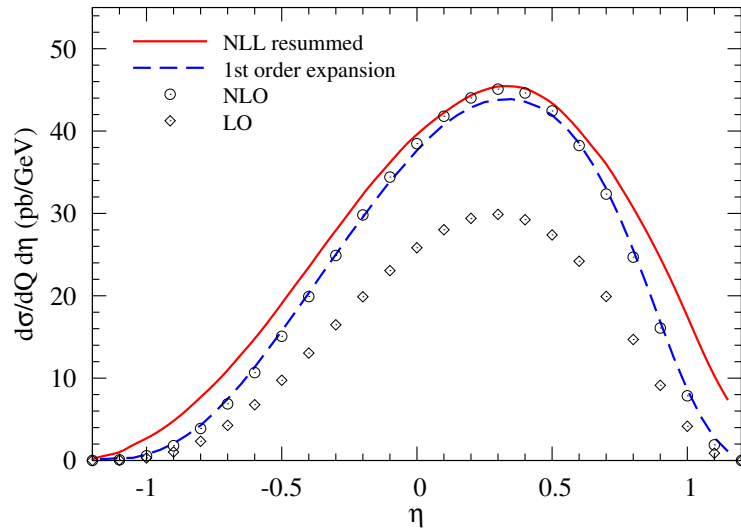
Figure 8.10.: Rapidity-differential Drell-Yan cross section $\mathrm{d}\sigma/\mathrm{d}Q\mathrm{d}\eta$ for $\pi^-\ p$ scattering at $\sqrt{S} = 19$ GeV and $\sqrt{\tau} = 0.3$. The LO, NLO and NLL-resummed cross sections as well as the first order expansion of the unmatched NLL-resummed cross section are shown as functions of the rapidity η of the dimuon pair.
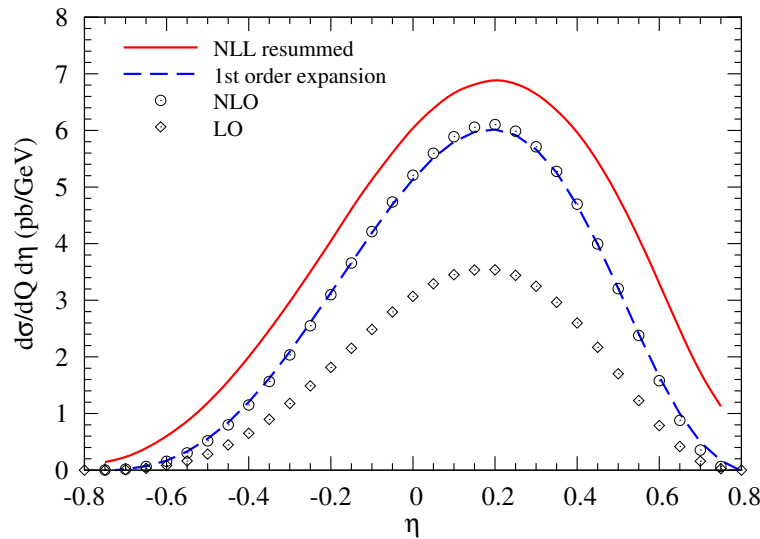

Figure 8.11.: Same as Fig. 8.10, but at $\sqrt{\tau} = 0.45$.

the resummed cross section and the fixed-order NLO and LO ones are shown. As before, we expand the unmatched resummed result in powers of α_s and find that the first order expansion agrees very well with the exact NLO result for $\sqrt{\tau} = 0.45$. For $\sqrt{\tau} = 0.3$, further away from threshold, the first order expansion of the threshold-resummed cross section
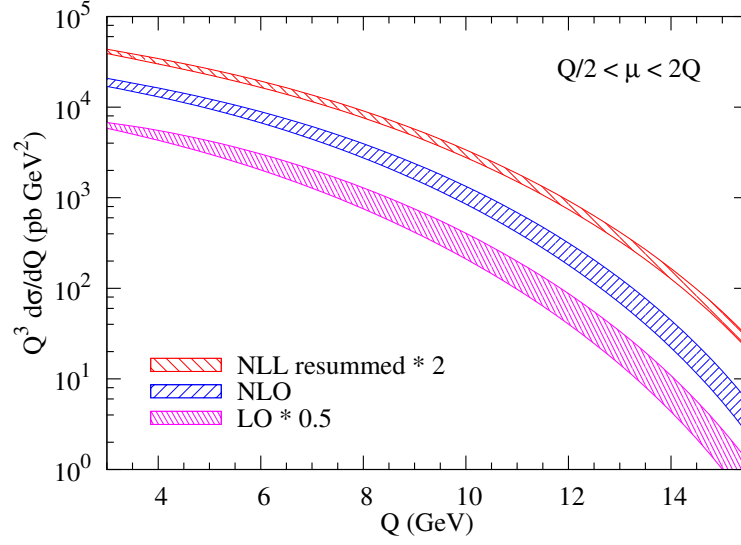
Figure 8.12.: Scale dependence of the LO, NLO and NLL-resummed rapidity-integrated Drell-Yan cross sections at $\sqrt{S} = 19$ GeV as function of Q. The factorization as well as the renormalization scale have been varied between $Q/2$ and $2Q$. Note that we have multiplied the LO cross section by $1/2$ and the resummed cross section by 2.

lies very slightly below the exact NLO result for central rapidities. This is due to the fact that the contributions from the threshold region $z \to 1$ do not entirely dominate the cross section in this rapidity region. As expected from our results in Figs. 8.8 and 8.9, at fixed rapidity the threshold resummation effects become more important as τ increases, resulting in a fairly large enhancement of the resummed cross section at $\sqrt{\tau} = 0.45$. Nevertheless, significant contributions from threshold resummation are still present in the cross section also for relatively modest values of τ.

The crucial quality test for any higher order calculation is the extent to which it reduces the scale ambiguity inherent to any perturbative QCD calculation. We examine the scale dependences of the rapidity-integrated and the rapidity-differential cross sections in Figs. 8.12 and 8.13, respectively. Again we show the LO, NLO and NLL-resummed results at $\sqrt{S} = 19$ GeV, now varying the renormalization and factorization scales between $\mu = Q/2$ and $\mu = 2Q$. Note that in Fig. 8.12 we have for better visibility multiplied the LO cross section by $1/2$ and the resummed one by 2. Evidently for the integrated cross section the scale dependence is decreased by resummation over the whole range of invariant mass Q, whereas going from LO to NLO reduces the scale dependence only marginally. Figure 8.13 shows the scale dependence of the rapidity distributions at $\sqrt{\tau} = 0.45$. Here we only show the NLL-resummed cross section and the NLO one. As one can see, the scale dependence
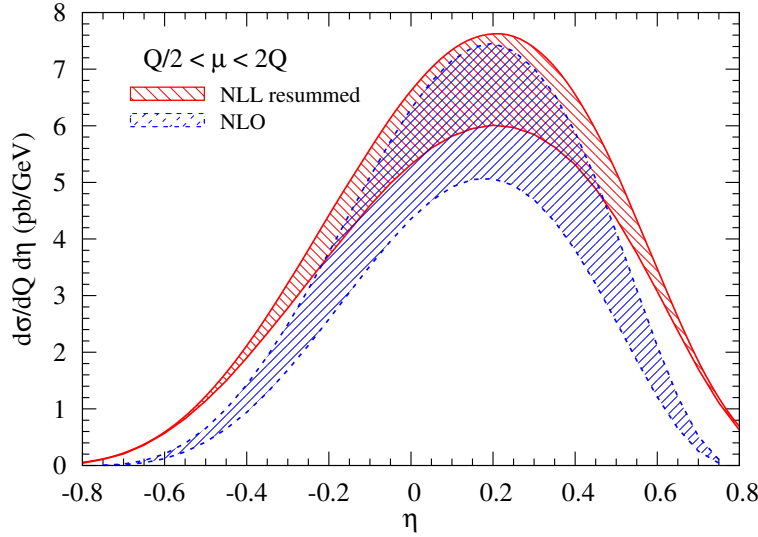
Figure 8.13.: Scale dependence of the NLO and NLL-resummed rapidity-differential Drell-Yan cross sections at $\sqrt{S} = 19$ GeV and $\sqrt{\tau} = 0.45$ as function of η. The factorization as well as the renormalization scale have been varied between $Q/2$ and $2Q$.

is again significantly improved by resummation. This applies to all values of rapidity; in fact the scale dependence almost vanishes at high η after resummation.

All in all, in this phenomenological study we find that threshold resummation has strong effects on the Drell-Yan cross section for pions scattering off a proton target at COMPASS. In fact, it leads to a significant enhancement above fixed-order calculations, even for moderate values of the invariant mass Q of the lepton pair. Another important finding is that the expansion of the resummed cross section to $\mathcal{O}(\alpha_s)$ agrees very well with the exact fixed-order calculation. This agreement demonstrates that the large threshold logarithms indeed make the main contribution to the Drell-Yan cross section and have to be taken into account to all orders. Even in cases where there is only a modest enhancement of the rapidity-integrated cross section, we find the shape of the rapidity-differential cross section to be very strongly affected by resummation at sufficiently large forward or backward rapidities. Finally, we have shown that the scale dependence of the perturbative cross section is substantially reduced when threshold-resummed contributions are included. Our results overall demonstrate that threshold resummation effects will be important in the analysis of future COMPASS data. While we have only addressed the spin-averaged Drell-Yan cross section in this thesis, we stress that threshold resummation effects are expected to be equally relevant also for corresponding spin-dependent cross sections, even though they may have a tendency to cancel in spin asymmetries. We also note that in the light of

our study cross sections and spin asymmetries at measured transverse momentum $q_\perp$ of the lepton pair, which will be a particular focus of the investigations at COMPASS, will require additional theoretical consideration.

Part III.

Single Longitudinal-Spin Asymmetries

9. Time-Reversal-Odd Spin Asymmetries

In this chapter we review some basic facts on single-spin asymmetries for processes involving both transversely and longitudinally polarized particles. We show that single longitudinal-spin asymmetries can originate from naive-time-reversal-odd (T-odd) effects, which arise only at higher orders in perturbation theory. Such T-odd observables can be observed in semi-inclusive deep-inelastic scattering (SIDIS). We schematically derive the leading perturbative contribution to T-odd effects and identify the corresponding Feynman diagrams in SIDIS.

9.1. Single-Spin Asymmetries

A single-spin asymmetry for an arbitrary high-energy scattering process is generally defined as the ratio

$$A = \frac{\frac{1}{2}(\mathrm{d}\sigma^S - \mathrm{d}\sigma^{-S})}{\frac{1}{2}(\mathrm{d}\sigma^S + \mathrm{d}\sigma^{-S})}, \tag{9.1}$$

where $\mathrm{d}\sigma^S$ is the hadronic differential cross section for a process with one polarized initial-state particle with spin vector S. In this definition we do not specify whether the particle is longitudinally or transversely polarized. In fact, to this day large single-spin asymmetries have mainly been observed in processes associated with transverse polarization. Although not predicted by theory, a surprisingly large asymmetry was first observed in the 1970s in Λ production at Fermilab [15]. This astonishing finding encouraged both theorists and experimentalists to investigate the origin and the phenomenology of these novel effects. In the last years, the main focus lay on the observation of large single transverse-spin asymmetries in SIDIS in the reaction

$$e + p^\uparrow \to e + h + X, \tag{9.2}$$

where $p^\uparrow$ is a transversely polarized proton and h denotes an observed hadron. Several experiments have been performed covering different kinematic regimes by SMC [121] and COMPASS [122, 123] at CERN, and the HERMES [124–126] collaboration at DESY. All of them confirmed the large size of the asymmetry. To understand and explain the physics behind these spin effects, QCD theorists have proposed two different mechanisms. The first one explains the asymmetries in terms of transverse-momentum dependent (TMD)

parton distributions for the polarized proton and TMD fragmentation functions for the final-state hadron [127–132]. In case of the SIDIS cross section the asymmetry involves TMD distribution functions which were first introduced by Sivers and are referred to as Sivers functions. The second approach relies on collinear factorization and is formulated in terms of twist-three multiparton correlation functions [133–137]. It is referred to as Efremov-Teryaev-Qiu-Sterman (ETQS) mechanism. Which one of the two mechanism applies, depends on the considered observable in the scattering reaction. Although the Sivers and the ETQS approach have their own domain of validity, it has been shown that they are equivalent (to some extent) in the region where their kinematic coverages overlap [138–141]. In the TMD approach the large spin asymmetries are due to the correlation of the intrinsic transverse momentum of the considered parton with the transverse spin of the proton, which defines a preferred direction perpendicular to the beam axis. This directional preference is also manifest in the ETQS approach in the dependence of the quark-gluon correlation functions on the transverse spin of the proton.

In case of longitudinal polarization large single-spin asymmetries were only recently detected in parity-violating observables in the production of $W^{\pm}$-bosons at RHIC [16, 17]. By contrast, in parity-conserving processes longitudinal-spin asymmetries turn out to be rather small. Such small asymmetries were observed by the HERMES collaboration in semi-inclusive deep-inelastic scattering off a hydrogen [126, 142] and a deuterium target [143]. Although for longitudinally polarized particles the spin vector is collinear to the beam axis and no transverse direction is preferred, the TMD factorization approach still gives rise to distribution functions, which induce non-vanishing longitudinal spin effects [144–147]. Some of these functions, however, are twist-three functions and are consequently suppressed by a factor $1/Q$, where Q is the momentum transfer in SIDIS. In the TMD approach it is therefore expected that the T-odd $\sin\phi$ asymmetry, which we will introduce in the following section, vanishes at high energies and hence high momentum transfer. However, perturbative corrections to the hard-scattering functions may as well account for single longitudinal-spin asymmetries in SIDIS. In this thesis, we investigate those perturbative effects. We will show that, if parity-violating interactions are excluded, asymmetries only arise at higher orders in perturbation theory and are hence suppressed by powers of α_s. In the following chapter, we will calculate the perturbative contributions to the single longitudinal-spin asymmetries to lowest order and make predictions for their magnitude in SIDIS. Although the asymmetries turn out to be small, we find that they may still be measured to a good accuracy at the planned high-luminosity high-energy electron-ion collider at RHIC (eRHIC).
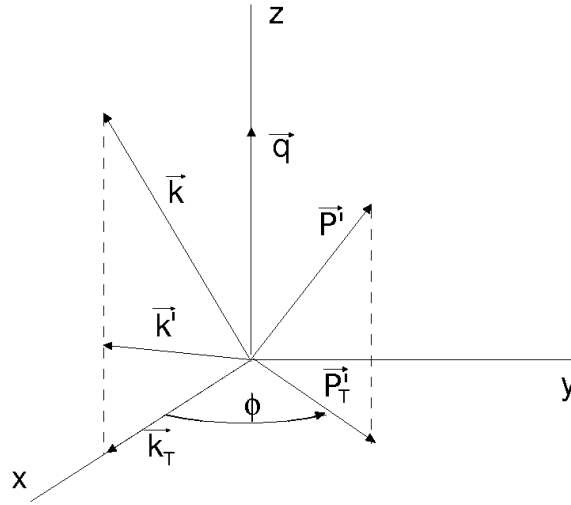
Figure 9.1.: Three-momentum kinematics for the process $e(k){+}p(P,S) \to e(k'){+}h(P'){+}X$ in the proton's rest frame.

9.2. Time-Reversal-Odd Effects

As mentioned above, the SIDIS process can schematically be written as

$$e(k) + p(P,S) \to e(k') + h(P') + X, \tag{9.3}$$

where k and k' denote the momenta of the electron before and after the scattering reaction, P is the momentum and S the spin of the initial state proton, and P' denotes the momentum of the observed hadron. The electron and the hadrons may interact via the electromagnetic or weak interaction. In the following, however, we only consider the electromagnetic case. The proton is longitudinally polarized and therefore its spin vector points along the beam axis. A spin-dependent observable can therefore only be associated with the momenta of the outgoing lepton and hadron transverse to the beam axis,

$$\vec{S} \cdot (\vec{k}_T \times \vec{P}'_T) \propto \sin\phi, \tag{9.4}$$

where ϕ is the angle between $\vec{k}_T$ and $\vec{P}'_T$ in the proton's rest frame. The kinematics are shown in Fig. 9.1. This observable is said to be T-odd, as it changes sign under reversal of both three-momenta and spins, and parity-even (P-even), as it is invariant under reversal of three-momenta. We note that 'T-odd' does not mean that the observable violates time-reversal invariance. Time reversal would also imply that the initial and final state of the scattering reaction are interchanged. A second linearly independent spin-dependent
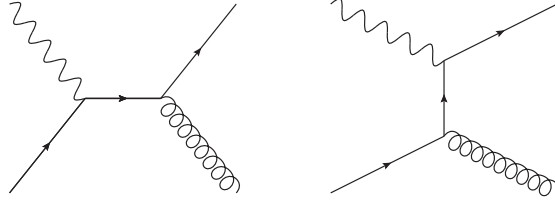
Figure 9.2.: LO (Born) diagrams for $\gamma^* + q \to q + G$.

observable can be deduced from the combination of momenta in Eq. (9.4),

$$\vec{S} \cdot (\vec{k}_T \times \vec{P}'_T)\vec{k}_T \cdot \vec{P}'_T \propto \sin(2\phi), \tag{9.5}$$

with $\vec{k}_T \cdot \vec{P}'_T \propto \cos\phi$. Equation (9.5) also defines a T-odd and P-even quantity. We restrict ourselves to the electromagnetic and strong interaction and do not allow for parity-violating interactions. Since this restriction forbids P-odd effects, we cannot construct any other spin-dependent observable. The single longitudinal-spin asymmetry in SIDIS is therefore proportional to the two T-odd observables in Eqs. (9.4) and (9.5),

$$A_L \equiv \frac{\frac{1}{2}(\mathrm{d}\sigma^+ - \mathrm{d}\sigma^-)}{\frac{1}{2}(\mathrm{d}\sigma^+ + \mathrm{d}\sigma^-)} \equiv \frac{\mathrm{d}\Delta\sigma}{\mathrm{d}\sigma} = D\sin\phi + E\sin(2\phi), \tag{9.6}$$

where $\mathrm{d}\sigma^{+/-}$ denotes the hadronic differential SIDIS cross section for a polarized proton beam with positive/negative helicity. We refer to $\mathrm{d}\Delta\sigma$ as the spin-dependent cross section and to $\mathrm{d}\sigma$ as the spin-averaged or unpolarized cross section.

Before we turn to the explicit perturbative calculation of the spin asymmetry A_L, let us first qualitatively study the form of the partonic cross section associated with T-odd effects. We thereby follow the discussions in Refs. [148, 149].

The matrix element S_{fi} for the scattering from an initial state i to a final state f can in general be written as

$$S_{fi} = \delta_{fi} + i(2\pi)^4\delta^{(4)}(P_f - P_i)T_{fi}, \tag{9.7}$$

where T_{fi} is the corresponding transition amplitude, P_f and P_i denote the sum of momenta of the final-state and initial-state particles, respectively. In quantum mechanics and quantum field theory the S-matrix is unitary, $S_{\Gamma i}S^*_{\Gamma f} = \delta_{fi}$. For the transition amplitude this implies the condition

$$T_{fi} - T^*_{if} = i\alpha_{fi}, \tag{9.8}$$

where α_{fi} is called the absorptive part of the transition amplitude T_{fi} and reads

$$\alpha_{fi} = \sum_\Gamma T^*_{\Gamma f}T_{\Gamma i}(2\pi)^4\delta^{(4)}(P_\Gamma - P_i) \tag{9.9}$$
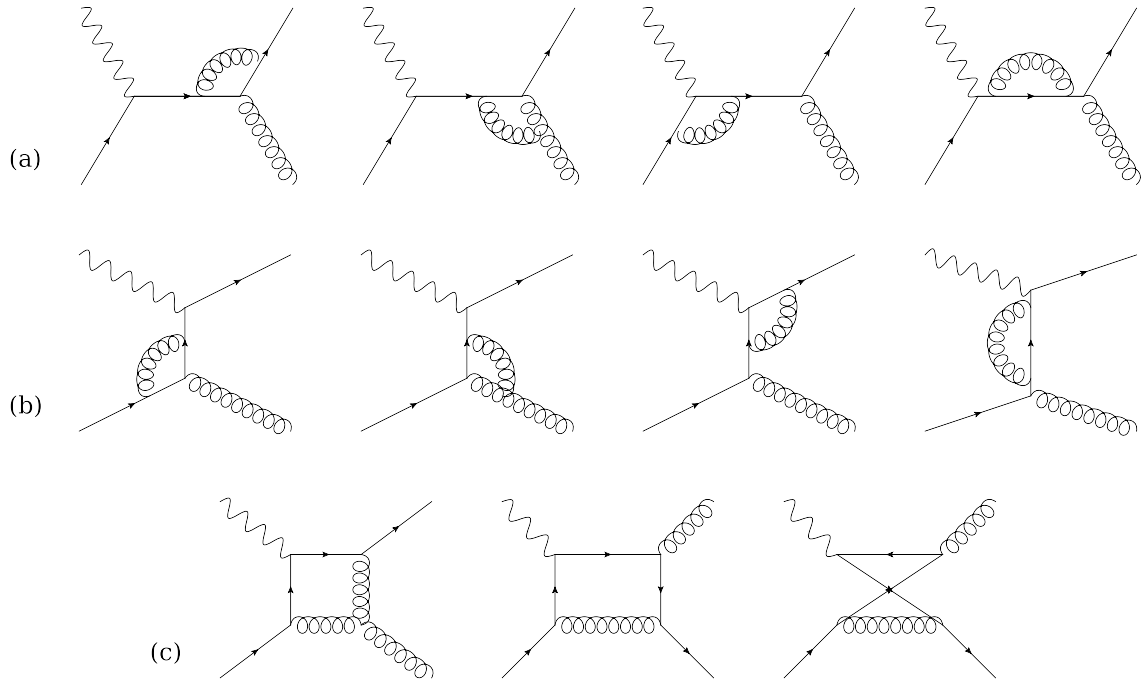
Figure 9.3.: One-loop absorptive diagrams for $\gamma^* + q \to q + G$: (a) s-channel diagrams, (b) t-channel diagrams, (c) box diagrams.

with the sum over Γ running over all possible states. If the S-matrix is a perturbative series, the absorptive part of a fixed-order transition amplitude is the sum of all higher-order diagrams with the same initial and final state. I.e. α_{fi} contains all virtual corrections to the transition amplitude T_{fi}. For example, in the case of SIDIS the dominant partonic channel is $\gamma^* + q \to q + G$. Its lowest-order contribution to the transition amplitude is given by the Born diagrams depicted in Fig. 9.2. The lowest-order contribution to the absorptive part of the Born amplitude is then given as the sum of all one-loop virtual corrections to the Born diagrams. The respective diagrams are depicted in Fig. 9.3.

The unitarity condition in Eq. (9.8) can readily be written as

$$T^*_{if} = T_{fi} - i\alpha_{fi}. \tag{9.10}$$

Multiplying both sides of the equation by its complex conjugate, we obtain

$$|T_{if}|^2 = |T_{fi}|^2 + |\alpha_{fi}|^2 + 2\text{Im}(T^*_{fi}\alpha_{fi}) \tag{9.11}$$

or

$$|T_{fi}|^2 = |T_{if}|^2 - 2\text{Im}(T^*_{fi}\alpha_{fi}) - |\alpha_{fi}|^2. \tag{9.12}$$

Let us now define the states $\tilde{i}$ and $\tilde{f}$ as the states made from i and f by reversing the directions of spins and three-momenta. As QCD preserves time-reversal invariance, the

absolute square of the transition amplitude is invariant under reversal of spins and three-momenta and simultaneous commutation of initial and final state, i.e.

$$|T_{fi}|^2 - |T_{\tilde{i}\tilde{f}}|^2 = 0 = |T_{if}|^2 - |T_{\widetilde{fi}}|^2. \tag{9.13}$$

T-odd effects, however, are defined as the difference of $|T_{fi}|^2$ and $|T_{\widetilde{fi}}|^2$ and may well be different from zero. Indeed, we find by means of Eqs. (9.12) and (9.13)

$$\begin{aligned}
|T_{fi}|^2 - |T_{\widetilde{fi}}|^2 &= |T_{if}|^2 - |T_{\widetilde{fi}}|^2 - 2\text{Im}(T_{fi}^* \alpha_{fi}) - |\alpha_{fi}|^2 \\
&= -2\text{Im}(T_{fi}^* \alpha_{fi}) - |\alpha_{fi}|^2. \tag{9.14}
\end{aligned}$$

As already mentioned, the lowest-order contribution to T_{fi} in SIDIS comes from the Born diagrams in Fig. 9.2 and the lowest-order contribution to α_{fi} is due to the absorptive diagrams in Fig. 9.3. The leading contribution to the term $T_{fi}^* \alpha_{fi}$ is then given by the interference of the Born term with its one-loop absorptive corrections and is of $\mathcal{O}(\alpha_s^2)$. Hence, the imaginary part of this interference term is the lowest-order contribution to T-odd observables in perturbation theory.

10. Single Longitudinal-Spin Asymmetry in SIDIS

In the previous chapter, we have identified the leading perturbative contribution to the single longitudinal-spin asymmetry in SIDIS and depicted the corresponding Feynman diagrams. We now turn to the explicit calculation of this contribution in perturbative QCD. In Sec. 10.1 we investigate the kinematics of the considered process and present the general form of the spin-dependent hadronic cross section. The calculation of the perturbative hard-scattering part is outlined in Sec. 10.2. We calculate the spin-dependent cross section to $\mathcal{O}(\alpha_s^2)$, which is the first non-vanishing order. In the derivation of the hard-scattering functions we make use of the one-loop result for e^+e^--annihilation from Ref. [150] by applying the crossing procedure for SIDIS developed in Ref. [151]. The last section of this chapter is then dedicated to SIDIS phenomenology at a future electron-ion collider at RHIC (eRHIC). We make predictions for the single longitudinal-spin asymmetry in the kinematic regime accessible by the planned collider and show the magnitude of the measured SIDIS cross section in this regime.

We note that perturbative T-odd effects in SIDIS were calculated for a polarized lepton beam incident on an unpolarized proton target in Refs. [149, 151, 152] including electromagnetic and weak interactions. For the Drell-Yan process leading perturbative contributions to T-odd asymmetries were calculated in Refs. [151, 153–155].

10.1. Spin-Dependent Hadronic Cross Section

Let us first recall our notation for momenta and spins in the SIDIS process:

$$e(k) + p(P, S) \rightarrow e(k') + h(P') + X. \tag{10.1}$$

We have already mentioned that we restrict ourselves to the case of electromagnetic interaction of the electron with the partons in the proton. The differential spin-dependent cross section defined in Eq. (9.6) may be written as the product of a leptonic tensor $L_{\mu\nu}$ and a spin-dependent hadronic tensor $\Delta W_{\mu\nu}$,

$$\frac{k_0' P_0' \, \mathrm{d}\Delta\sigma}{\mathrm{d}^3\vec{k'} \, \mathrm{d}^3\vec{P'}} = \frac{\alpha^2}{2Sq^4} L^{\mu\nu} \Delta W_{\mu\nu}, \tag{10.2}$$

where $S = (P + k)^2$ is the center-of-mass energy squared and $q = k - k'$ is the spacelike momentum of the virtual photon. We integrate over the azimuthal angle of the scattered lepton and express the cross section in terms of the invariants

$$Q^2 = -q^2, \quad x = \frac{Q^2}{2P \cdot q}, \quad y = \frac{P \cdot q}{P \cdot k}, \quad z = \frac{P \cdot P'}{P \cdot q} \tag{10.3}$$

to find

$$\frac{\mathrm{d}\Delta\sigma}{\mathrm{d}x \; \mathrm{d}Q^2 \; \mathrm{d}z \; \mathrm{d}\kappa^2 \; \mathrm{d}\phi} = \frac{\pi\alpha^2 y^2}{4Q^4 z} L^{\mu\nu} \Delta W_{\mu\nu}, \tag{10.4}$$

where

$$\kappa^2 = \frac{P_T'^2}{Q^2} \tag{10.5}$$

with ϕ defined as the azimuthal angle between $\vec{P}_T'$ and the lepton scattering plane (see Fig. 9.1).

The spin-averaged leptonic tensor is of the form,

$$L_{\mu\nu} = 2 \left(k_\mu k_\nu' + k_\nu k_\mu' + \frac{q^2}{2} g_{\mu\nu} \right). \tag{10.6}$$

The hadronic tensor is defined as

$$\Delta W_{\mu\nu} = \sum_{a,b} \int_x^1 \frac{\mathrm{d}\xi}{\xi} \int_z^1 \frac{\mathrm{d}\eta}{\eta^2} D_a^H(\eta) e_{ab} \Delta H_{\mu\nu}^{ab} \Delta f_b^p(\xi), \tag{10.7}$$

where $\Delta f_b^p(\xi)$ is the helicity distribution of a parton b in a proton with momentum fraction ξ and $D_a^H(\eta)$ is the fragmentation function for a parton a fragmenting into a hadron H with momentum fraction η. The coupling e_{ab} equals e_q^2 for all scattering processes at lowest order. $\Delta H_{\mu\nu}^{ab}$ is the hard-scattering function, which is given as the difference of the helicity-dependent scattering amplitudes for the partonic process

$$\gamma^*(q) + b(p, \pm) \to a(p') + X, \tag{10.8}$$

where p is the momentum of the incoming polarized parton b and p' is the momentum of the outgoing unpolarized parton a. The hard-scattering function has a general form consisting of nine different gauge invariant terms [151],

$$\begin{aligned}
\Delta H_{\mu\nu}^{ab} =& \Delta H_1^{ab} \left(g_{\mu\nu} - \frac{q_\mu q_\nu}{q^2} \right) + \Delta H_2^{ab} q^{-2} \hat{p}_\mu \hat{p}_\nu + \Delta H_3^{ab} q^{-2} \hat{p}_\mu' \hat{p}_\nu' \\
&+ \Delta H_4^{ab} q^{-2} (\hat{p}_\mu \hat{p}_\nu' + \hat{p}_\nu \hat{p}_\mu') + \Delta H_5^{ab} q^{-2} (\hat{p}_\mu \hat{p}_\nu' - \hat{p}_\nu \hat{p}_\mu') + \Delta H_6^{ab} q^{-2} i\epsilon_{\mu\nu\alpha\beta} q^\alpha p^\beta \\
&+ \Delta H_7^{ab} q^{-2} i\epsilon_{\mu\nu\alpha\beta} q^\alpha p'^\beta + \Delta H_8^{ab} q^{-4} (\hat{p}_\mu \tilde{F}_\nu + \hat{p}_\nu \tilde{F}_\mu) + \Delta H_9^{ab} q^{-4} (\hat{p}_\mu' \tilde{F}_\nu + \hat{p}_\nu' \tilde{F}_\mu),
\end{aligned} \tag{10.9}$$

with

$$\hat{p}_\mu = p_\mu - \frac{p \cdot q}{q^2} q_\mu,$$

$$\hat{p}'_\mu = p'_\mu - \frac{p' \cdot q}{q^2} q_\mu,$$

$$\tilde{F}_\mu = i\epsilon_{\mu\alpha\beta\gamma} p^\alpha p'^\beta q^\gamma. \tag{10.10}$$

We use the convention $\epsilon^{0123} = -1$ for the antisymmetric tensor throughout. The first five terms in Eq. (10.9) are independent of the parton's spin. Therefore the structure functions ΔH_1^{ab} to ΔH_5^{ab} vanish. Since the hadronic tensor is contracted with the spin-averaged leptonic tensor $L^{\mu\nu}$ in Eq. (10.6), which is symmetric in μ and ν, antisymmetric terms in μ and ν in Eq. (10.9) do contribute. Hence, one can neglect the terms with ΔH_6^{ab} and ΔH_7^{ab}. The terms proportional to ΔH_8^{ab} and ΔH_9^{ab} are T-odd quantities. As we have shown in the previous chapter, their leading contributions come from the interference of the Born diagrams shown in Fig. 9.2 with the absorptive part of the one-loop diagrams shown in Fig. 9.3. These contributions are of $\mathcal{O}(\alpha_s^2)$. The absorptive part of the diagrams in Fig. 9.3 can be derived from the one-loop result for e^+e^--annihilation in Ref. [150]. In the following section we sketch the perturbative calculation of the relevant functions ΔH_8^{ab} and ΔH_9^{ab}.

10.2. Hard-Scattering Functions to $\mathcal{O}(\alpha_s^2)$

In general, the hard-scattering function for the partonic process $\gamma^*(q) + b(p) \to a(p') + X$ with partons a and b is defined as

$$\Delta H_{\mu\nu}^{ab} = \frac{1}{2} \left(|\mathcal{M}^+|_{\mu\nu}^2 (b \to a) - |\mathcal{M}^-|_{\mu\nu}^2 (b \to a) \right) \mathcal{P}, \tag{10.11}$$

with the difference of the scattering amplitudes $|\mathcal{M}|_{\mu\nu}^2 (b \to a)$ for positive (+) and negative helicity (-) of the initial-state parton and a phase space factor $\mathcal{P}$. Each diagram in Figs. 9.2 and 9.3 contains 2 external partons. One of these is unobserved and its phase space is integrated over. The factor $\mathcal{P}$ is therefore of the form

$$\mathcal{P} = \frac{1}{(2\pi)^4} \int \frac{d^3\vec{p}_3}{(2\pi)^3 2E_3} (2\pi)^4 \delta^{(4)}(p + q - p' - p_3) = \frac{1}{(2\pi)^3} \delta\left([p + q - p']^2\right)$$

$$= \frac{\hat{z}}{(2\pi)^3 Q^2} \delta\left(\hat{\kappa}^2 - \frac{1 - \hat{x}}{\hat{x}} \hat{z}(1 - \hat{z})\right), \tag{10.12}$$

where we have introduced the partonic analogs of the invariants x and z,

$$\hat{x} = \frac{Q^2}{2p \cdot q} = \frac{x}{\xi}, \quad \hat{z} = \frac{p \cdot p'}{p \cdot q} = \frac{z}{\eta}, \tag{10.13}$$

and of κ,

$$\hat{\kappa} = \frac{p'_T}{Q} = \frac{\kappa}{\eta}. \tag{10.14}$$

Since the phase space factor is independent of the underlying partonic process involving partons a and b, we define dimensionless functions $\Delta h_{8,9}^{ab}$, which contain the full information on the partonic process, and rewrite the functions $\Delta H_{8,9}^{ab}$ in Eq. (10.9) as

$$\Delta H_{8,9}^{ab} = \frac{\hat{z}}{(2\pi)^3 Q^2} \delta \left(\hat{\kappa}^2 - \frac{1-\hat{x}}{\hat{x}} \hat{z}(1-\hat{z}) \right) \Delta h_{8,9}^{ab}(\alpha_s, \hat{x}, \hat{z}). \tag{10.15}$$

The functions $\Delta h_{8,9}^{ab}$ can then easily be determined by comparing the expansion of $\Delta H_{\mu\nu}^{ab}$ in Eq. (10.9) with the calculated squared scattering amplitude in Eq. (10.11).

Let us now calculate this amplitude for the partonic process $\gamma^*(q) + q(p) \to q(p') + X$. As mentioned above, the lowest order non-vanishing contribution to $\Delta H_{\mu\nu}$ is due to the interference of the Born diagrams in Fig. 9.2 with the absorptive diagrams in Fig. 9.3. The corresponding squared scattering amplitude can be written as a trace in Dirac and color space,

$$|\mathcal{M}^{\pm}|_{\mu\nu}^2(q \to q) = \frac{1}{N} \left(-Tr \left[\slashed{p}' T_{\mu\beta}^q \frac{1 \pm \gamma_5}{2} \slashed{p} \bar{B}_{\nu\alpha}^q g^{\beta\alpha} \right] - Tr \left[\slashed{p}' B_{\mu\beta}^q \frac{1 \pm \gamma_5}{2} \slashed{p} \bar{T}_{\nu\alpha}^q g^{\beta\alpha} \right] \right), \tag{10.16}$$

with the number of colors $N = 3$ and the Born term

$$B_{\mu\beta}^q = gt^a \left(\gamma_\mu \frac{\slashed{p} - \slashed{p}_3}{2p \cdot p_3} \gamma_\beta - \gamma_\beta \frac{\slashed{p}' + \slashed{p}_3}{2p' \cdot p_3} \gamma_\mu \right). \tag{10.17}$$

The transition amplitude $T_{\mu\beta}^q$ contains all contributions from the absorptive diagrams. By applying crossing one may obtain this transition amplitude from the absorptive corrections to the annihilation process $e^+ + e^- \to \gamma^* \to q + \bar{q} + G$ [151]. In the following we briefly outline the most important steps of this crossing procedure.

The amplitude for the one-loop absorptive corrections to the process $\gamma^* \to q(p_1) + \bar{q}(p_2) + G(p_3)$ may be written as

$$\bar{u}(p_1) T_{\mu\beta} v(p_2) \epsilon^{*\beta}(p_3), \tag{10.18}$$

where $T_{\mu\beta}$ is of $\mathcal{O}(\alpha_s^{3/2})$. The diagrams contributing to the expression in (10.18) are equal to the absorptive leptoproduction diagrams in Fig. 9.3 except that all three external partons are in the final state and the virtual photon is timelike rather than spacelike. The transition amplitude may be expanded in terms of seven independent covariant terms [150],

$$\begin{aligned} T_{\mu\beta} = &q^{-4} N_1 \hat{p}_{+\mu} \tilde{p}_{-\beta} \slashed{p}_3 + q^{-4} N_2 \hat{p}_{-\mu} \tilde{p}_{-\beta} \slashed{p}_3 + q^{-2} N_3 \hat{\gamma}_\mu \tilde{p}_{-\beta} \\ &+ q^{-2} N_4 \hat{p}_{+\mu} \tilde{\gamma}_\beta + q^{-2} N_5 \hat{p}_{-\mu} \tilde{\gamma}_\beta + q^{-2} N_6 \hat{\tilde{g}}_{\mu\beta} \slashed{p}_3 \\ &+ N_7 \left(\gamma_\mu \frac{\slashed{p}_2 + \slashed{p}_3}{2p_2 \cdot p_3} \gamma_\beta - \gamma_\beta \frac{\slashed{p}_1 + \slashed{p}_3}{2p_1 \cdot p_3} \gamma_\mu \right), \end{aligned} \tag{10.19}$$

where $(l = 1, \ldots, 7)$

$$N_l = g^3(\tilde{N}_l i f^{bac} t^c t^b + \hat{N}_l t^b t^a t^b + N_l^{(ct)} t^a) \tag{10.20}$$

and $q = p_1 + p_2 + p_3$, $p_\pm = p_1 \pm p_2$. The gauge invariant completions are defined as

$$\hat{p}_\mu = p_\mu - \frac{p \cdot q}{q^2} q_\mu,$$

$$\hat{\gamma}_\mu = \gamma_\mu - \frac{\slashed{q}}{q^2} q_\mu,$$

$$\tilde{p}_\beta = p_\beta - \frac{p \cdot p_3}{p_3 \cdot q} q_\beta,$$

$$\tilde{\gamma}_\beta = \gamma_\beta - \frac{\slashed{p}_3}{p_3 \cdot q} q_\beta,$$

$$\hat{\tilde{g}}_{\mu\beta} = g_{\mu\beta} - \frac{q_\beta p_{3\mu}}{p_3 \cdot q}. \tag{10.21}$$

The scalar functions $\tilde{N}_l$, $\hat{N}_l$ and $N_l^{(ct)}$ $(l = 1, \ldots, 7)$ can be found in Eq. (7) and Table 1 and 2 of Ref. [150].

The transition amplitude $T_{\mu\beta}^q$ for the quark-quark process in SIDIS is obtained from the amplitude $T_{\mu\beta}$ in Eq. (10.19) by the change of momenta,

$$p_1 \to p', \quad p_2 \to -p, \tag{10.22}$$

which corresponds to replacing the outgoing antiquark with momentum p_2 by an incoming quark with momentum p. The functions $\tilde{N}_l$ and $\hat{N}_l$ contain logarithmic functions of the kinematic variables $y_{ij} = 2p_i \cdot p_j / q^2$, namely $\ln(y_{ij})$, $\ln(1-y_{ij})$ and the dilogarithm $\text{Li}_2(y_{ij})$. Crossing results in a sign change of external momenta, which may lead to a discontinuous change of the kinematic variables y_{ij}. Their new values may lie on the branch cuts of the domains of definition of the logarithmic functions leading to ambiguous results. To circumvent this ambiguity one has to perform an analytic continuation of the logarithmic functions and take care of small imaginary parts of the Feynman propagators specified by the $i\eta$ prescriptions. For the quark-quark channel one finds the following replacements [151]:

$$\ln(1 - y_{12}) \to \ln\left(\frac{2p \cdot p'}{-q^2} - 1\right) - i\pi,$$

$$\text{Li}_2(y_{12}) \to -\text{Li}_2\left(1 - \frac{2p \cdot p'}{-q^2}\right) + i\pi \ln\left(\frac{2p \cdot p'}{-q^2}\right) - \ln\left(\frac{2p \cdot p'}{-q^2}\right)\ln\left(\frac{2p \cdot p'}{-q^2} - 1\right) + \zeta(2),$$

$$\ln(y_{13}) \to \ln\left(\frac{2p' \cdot p_3}{-q^2}\right) - i\pi,$$

$$\ln(1 - y_{23}) \to \ln\left(\frac{2p \cdot p_3}{-q^2} - 1\right) - i\pi,$$

$$\text{Li}_2(y_{23}) \to -\text{Li}_2\left(1 - \frac{2p \cdot p_3}{-q^2}\right) + i\pi \ln\left(\frac{2p \cdot p_3}{-q^2}\right) - \ln\left(\frac{2p \cdot p_3}{-q^2}\right)\ln\left(\frac{2p \cdot p_3}{-q^2} - 1\right) + \zeta(2). \tag{10.23}$$

With these prescriptions the transition amplitude $T_{\mu\beta}^q$ is easily calculated. It is then straightforward to evaluate the trace in Eq. (10.16) and find the expression for the hard-scattering function $\Delta H_{\mu\nu}^{qg}$. We refrain from showing the entire calculation and simply collect the results at the end of this section starting from Eq. (10.32).

Analogously the squared matrix elements for the gluon-initiated partonic channel $\gamma^*(q) + G(p) \to q(p') + X$ is calculated. The trace in Dirac and color space is of the form

$$|\mathcal{M}^\pm|_{\mu\nu}^2(G \to q) = \frac{1}{N^2 - 1}\left(Tr\left[\not{p}'T_{\mu\beta}^G\not{p}_3\bar{B}_{\nu\alpha}^G\epsilon_\pm^\beta\epsilon_\pm^{*\alpha}\right] + Tr\left[\not{p}'B_{\mu\beta}^G\not{p}_3\bar{T}_{\nu\alpha}^G\epsilon_\pm^\beta\epsilon_\pm^{*\alpha}\right]\right), \quad (10.24)$$

where the corresponding Born term is

$$B_{\mu\beta}^G = gt^a\left(\gamma_\mu\frac{\not{p}_3 - \not{p}}{-2p \cdot p_3}\gamma_\beta - \gamma_\beta\frac{\not{p}' - \not{p}}{-2p' \cdot p}\gamma_\mu\right). \quad (10.25)$$

In Eq. (10.11) we calculate the difference of the squared matrix element for right-handed and left-handed gluons. In its derivation we encounter the difference

$$S^{\beta\alpha} = \epsilon_+^\beta\epsilon_+^{*\alpha} - \epsilon_-^\beta\epsilon_-^{*\alpha}. \quad (10.26)$$

The polarization tensor $S^{\beta\alpha}$ can be expressed in terms of Lorentz vectors and the completely antisymmetric tensor as

$$S_{\beta\alpha} = \frac{i}{p \cdot q}\epsilon_{\beta\alpha\rho\sigma}p^\rho q^\sigma. \quad (10.27)$$

One can make this clear by considering a gluon moving in the 3-direction and $q = (0, 0, 0, -Q)$. The gluon's polarization vector has the form

$$\epsilon_\pm = \frac{1}{2}(0, 1, \pm i, 0). \quad (10.28)$$

Hence, the polarization tensor according to the definition in Eq. (10.26) reads

$$S^{\beta\alpha} = \begin{pmatrix} 0 & 0 & 0 & 0 \\ 0 & 0 & -i & 0 \\ 0 & i & 0 & 0 \\ 0 & 0 & 0 & 0 \end{pmatrix}, \quad (10.29)$$

which is equal to the expression in Eq. (10.27).

The transition amplitude $T_{\mu\beta}^G$ can be derived from the amplitudes $T_{\mu\beta}$ in e^+e^- annihilation by making the change of external momenta,

$$p_1 \to p', \quad p_3 \to -p, \quad p_2 \to p_3. \quad (10.30)$$

The resulting replacements for the logarithmic functions read [151]

$$\ln(y_{12}) \to \ln\left(\frac{2p' \cdot p_3}{-q^2}\right) - i\pi,$$

$$\ln(1 - y_{13}) \to \ln\left(\frac{2p \cdot p'}{-q^2} - 1\right) - i\pi,$$

$$\text{Li}_2(y_{13}) \to -\text{Li}_2\left(1 - \frac{2p \cdot p'}{-q^2}\right) + i\pi \ln\left(\frac{2p \cdot p'}{-q^2}\right) - \ln\left(\frac{2p \cdot p'}{-q^2}\right)\ln\left(\frac{2p \cdot p'}{-q^2} - 1\right) + \zeta(2),$$

$$\ln(1 - y_{23}) \to \ln\left(\frac{2p \cdot p_3}{-q^2} - 1\right) - i\pi,$$

$$\text{Li}_2(y_{23}) \to -\text{Li}_2\left(1 - \frac{2p \cdot p_3}{-q^2}\right) + i\pi \ln\left(\frac{2p \cdot p_3}{-q^2}\right) - \ln\left(\frac{2p \cdot p_3}{-q^2}\right)\ln\left(\frac{2p \cdot p_3}{-q^2} - 1\right) + \zeta(2).$$

$$\tag{10.31}$$

These crossing prescriptions allow to evaluate the $\mathcal{O}(\alpha_s^2)$ contributions to the hard-scattering function $\Delta H_{\mu\nu}^{qG}$.

As mentioned earlier, comparing the results for the hard-scattering functions $\Delta H_{\mu\nu}^{ab}$ with their expansion in Eqs. (10.9) and (10.15) we can read off the dimensionless functions $\Delta h_{8,9}^{ab}$. For the quark-quark channel we find

$$\Delta h_8^{qq} = -8i\pi\alpha_s^2(Q)\frac{\hat{x}^3(1 - \hat{x} - \hat{z})}{(1 - \hat{x})(1 - \hat{z})}$$
$$\times \left[\frac{1}{2}C_F C_A + C_F\left(C_F - \frac{C_A}{2}\right)\left(\frac{3 - \hat{z}}{1 - \hat{z}} + \ln(\hat{z})\frac{2}{(1 - \hat{z})^2}\right)\right],$$

$$\Delta h_9^{qq} = 8i\pi\alpha_s^2(Q)\frac{\hat{x}^3}{(1 - \hat{x})(1 - \hat{z})}$$
$$\times \left[\frac{3}{2}C_F C_A + C_F\left(C_F - \frac{C_A}{2}\right)\left(\frac{1 - 3\hat{z}}{1 - \hat{z}} + \ln(\hat{z})\frac{2(1 - 2\hat{z})}{(1 - \hat{z})^2}\right)\right]. \tag{10.32}$$

The functions for the antiquark-initiated channel,

$$\gamma^*(q) + \bar{q}(p, \pm) \to \bar{q}(p') + X,$$

are due to CP-invariance equal to those of the quark-initiated partonic process,

$$\Delta h_8^{\bar{q}\bar{q}} = \Delta h_8^{qq}, \quad \Delta h_9^{\bar{q}\bar{q}} = \Delta h_9^{qq}. \tag{10.33}$$

For the partonic channel with a gluon in the initial state and a fragmenting quark in the final state the corresponding functions read

$$\Delta h_8^{qG} = -8i\pi\alpha_s^2(Q)\frac{\hat{x}^3}{\hat{z}(1 - \hat{z})}\left(C_F - \frac{C_A}{2}\right)$$
$$\times \left[2(1 - \hat{z}) + \frac{2x}{\hat{z}} + \frac{\hat{z} - \hat{x} - 1}{\hat{z}(1 - \hat{z})} - \frac{\hat{x} + \hat{z} - 1}{(1 - \hat{z})^2}\ln\hat{z} + \frac{\hat{x} - \hat{z} - 1}{\hat{z}^2}\ln(1 - \hat{z})\right],$$

$$\Delta h_9^{qG} = - 8i\pi\alpha_s^2(Q) \left(C_F - \frac{C_A}{2} \right) \frac{\hat{x}^3}{\hat{z}(1-\hat{z})}$$
$$\times \left[\frac{1 - 2\hat{z} + 2\hat{z}^2}{\hat{z}(1-\hat{z})} + \frac{1}{(1-\hat{z})^2} \ln \hat{z} + \frac{1}{\hat{z}^2} \ln(1-\hat{z}) \right]. \qquad (10.34)$$

With these results we can calculate the spin-dependent hadronic cross section in SIDIS to $\mathcal{O}(\alpha_s^2)$. To this end, we explicitly contract the leptonic tensor $L^{\mu\nu}$ in Eq. (10.6) with the hadronic tensor $\Delta W_{\mu\nu}$ in Eq. (10.7) to obtain

$$L^{\mu\nu}\Delta W_{\mu\nu} = \sum_{a,b} \int_x^1 \frac{\mathrm{d}\xi}{\xi} \int_z^1 \frac{\mathrm{d}\eta}{\eta^2} D_a^H(\eta)\Delta f_b^p(\xi)\frac{2\hat{z}e_{ab}}{(2\pi)^3 y^2} \left(D^{ab} \sin\phi + E^{ab}\sin(2\phi) \right)$$
$$\times \delta\left(\hat{\kappa}^2 - \frac{1-\hat{x}}{\hat{x}}\hat{z}(1-\hat{z}) \right) \qquad (10.35)$$

with

$$D^{ab} = \sqrt{1-y}(2-y)i\frac{\hat{\kappa}}{2\hat{x}} \left[\frac{1}{\hat{x}}\Delta h_8^{ab} + \left(\hat{z} + \frac{\hat{\kappa}^2}{\hat{z}} \right) \Delta h_9^{ab} \right],$$
$$E^{ab} = -(1-y)i\frac{\hat{\kappa}^2}{\hat{x}}\Delta h_9^{ab}. \qquad (10.36)$$

As expected, the T-odd structure of the hadronic tensor results in asymmetries proportional to $\sin\phi$ and $\sin(2\phi)$. The coefficients D^{ab} and E^{ab} are given in terms of the dimensionless functions in Eqs. (10.32-10.34) for the qq, $\bar{q}\bar{q}$ and qG partonic channels. At the given order in perturbation theory, however, there are three more partonic processes contributing to the cross section, namely Gq, $G\bar{q}$ and $\bar{q}G$. The corresponding hard-scattering functions may be obtained by interchanging the two external final-state momenta p' and p_3 in the calculation of the matrix elements for the processes qq, $\bar{q}\bar{q}$ and qG, respectively. The resulting coefficients are

$$D^{Gq}(\hat{z}) = -D^{qq}(1-\hat{z}), \quad E^{Gq}(\hat{z}) = E^{qq}(1-\hat{z}),$$
$$D^{G\bar{q}}(\hat{z}) = -D^{\bar{q}\bar{q}}(1-\hat{z}), \quad E^{G\bar{q}}(\hat{z}) = E^{\bar{q}\bar{q}}(1-\hat{z}),$$
$$D^{\bar{q}G}(\hat{z}) = -D^{qG}(1-\hat{z}), \quad E^{\bar{q}G}(\hat{z}) = E^{qG}(1-\hat{z}). \qquad (10.37)$$

Let us now make some qualitative statements about the single longitudinal-spin asymmetry in SIDIS. The color factor for contributions associated with initial state gluons $C_F - C_A/2$ is smaller by more than an order of magnitude compared to the leading color factor $\frac{3}{2}C_F C_A$ for the quark-initiated partonic channel. The asymmetry is therefore dominated by contributions from initial-state quarks. This argument is even emphasized by analyses of spin-dependent observables which suggest that the helicity parton distribution function for the gluon ΔG is close to zero [46, 47].

By making use of the delta function in Eq. (10.35) one may evaluate Eq. (10.36) for the quark-quark channel and find that the coefficient D^{qq} is negative for arbitrary values

of $\hat{x}$ and $\hat{z}$. It behaves as $(1 - \hat{z})^{-1/2}$ at large $\hat{z}$. From Eq. (10.37) we see that the corresponding function D^{Gq} for an fragmenting gluon is positive and behaves as $\hat{z}^{-1/2}$ at small $\hat{z}$. Hence, we expect that, at hadron level, fragmenting quarks dominate the $\sin\phi$ asymmetry for moderate and large values of z. At small z the asymmetry changes sign due to large contributions from fragmenting gluons. By contrast, the $\sin(2\phi)$ asymmetry does not change sign as a function of z because the corresponding coefficients E^{qq} and E^{Gq} are both positive.

10.3. Phenomenological Results for eRHIC

In this section we investigate the numerical magnitude of the T-odd single-spin asymmetry,

$$A_L \equiv \frac{\frac{1}{2}\left(\mathrm{d}\sigma^+ - \mathrm{d}\sigma^-\right)}{\frac{1}{2}\left(\mathrm{d}\sigma^+ + \mathrm{d}\sigma^-\right)} \equiv \frac{\mathrm{d}\Delta\sigma}{\mathrm{d}\sigma} \tag{10.38}$$

from Eq. (9.6). As can be seen from Eqs. (10.4) and (10.35) the calculation of the numerator involves convolution integrals of helicity parton distributions and fragmentation functions with the hard-scattering part, which we calculated to $O(\alpha_s^2)$. For our numerical estimates we use the deFlorian-Sassot-Stratmann-Vogelsang (DSSV) [46, 47] NLO helicity PDFs and the deFlorian-Sassot-Stratmann (DSS) [73] NLO fragmentation functions. The denominator of Eq. (10.38) is the spin-averaged semi-inclusive leptoproduction cross section. Its leading contribution for nonzero P'_T is of $\mathcal{O}(\alpha_s)$ and was calculated in Ref. [156]. In Appendix A.3 we collect the results for the spin-averaged cross section. We use the unpolarized CTEQ6M [5] NLO PDFs and the DSS NLO fragmentation functions for the numerical calculation of the denominator. Since the first non-vanishing contributions to the numerator are of $\mathcal{O}(\alpha_s^2)$, leading-order expressions in the denominator are sufficient to evaluate the asymmetry A_L to $\mathcal{O}(\alpha_s)$.

As we have shown in the previous section, the T-odd structure of the cross section leads to asymmetries proportional to $\sin\phi$ and $\sin(2\phi)$. In order to project out the individual terms, we integrate the cross sections over ϕ with a corresponding weighting factor. We thereby define the average asymmetry

$$\langle \sin(n\phi) \rangle \equiv \frac{\int \mathrm{d}x \mathrm{d}z \mathrm{d}\phi \sin(n\phi) \frac{\mathrm{d}\Delta\sigma}{\mathrm{d}x \mathrm{d}Q^2 \mathrm{d}z \mathrm{d}\kappa^2 \mathrm{d}\phi}}{\int \mathrm{d}x \mathrm{d}z \mathrm{d}\phi \frac{\mathrm{d}\sigma}{\mathrm{d}x \mathrm{d}Q^2 \mathrm{d}z \mathrm{d}\kappa^2 \mathrm{d}\phi}}, \tag{10.39}$$

where we also integrate over the hadronic variables x and z. The limits of the x and z integration are determined through the kinematic constraint

$$\frac{P'^2_T}{Q^2} \leq \frac{1-x}{x} z(1-z). \tag{10.40}$$

Since fragmentation functions are only poorly known for very small values of z, we introduce an additional lower bound for the integral at $z_{\min} = 0.05$. This bound, of course,
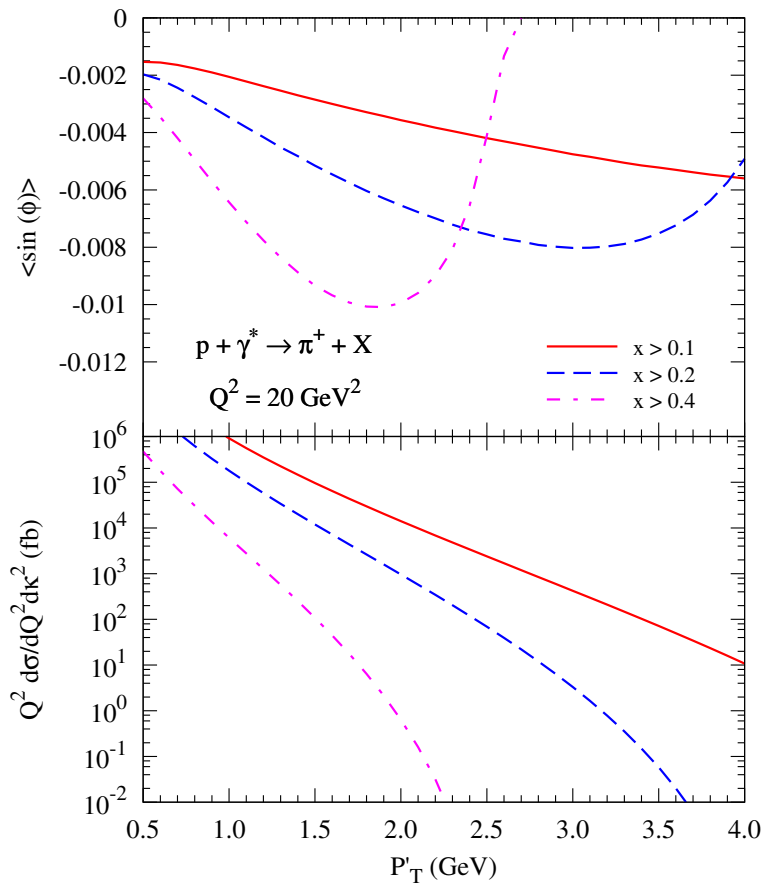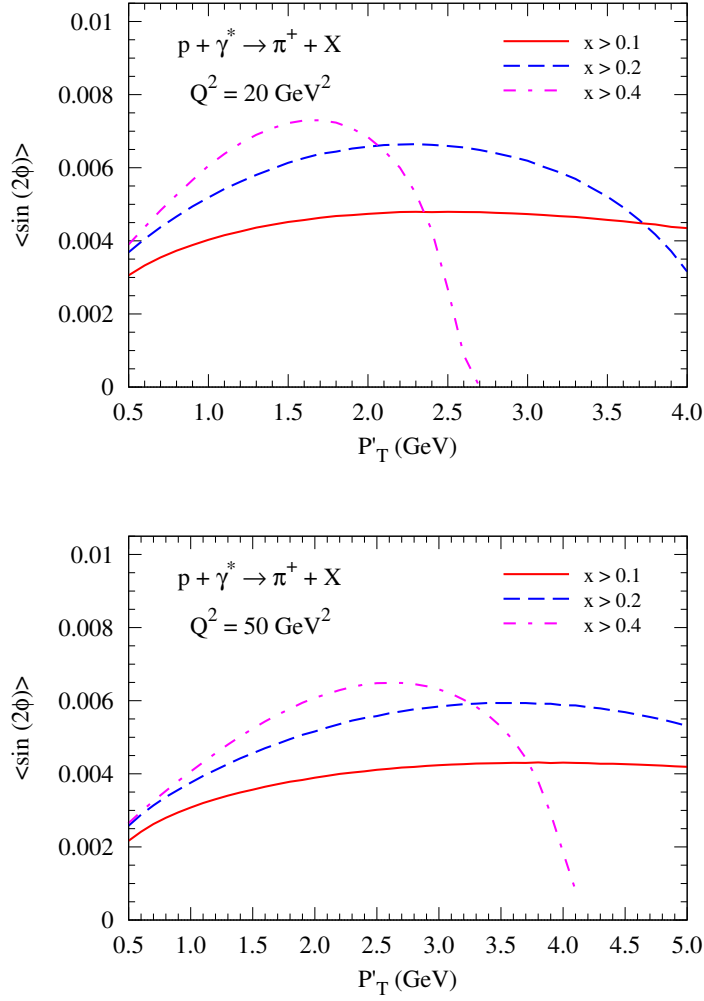
Figure 10.1.: The upper plot shows the asymmetry $\langle\sin\phi\rangle$ in π^+ production as a function of P_T' for $\sqrt{S} = 63$ GeV and $Q^2 = 20$ GeV^2. The solid, dashed and dot-dashed lines correspond to $x > 0.1$, 0.2 and 0.4, respectively. The lower plot shows the corresponding unpolarized cross section $Q^2\mathrm{d}\sigma/\mathrm{d}Q^2\mathrm{d}\kappa^2$.

only affects the result for the asymmetry at low P_T'. In the following considerations we also vary the lower bound $x_{\min}$ of the integral over x.

We estimate the single longitudinal-spin asymmetry for the medium energy kinematics of the eRHIC collider design. At the medium energy stage it is planned to collide a 4 GeV electron beam with a 250 GeV beam of polarized protons. The resulting center-of-mass energy is $\sqrt{S} = 63$ GeV. In Fig. 10.1 the asymmetry $\langle\sin\phi\rangle$ for the production of a π^+ meson at $Q^2 = 20$ GeV^2 is shown. Also shown is the unpolarized cross section $Q^2\mathrm{d}\sigma/\mathrm{d}Q^2\mathrm{d}\kappa^2$ which corresponds to the denominator of the asymmetry in Eq. (10.39). As can be seen, the asymmetry is negative and of the order of one per cent. It is largest for large lower bounds of x which indicates that the main contribution to the asymmetry comes from the helicity distribution of the valence quarks in the proton. The peak of the asymmetry as a function of the transverse momentum of the π^+ meson is strongly
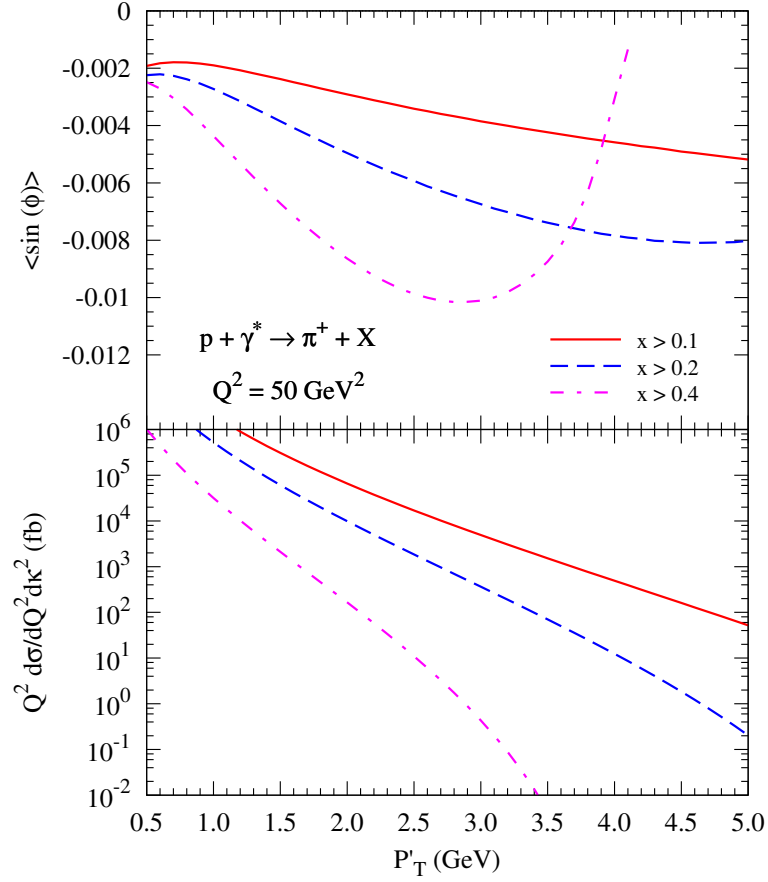
Figure 10.2.: Same as Fig. 10.1 at $Q^2 = 50$ GeV^2.

correlated to the lower bound $x_{\min}$ of the x integral. The larger $x_{\min}$, the smaller is the transverse momentum for which the peak occurs and the higher is the peak of the asymmetry. In Fig. 10.2 the asymmetry $\langle \sin \phi \rangle$, again for π^+ production, is shown at $Q^2 = 50$ GeV^2. The height of the peak and the shape of the asymmetry is hardly altered when going from $Q^2 = 20$ GeV^2 to $Q^2 = 50$ GeV^2. In fact, it turns out that the size of the asymmetry is rather stable as a function of Q^2. Only at large momentum transfer the asymmetry is suppressed since it is proportional to $\alpha_s(Q)$. The unpolarized cross section $Q^2 \mathrm{d}\sigma/\mathrm{d}Q^2 \mathrm{d}\kappa^2$ at $Q^2 = 20$ GeV^2 and $Q^2 = 50$ GeV^2, depicted in the lower panels of Figs. 10.1 and 10.2, is of the order of 1 - 100 fb in the kinematic domain where the asymmetry is largest. The luminosity for the eRHIC design in this setup is of the order of 10^{-5} fb^{-1}s^{-1}. It should therefore be well-feasible to obtain a clear signal for the asymmetry at eRHIC.

The asymmetry $\langle \sin(2\phi) \rangle$ for π^+ production at $Q^2 = 20$ GeV^2 and $Q^2 = 50$ GeV^2 is shown in Fig. 10.3. It is positive and in general smaller than the $\langle \sin \phi \rangle$ asymmetry. Again the asymmetry is largest for the largest lower bound $x_{\min}$. As already mentioned, this suggests that contributions from valence quarks dominate the cross section. We make
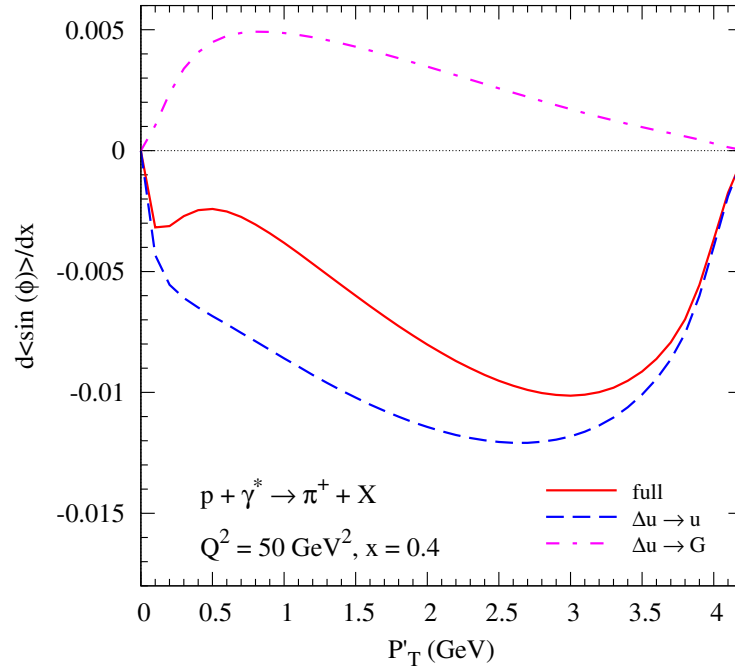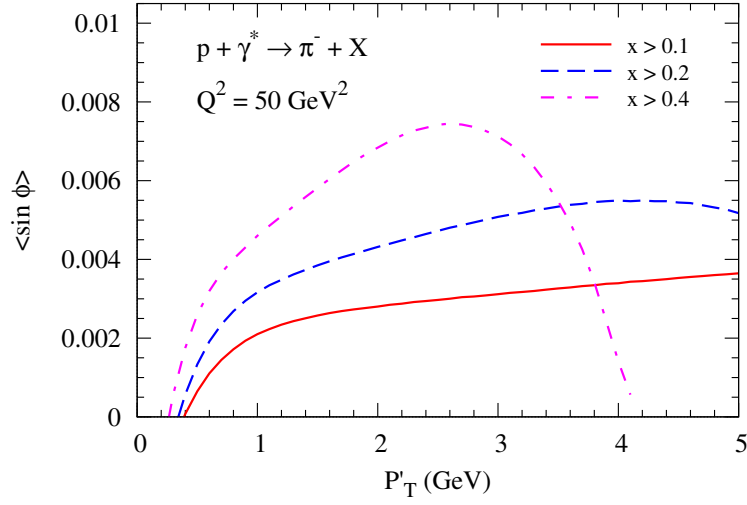
Figure 10.3.: The asymmetry $\langle \sin(2\phi) \rangle$ in π^+ production as a function of P_T' for $\sqrt{S} = 63$ GeV and $Q^2 = 20$ GeV^2 (upper plot) as well as $Q^2 = 50$ GeV^2 (lower plot). The solid, dashed and dot-dashed lines correspond to $x > 0.1$, 0.2 and 0.4, respectively.

this clear in Fig. 10.4, where the individual contributions from the partonic channels $\Delta u + \gamma^* \to u + X$ and $\Delta u + \gamma^* \to G + X$ to the differential asymmetry $\mathrm{d}\langle \sin \phi \rangle / \mathrm{d}x$ are shown at $Q^2 = 50$ GeV^2 and $x = 0.4$ in π^+ production. As discussed in the previous section, the hard-scattering functions corresponding to the quark-quark and quark-gluon process have different signs. It can be seen in Fig. 10.4 that the sum of both contributions almost entirely builds up the overall asymmetry. Hence, contributions from the helicity distributions $\Delta \bar{u}$, Δd, $\Delta \bar{d}$, Δs and $\Delta \bar{s}$ as well as ΔG are negligible for fragmentation into π^+ mesons.

Figure 10.4.: The differential asymmetry $d\langle\sin\phi\rangle/dx$ in π^+ production as a function of P'_T for $\sqrt{S} = 63$ GeV, $Q^2 = 50$ GeV^2 and $x = 0.4$. Individual contributions from the partonic processes $\Delta u + \gamma^* \to u + X$ and $\Delta u + \gamma^* \to G + X$ are also shown.

We also study the fragmentation into negatively charged mesons. Figure 10.5 shows the asymmetry $\langle\sin\phi\rangle$ at $Q^2 = 50$ GeV^2 for π^- production. The asymmetry is positive and its peak is a little lower than for the production of positively charged pions. Although not shown in the figure, the unpolarized cross section at the transverse momentum of the peak is smaller by a factor of 3 compared to the case of π^+ production. Now, let us again investigate the main partonic contributions to the asymmetry. The most important channels in this case are $\Delta d + \gamma^* \to d + X$, $\Delta u + \gamma^* \to u + X$ and $\Delta u + \gamma^* \to G + X$. Their contributions are shown in Fig. 10.6. Since the helicity PDF Δd is negative in the valence region, its contribution to the asymmetry is positive. It is noticeable that even for fragmentation into a negatively charged meson the asymmetry is dominated by the helicity distribution Δu. This statement also holds true if one considers heavier mesons in the final state, such as kaons.

A precise measurement of the single longitudinal-spin asymmetries in SIDIS would therefore provide clear information on the functional form of Δu. On the other hand, a determination of the still rather poorly known helicity distributions of the sea quarks and the gluon is not possible. Beside the analysis of helicity PDFs, an experimental confirmation of these higher-order perturbative T-odd effects would be desirable by itself.

Figure 10.5.: The asymmetry $\langle \sin \phi \rangle$ in π^- production as a function of P_T' for $\sqrt{S} = 63$ GeV and $Q^2 = 50$ GeV^2. The solid, dashed and dot-dashed lines correspond to $x > 0.1$, 0.2 and 0.4, respectively.

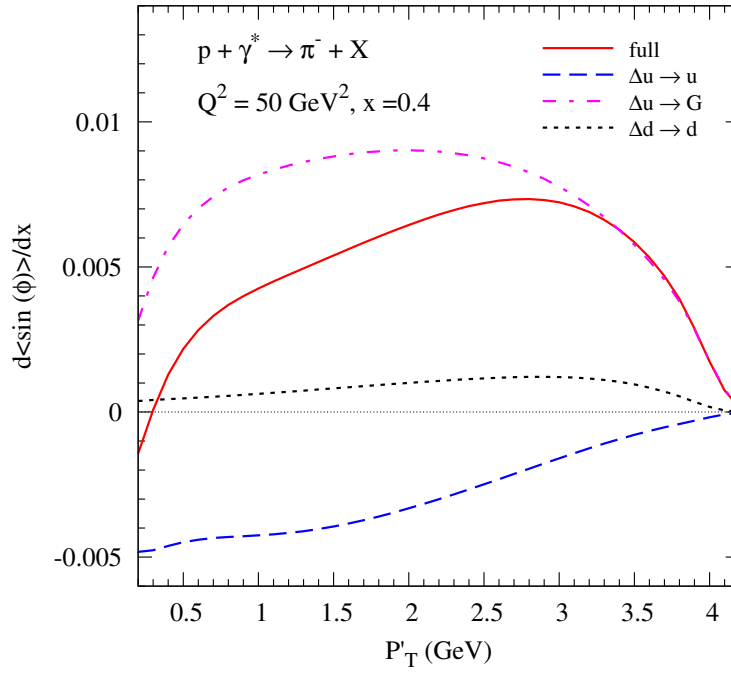Figure 10.6.: The differential asymmetry $d\langle \sin \phi \rangle/dx$ in π^- production as a function of P_T' for $\sqrt{S} = 63$ GeV, $Q^2 = 50$ GeV^2 and $x = 0.4$. Also shown are individual contributions from the partonic processes, $\Delta u + \gamma^* \to u + X$, $\Delta u + \gamma^* \to G + X$ and $\Delta d + \gamma^* \to d + X$.

11. Summary and Conclusions

We started out with an outline of the fundamental concepts of perturbative QCD, including asymptotic freedom, factorization, regularization and renormalization. We reviewed the current status of global PDF analyses for both protons and pions. While the PDFs of the proton are well-known, especially in the valence region, the analysis of pion PDFs suffers from the lack of reliable data. Information on the pion's parton distributions mainly comes from Drell-Yan data, which primarily constrain the valence distribution. However, results from fixed-order analyses of these data seemed to be at odds with theoretical predictions. We rederived the fixed LO and NLO hard-scattering functions for the Drell-Yan process and identified large logarithmic contributions to the cross section. These logarithms, which in particular dominate the cross section near the partonic threshold, are associated with soft-gluon radiation and have to be taken into account to all orders in perturbation theory. We outlined the proof of exponentiation of soft-gluon diagrams in non-abelian gauge theories by Gatheral, Frenkel and Taylor [81, 82], which allows for the resummation of large perturbative corrections to all orders, and presented NLL threshold-resummed formulae for the Drell-Yan cross section, originally derived by Sterman [13] and Catani and Trentadue [14].

Next, we performed an analysis of pion Drell-Yan data including NLL threshold resummation and determined a new valence PDF of the pion. Our obtained valence distribution is much softer in the high-x region than that obtained from fixed-order analyses, behaving roughly as $(1-x)^2$. The extracted high-x behavior agrees very well with predictions from perturbative QCD and nonperturbative Dyson-Schwinger equation approaches. We also found that in the kinematic regime of the Drell-Yan data the scale dependence of the cross section, which is the main theoretical uncertainty, is vastly reduced by resummation. However, the analysis also showed that due to the large overall systematic uncertainty of the available Drell-Yan data it is not possible to accurately determine the second moment of the pion's valence distribution, i.e. the total fraction of the pion's momentum carried by the valence quarks. We hope that the upcoming fixed-target Drell-Yan experiment at COMPASS provides data with a well-understood normalization and helps to resolve this issue. To contribute to the future analysis of these data, we performed a phenomenological study of the Drell-Yan cross section at COMPASS. To this end, we analyzed both rapidity-integrated and rapidity-differential cross sections. It turned out that in the kinematic regime accessed by the COMPASS experiment resummation leads to a significant

enhancement of the cross section above fixed-order calculations, even for moderate values of the invariant mass Q of the produced lepton pair. Particularly large corrections arise at large forward and backward rapidities of the lepton pair which significantly alter the shape of the rapidity-differential cross section.

We conclude that the inclusion of large perturbative corrections near the partonic threshold to all orders is crucial for the analysis of Drell-Yan data, especially in the fixed-target regime. Our results clearly show that the form of the extracted parton distributions is strongly affected by resummation. Indeed, our obtained valence distribution of the pion is in much better agreement with predictions from perturbative-QCD counting rules than the ones obtained in fixed-order analyses. This finding unmistakably demonstrates the importance of higher-order QCD calculations for the field of strong-interaction physics.

The second major topic of this thesis are single longitudinal-spin asymmetries in SIDIS. After reviewing some basic facts on spin asymmetries, we demonstrated that, if parity-violating interactions are neglected, single longitudinal-spin asymmetries in SIDIS are measurable in terms of T-odd observables. In perturbation theory T-odd effects only arise at higher orders due to the interference of the absorptive part of a transition amplitude with its leading-order (Born) term. We calculated the respective leading T-odd contributions to the partonic hard-scattering functions in SIDIS, which are of $\mathcal{O}(\alpha_s^2)$, and presented a formula for the calculation of the single longitudinal-spin asymmetry at hadron level. In a phenomenological study relevant for a future high-precision high-luminosity electron-ion collider at RHIC, we found that the expected asymmetry is small but still measurable. We also found that polarized u-quarks in the proton make the main contribution to the asymmetry in pion production. Gluonic contributions are down by more than an order of magnitude and therefore negligible.

Since T-odd longitudinal-spin asymmetries are pure higher-order QCD effects, we state, in conclusion, that the precise measurement of such observables at a future high-luminosity electron-ion collider may serve as a thorough test of the predictive power of fixed higher-order perturbative calculations.
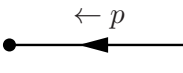
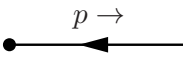# A. Feynman Rules, Cross Section Formulae

A.1. Feynman Rules

In this appendix the Feynman rules for the calculation of matrix elements in QCD are presented. Solid, curly and dashed lines represent quarks, gluons and ghosts, respectively. We denote the color indices for quarks by i, j and for gluons by a, b, c. It is understood that momentum is conserved at each vertex and it is integrated over each undetermined loop momentum. The normalization of the loop integrals is $\int \mathrm{d}^d k / (2\pi)^d$. For each closed fermion or ghost loop the matrix element is dressed with a factor of (-1).

For external-particle legs we have the rules (with p and s denoting the momentum and spin of the (anti)quark, and k and λ denoting the momentum and helicity of the gluon):

incoming quark

$$p \rightarrow \qquad = u(p, s)$$

outgoing quark

$$\leftarrow p \qquad = \bar{u}(p, s)$$

incoming antiquark

$$p \rightarrow \qquad = \bar{v}(p, s)$$

outgoing antiquark

$$\leftarrow p \qquad = v(p, s)$$

incoming gluon

$$k \rightarrow \qquad = \epsilon_\mu(k, \lambda)$$
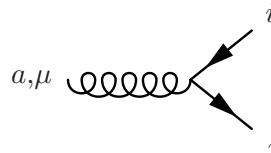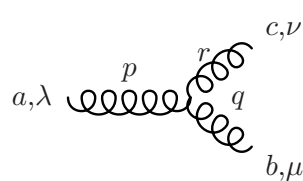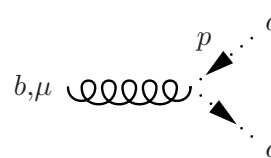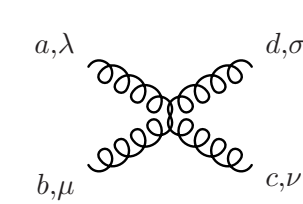
outgoing gluon $= \epsilon_\mu^*(k,\lambda)$

The quark, gluon and ghost propagators are (with the gauge parameter ξ):

          $i\delta_{ij}\dfrac{\not{p}+m}{p^2-m^2+i\eta}$

          $\dfrac{-i\delta^{ab}}{k^2+i\eta}\left[g_{\mu\nu}-(1-\xi)\dfrac{k_\mu k_\nu}{k^2}\right]$

          $\dfrac{i\delta^{ab}}{p^2+i\eta}$

The interaction of quarks, gluons and ghosts is contained in the Feynman rules for the vertices. Note that at the three-gluon vertex all momenta are chosen to be outgoing:

          $ig\gamma_\mu t_{ij}^a$

          $gf^{abc}[(p-q)_\nu g_{\rho\mu}+(q-r)_\rho g_{\mu\nu}+(r-p)_\mu g_{\nu\rho}]$

          $-gf^{abc}p_\mu$

$-ig^2 f^{abe}f^{cde}(g_{\rho\nu}g_{\mu\sigma}-g_{\rho\sigma}g_{\mu\nu})$

$-ig^2 f^{ace}f^{bde}(g_{\rho\mu}g_{\nu\sigma}-g_{\rho\sigma}g_{\mu\nu})$

$-ig^2 f^{ade}f^{cbe}(g_{\rho\nu}g_{\mu\sigma}-g_{\rho\mu}g_{\sigma\nu})$

When we calculate the absolute square of matrix elements, we encounter projection

operators for external quarks, antiquarks and gluons. For definite helicity $\lambda = \pm 1$ these projection operators are given by

$$u(p, \lambda)\bar{u}(p, \lambda) = \frac{1 + \gamma_5 \lambda}{2}(\not{p} + m),$$

$$v(p, \lambda)\bar{v}(p, \lambda) = \frac{1 - \gamma_5 \lambda}{2}(\not{p} - m),$$

$$\epsilon^\mu(k, \lambda)\epsilon^{*\nu}(k, \lambda) = \frac{1}{2}\left[-g^{\mu\nu} + \frac{k^\mu r^\nu + k^\nu r^\mu}{q \cdot r} + \frac{i}{k \cdot r}\lambda\epsilon^{\mu\nu\rho\sigma}k_\rho r_\sigma\right],$$

where r is an arbitrary vector with $r^2 = 0$ and $k \cdot r \neq 0$.

A.2. NLO Hard-Scattering Functions for the Drell-Yan Process

In this appendix we collect the $\mathcal{O}(\alpha_s)$ hard-scattering functions $\tilde{\omega}_{ab}^{(1)}$ for the rapidity-differential Drell-Yan cross section defined in Eq. (5.14). The parton-level expressions were derived in the DIS factorization scheme in Ref. [78]. In the $\overline{\text{MS}}$-scheme they can be found in the Appendix of Ref. [9]. However, we note that Ref. [9] adopts a non-standard polarization average for incoming gluons in dimensional regularization. We correct for this and collect the expressions for the NLO hard-scattering functions in the $\overline{\text{MS}}$-scheme for renormalization and factorization scale $\mu = Q$.

The $\mathcal{O}(\alpha_s)$ corrections to the quark-antiquark annihilation channel read

$$\tilde{\omega}_{q\bar{q}}^{(1)} = \frac{C_F}{2}x_1 x_2 \delta(x_1 - x_1^0)\delta(x_2 - x_2^0)\left(-8 + \frac{\pi^2}{3} + \ln^2(1 - x_1^0) + \ln^2(1 - x_2^0) + 2\text{Li}_2(x_1^0)\right.$$

$$\left. + 2\text{Li}_2(x_2^0) + 2\ln\frac{x_1^0}{1 - x_1^0}\ln\frac{x_2^0}{1 - x_2^0}\right)$$

$$+ \frac{C_F}{2}x_1 x_2 \delta(x_2 - x_2^0)\left(\frac{x_1^2 + (x_1^0)^2}{x_1^2(x_1 - x_1^0)_+}\ln\frac{2x_1^0(1 - x_2^0)}{x_2^0(x_1 + x_1^0)} + \frac{1}{x_1} - \frac{x_1^0}{x_1^2} - \frac{x_1^2 + (x_1^0)^2}{x_1^2(x_1 - x_1^0)}\ln\frac{x_1^0}{x_1}\right.$$

$$\left. + \frac{x_1^2 + (x_1^0)^2}{x_1^2}\left[\frac{\ln(1 - x_1^0/x_1)}{x_1 - x_1^0}\right]_+\right)$$

$$+ (1 \leftrightarrow 2)$$

$$+ C_F x_1 x_2\left(\frac{G^A(x_1, x_2)}{\left[(x_1 - x_1^0)(x_2 - x_2^0)\right]_+} + H^A(x_1, x_2)\right), \tag{A.1}$$

where the functions G^A and H^A are

$$G^A(x_1, x_2) = \frac{(\tau + x_1 x_2)\left[\tau^2 + (x_1 x_2)^2\right]}{(x_1 x_2)^2(x_1 + x_1^0)(x_2 + x_2^0)},$$

$$H^A(x_1, x_2) = \frac{-2\tau(\tau + x_1 x_2)}{x_1 x_2(x_1 x_1^0 + x_2 x_2^0)^2}. \tag{A.2}$$

Here, the plus-prescriptions are defined by

$$\int_{x_1^0}^1 dx_1 \frac{f(x_1)}{(x_1 - x_1^0)_+} = \int_{x_1^0}^1 dx_1 \frac{f(x_1) - f(x_1^0)}{x_1 - x_1^0},$$

$$\int_{x_1^0}^1 dx_1 \int_{x_2^0}^1 dx_2 \frac{f(x_1, x_2)}{[(x_1 - x_1^0)(x_2 - x_2^0)]_+} = \int_{x_1^0}^1 dx_1 \int_{x_2^0}^1 dx_2$$

$$\times \frac{f(x_1, x_2) - f(x_1, x_2^0) - f(x_1^0, x_2) + f(x_1^0, x_2^0)}{(x_1 - x_1^0)(x_2 - x_2^0)}. \tag{A.3}$$

The hard-scattering function for the QCD Compton process is given by

$$\tilde{\omega}_{qG}^{(1)} = \frac{1}{2} x_1 x_2 \delta(x_2 - x_2^0) \left(\frac{(x_1^0)^2 + (x_1 - x_1^0)^2}{2x_1^3} \left[\ln \frac{2(1 - x_2^0)(x_1 - x_1^0)}{x_2^0(x_1 + x_1^0)} - 1 \right] + \frac{1}{2x_1} \right)$$

$$+ \frac{1}{2} x_1 x_2 \left(\frac{G^C(x_1, x_2)}{(x_2 - x_2^0)_+} + H^C(x_1, x_2) \right), \tag{A.4}$$

where

$$G^C(x_1, x_2) = \frac{x_2^0(\tau + x_1 x_2)[\tau^2 + (\tau - x_1 x_2)^2]}{x_1^3 x_2^2 (x_1 x_2^0 + x_2 x_1^0)(x_2 + x_2^0)},$$

$$H^C(x_1, x_2) = \frac{\tau(\tau + x_1 x_2)[x_1 x_2^2 x_1^0 + \tau(x_1 x_2^0 + 2x_2 x_1^0)]}{(x_1 x_2)^2 (x_1 x_2^0 + x_2 x_1^0)^3}. \tag{A.5}$$

A.3. LO Spin-Averaged SIDIS Cross Section

We collect the lowest-order perturbative contributions to the unpolarized SIDIS cross section for non-vanishing P_T'. The respective expressions were first derived in Ref. [156].

Similar to Eq. (10.4) the unpolarized SIDIS cross section is of the form,

$$\frac{d\sigma}{dx \, dQ^2 \, dz \, d\kappa^2 \, d\phi} = \frac{\pi \alpha^2 y^2}{4Q^4 z} L^{\mu\nu} W_{\mu\nu}, \tag{A.6}$$

where the contraction of the leptonic and hadronic tensor is given by

$$L^{\mu\nu} W_{\mu\nu} = \sum_{a,b} \int_x^1 \frac{d\xi}{\xi} \int_z^1 \frac{d\eta}{\eta^2} D_a^H(\eta) f_b^p(\xi) \frac{2\hat{z} e_{ab}}{(2\pi)^3 y^2} \left(A^{ab} + B^{ab} \cos\phi + C^{ab} \cos(2\phi) \right)$$

$$\times \delta \left(\hat{\kappa}^2 - \frac{1 - \hat{x}}{\hat{x}} \hat{z}(1 - \hat{z}) \right) \tag{A.7}$$

with $e_{ab} = e_q^2$. The fragmentation function for a parton a into a hadron H is denoted by D_a^H and f_b^p is the unpolarized PDF for a parton b in a proton.

For the quark-quark and the antiquark-antiquark channel the coefficients read

$$A^{qq} = A^{\bar{q}\bar{q}} = g^2 C_F \left(16(1-y)\hat{x}\hat{z} + 2\left[1 + (1-y)^2\right] \left[(1-\hat{x})(1-\hat{z}) + \frac{1 + \hat{x}^2\hat{z}^2}{(1-\hat{x})(1-\hat{z})}\right]\right),$$

$$B^{qq} = B^{\bar{q}\bar{q}} = -8g^2 C_F \sqrt{1-y}(2-y)\sqrt{\frac{\hat{x}\hat{z}}{(1-\hat{x})(1-\hat{z})}}\left[\hat{x}\hat{z} + (1-\hat{x})(1-\hat{z})\right],$$

$$C^{qq} = C^{\bar{q}\bar{q}} = 8g^2 C_F(1-y)\hat{x}\hat{z}. \tag{A.8}$$

Note that due to a different normalization the coefficients in Eq. (A.8) differ by a factor of 2 from the coefficients in Ref. [156].

For the gluon-initiated partonic subprocess the respective coefficients are

$$A^{qG} = 16g^2(1-y)\hat{x}(1-\hat{x}) + g^2\left[1 + (1-y)^2\right]\left[\hat{x}^2 + (1-\hat{x})^2\right]\frac{\hat{z}^2 + (1-\hat{z})^2}{\hat{z}(1-\hat{z})},$$

$$B^{qG} = -4g^2\sqrt{1-y}(2-y)\sqrt{\frac{\hat{x}(1-\hat{x})}{\hat{z}(1-\hat{z})}}(1-2\hat{x})(1-2\hat{z}),$$

$$C^{qG} = 8g^2(1-y)\hat{x}(1-\hat{x}). \tag{A.9}$$

The partonic hard-scattering cross sections for the remaining channels can be obtained from the expressions above by:

$$A^{Gq}(\hat{z}) = A^{qq}(1-\hat{z}), \quad B^{Gq}(\hat{z}) = B^{qq}(1-\hat{z}), \quad C^{Gq}(\hat{z}) = C^{qq}(1-\hat{z}),$$
$$A^{G\bar{q}}(\hat{z}) = A^{\bar{q}\bar{q}}(1-\hat{z}), \quad B^{G\bar{q}}(\hat{z}) = B^{\bar{q}\bar{q}}(1-\hat{z}), \quad C^{G\bar{q}}(\hat{z}) = C^{\bar{q}\bar{q}}(1-\hat{z}),$$
$$A^{\bar{q}G}(\hat{z}) = A^{qG}(1-\hat{z}), \quad B^{\bar{q}G}(\hat{z}) = B^{qG}(1-\hat{z}), \quad C^{\bar{q}G}(\hat{z}) = C^{qG}(1-\hat{z}). \tag{A.10}$$

Acknowledgements

Bibliography

[1] M. Gell-Mann, Phys.Lett. **8**, 214 (1964).

[2] G. Zweig in CERN-TH-401.

[3] D. Gross and F. Wilczek, Phys.Rev.Lett. **30**, 1343 (1973).

[4] H. Politzer, Phys.Rev.Lett. **30**, 1346 (1973).

[5] J. Pumplin *et al.*, JHEP **07**, 012 (2002), arXiv:hep-ph/0201195.

[6] A. D. Martin, W. J. Stirling, R. S. Thorne, and G. Watt, Eur. Phys. J. **C63**, 189 (2009), arXiv:0901.0002 [hep-ph].

[7] R. D. Ball *et al.*, Nucl. Phys. **B838**, 136 (2010), arXiv:1002.4407 [hep-ph].

[8] J. S. Conway *et al.*, Phys. Rev. **D39**, 92 (1989).

[9] P. J. Sutton, A. D. Martin, R. G. Roberts, and W. J. Stirling, Phys. Rev. **D45**, 2349 (1992).

[10] M. Gluck, E. Reya, and I. Schienbein, Eur. Phys. J. **C10**, 313 (1999), arXiv:hep-ph/9903288.

[11] K. Wijesooriya, P. E. Reimer, and R. J. Holt, Phys. Rev. **C72**, 065203 (2005), arXiv:nucl-ex/0509012.

[12] R. J. Holt and C. D. Roberts, Rev. Mod. Phys. **82**, 2991 (2010), arXiv:1002.4666 [nucl-th].

[13] G. Sterman, Nucl. Phys. **B281**, 310 (1987).

[14] S. Catani and L. Trentadue, Nucl. Phys. **B327**, 323 (1989).

[15] G. Bunce *et al.*, Phys.Rev.Lett. **36**, 1113 (1976).

[16] M. Aggarwal *et al.* (STAR Collaboration), Phys.Rev.Lett. **106**, 062002 (2011), arXiv:1009.0326 [hep-ex].

[17] A. Adare *et al.* (PHENIX Collaboration), Phys.Rev.Lett. **106**, 062001 (2011), arXiv:1009.0505 [hep-ex].

[18] L. Faddeev and V. Popov, Phys.Lett. **B25**, 29 (1967).

[19] R. Slansky, Phys. Rept. **79**, 1 (1981).

[20] S. Bethke, Eur. Phys. J. **C64**, 689 (2009), arXiv:0908.1135 [hep-ph].

[21] F. Bloch and A. Nordsieck, Phys. Rev. **52**, 54 (1937).

[22] T. Kinoshita, J. Math. Phys. **3**, 650 (1962).

[23] T. D. Lee and M. Nauenberg, Phys. Rev. **133**, B1549 (1964).

[24] J. D. Jackson , John Wiley & Sons (1962).

[25] G. 't Hooft and M. J. G. Veltman, Nucl. Phys. **B44**, 189 (1972).

[26] C. G. Bollini and J. J. Giambiagi, Nuovo Cim. **B12**, 20 (1972).

[27] C. G. Bollini and J. J. Giambiagi, Phys. Lett. **B40**, 566 (1972).

[28] P. Breitenlohner and D. Maison, Commun.Math.Phys. **52**, 11 (1977).

[29] A. A. Slavnov, Theor. Math. Phys. **10**, 99 (1972).

[30] J. C. Taylor, Nucl. Phys. **B33**, 436 (1971).

[31] G. 't Hooft, Nucl.Phys. **B61**, 455 (1973).

[32] W. A. Bardeen, A. Buras, D. Duke, and T. Muta, Phys.Rev. **D18**, 3998 (1978).

[33] D. Amati, R. Petronzio, and G. Veneziano, Nucl.Phys. **B140**, 54 (1978).

[34] D. Amati, R. Petronzio, and G. Veneziano, Nucl.Phys. **B146**, 29 (1978).

[35] S. B. Libby and G. F. Sterman, Phys.Rev. **D18**, 3252 (1978).

[36] R. Ellis, H. Georgi, M. Machacek, H. Politzer, and G. G. Ross, Nucl.Phys. **B152**, 285 (1979).

[37] J. C. Collins, D. E. Soper, and G. F. Sterman, Phys.Lett. **B134**, 263 (1984).

[38] J. C. Collins, D. E. Soper, and G. Sterman, Nucl. Phys. **B261**, 104 (1985).

[39] J. C. Collins, D. E. Soper, and G. F. Sterman, Adv.Ser.Direct.High Energy Phys. **5**, 1 (1988), to be publ. in 'Perturbative QCD' (A.H. Mueller, ed.) (World Scientific Publ., 1989), arXiv:hep-ph/0409313 [hep-ph].

[40] G. C. Nayak, J.-W. Qiu, and G. F. Sterman, Phys.Rev. **D72**, 114012 (2005), arXiv:hep-ph/0509021 [hep-ph].

[41] Y. L. Dokshitzer, Sov. Phys. JETP **46**, 641 (1977).

[42] G. Altarelli and G. Parisi, Nucl. Phys. **B126**, 298 (1977).

[43] V. N. Gribov and L. N. Lipatov, Sov. J. Nucl. Phys. **15**, 438 (1972).

[44] S. Moch, J. Vermaseren, and A. Vogt, Nucl.Phys. **B688**, 101 (2004), arXiv:hep-ph/0403192 [hep-ph].

[45] A. Vogt, S. Moch, and J. Vermaseren, Nucl.Phys. **B691**, 129 (2004), arXiv:hep-ph/0404111 [hep-ph].

[46] D. de Florian, R. Sassot, M. Stratmann, and W. Vogelsang, Phys. Rev. Lett. **101**, 072001 (2008), arXiv:0804.0422 [hep-ph].

[47] D. de Florian, R. Sassot, M. Stratmann, and W. Vogelsang, Phys. Rev. **D80**, 034030 (2009), arXiv:0904.3821 [hep-ph].

[48] M. Gluck, E. Reya, M. Stratmann, and W. Vogelsang, Phys. Rev. **D63**, 094005 (2001), arXiv:hep-ph/0011215.

[49] D. de Florian, G. A. Navarro, and R. Sassot, Phys. Rev. **D71**, 094018 (2005), arXiv:hep-ph/0504155.

[50] R. Mertig and W. van Neerven, Z.Phys. **C70**, 637 (1996), arXiv:hep-ph/9506451 [hep-ph].

[51] W. Vogelsang, Nucl.Phys. **B475**, 47 (1996), arXiv:hep-ph/9603366 [hep-ph].

[52] W. Vogelsang, Phys.Rev. **D54**, 2023 (1996), arXiv:hep-ph/9512218 [hep-ph].

[53] M. Diehl, Phys. Rept. **388**, 41 (2003), arXiv:hep-ph/0307382.

[54] A. V. Belitsky and A. V. Radyushkin, Phys. Rept. **418**, 1 (2005), arXiv:hep-ph/0504030.

[55] M. Gockeler *et al.* (QCDSF), Phys. Rev. Lett. **92**, 042002 (2004), arXiv:hep-ph/0304249.

[56] P. Hagler *et al.* (LHPC), Phys. Rev. **D77**, 094502 (2008), arXiv:0705.4295 [hep-lat].

[57] P. Bordalo *et al.* (NA10), Phys. Lett. **B193**, 373 (1987).

[58] G. Alverson *et al.* (FERMILAB-E706), Phys. Rev. **D48**, 5 (1993).

[59] G. R. Farrar and D. R. Jackson, Phys.Rev.Lett. **43**, 246 (1979).

[60] E. L. Berger and S. J. Brodsky, Phys.Rev.Lett. **42**, 940 (1979).

[61] S. J. Brodsky and F. Yuan, Phys.Rev. **D74**, 094018 (2006), arXiv:hep-ph/0610236 [hep-ph].

[62] F. Yuan, Phys.Rev. **D69**, 051501 (2004), arXiv:hep-ph/0311288 [hep-ph].

[63] M. Hecht, C. D. Roberts, and S. Schmidt, Phys.Rev. **C63**, 025213 (2001), arXiv:nucl-th/0008049 [nucl-th].

[64] T. Nguyen, A. Bashir, C. D. Roberts, and P. C. Tandy(2011), arXiv:1102.2448 [nucl-th].

[65] T. Shigetani, K. Suzuki, and H. Toki, Phys.Lett. **B308**, 383 (1993), arXiv:hep-ph/9402286 [hep-ph].

[66] A. Dorokhov and L. Tomio, Phys.Rev. **D62**, 014016 (2000).

[67] T. Frederico and G. Miller, Phys.Rev. **D50**, 210 (1994).

[68] P. Rijken and W. van Neerven, Nucl.Phys. **B487**, 233 (1997), arXiv:hep-ph/9609377 [hep-ph].

[69] S. Kretzer, Phys.Rev. **D62**, 054001 (2000), arXiv:hep-ph/0003177 [hep-ph].

[70] S. Albino, B. Kniehl, and G. Kramer, Nucl.Phys. **B725**, 181 (2005), arXiv:hep-ph/0502188 [hep-ph].

[71] B. A. Kniehl, G. Kramer, and B. Potter, Nucl.Phys. **B582**, 514 (2000), arXiv:hep-ph/0010289 [hep-ph].

[72] M. Hirai, S. Kumano, T.-H. Nagai, and K. Sudoh, Phys.Rev. **D75**, 094009 (2007), arXiv:hep-ph/0702250 [hep-ph].

[73] D. de Florian, R. Sassot, and M. Stratmann, Phys.Rev. **D75**, 114010 (2007), arXiv:hep-ph/0703242 [hep-ph].

[74] D. de Florian, R. Sassot, and M. Stratmann, Phys.Rev. **D76**, 074033 (2007), arXiv:0707.1506 [hep-ph].

[75] S. Drell and T.-M. Yan, Phys.Rev.Lett. **25**, 316 (1970).

[76] G. Altarelli, R. K. Ellis, and G. Martinelli, Nucl. Phys. **B157**, 461 (1979).

[77] T. Gehrmann, Nucl.Phys. **B498**, 245 (1997), arXiv:hep-ph/9702263 [hep-ph].

[78] J. Kubar, M. Le Bellac, J. L. Meunier, and G. Plaut, Nucl. Phys. **B175**, 251 (1980).

[79] D. R. Yennie, S. C. Frautschi, and H. Suura, Ann. Phys. **13**, 379 (1961).

[80] G. Sterman in *Tallahassee 1981, Proceedings, Perturbative Quantum Chromodynamics*, 22-40.

[81] J. G. M. Gatheral, Phys. Lett. **B133**, 90 (1983).

[82] J. Frenkel and J. C. Taylor, Nucl. Phys. **B246**, 231 (1984).

[83] M. E. Peskin and D. V. Schroeder , Reading, Perseus Books (1995), ch. 6.5.

[84] C. F. Berger(2003), arXiv:hep-ph/0305076.

[85] J. Frenkel, J. Gatheral, and J. Taylor, Nucl.Phys. **B233**, 307 (1984).

[86] E. Laenen, G. Stavenga, and C. D. White, JHEP **0903**, 054 (2009), arXiv:0811.2067 [hep-ph].

[87] E. Laenen, L. Magnea, G. Stavenga, and C. D. White, JHEP **1101**, 141 (2011), arXiv:1010.1860 [hep-ph].

[88] S. Forte and G. Ridolfi, Nucl.Phys. **B650**, 229 (2003), arXiv:hep-ph/0209154 [hep-ph].

[89] A. V. Manohar, Phys.Rev. **D68**, 114019 (2003), arXiv:hep-ph/0309176 [hep-ph].

[90] A. Idilbi and X.-d. Ji, Phys.Rev. **D72**, 054016 (2005), arXiv:hep-ph/0501006 [hep-ph].

[91] T. Becher, M. Neubert, and G. Xu, JHEP **0807**, 030 (2008), arXiv:0710.0680 [hep-ph].

[92] A. Vogt, Phys.Lett. **B497**, 228 (2001), arXiv:hep-ph/0010146 [hep-ph].

[93] J. Kodaira and L. Trentadue, Phys. Lett. **B112**, 66 (1982).

[94] T. O. Eynck, E. Laenen, and L. Magnea, JHEP **06**, 057 (2003), arXiv:hep-ph/0305179.

[95] M. Beneke and V. M. Braun(2000), arXiv:hep-ph/0010208 [hep-ph].

[96] S. Catani, M. L. Mangano, P. Nason, and L. Trentadue, Nucl. Phys. **B478**, 273 (1996), arXiv:hep-ph/9604351.

[97] S. Catani, M. L. Mangano, and P. Nason, JHEP **07**, 024 (1998), arXiv:hep-ph/9806484.

[98] R. Bonciani, S. Catani, M. L. Mangano, and P. Nason, Nucl.Phys. **B529**, 424 (1998), arXiv:hep-ph/9801375 [hep-ph].

[99] G. F. Sterman and W. Vogelsang(1999), arXiv:hep-ph/9910371 [hep-ph].

[100] D. de Florian, A. Kulesza, and W. Vogelsang, JHEP **0602**, 047 (2006), arXiv:hep-ph/0511205 [hep-ph].

[101] D. de Florian and W. Vogelsang, Phys.Rev. **D71**, 114004 (2005), arXiv:hep-ph/0501258 [hep-ph].

[102] L. G. Almeida, G. F. Sterman, and W. Vogelsang, Phys.Rev. **D80**, 074016 (2009), arXiv:0907.1234 [hep-ph].

[103] A. Kulesza, G. Sterman, and W. Vogelsang, Phys. Rev. **D69**, 014012 (2004), arXiv:hep-ph/0309264.

[104] A. Kulesza, G. Sterman, and W. Vogelsang, Phys. Rev. **D66**, 014011 (2002), arXiv:hep-ph/0202251.

[105] S. Catani, D. de Florian, and M. Grazzini, JHEP **01**, 015 (2002), arXiv:hep-ph/0111164.

[106] G. Bozzi, S. Catani, D. de Florian, and M. Grazzini, Nucl.Phys. **B791**, 1 (2008), arXiv:0705.3887 [hep-ph].

[107] G. Sterman and W. Vogelsang, JHEP **02**, 016 (2001), arXiv:hep-ph/0011289.

[108] A. Mukherjee and W. Vogelsang, Phys. Rev. **D73**, 074005 (2006), arXiv:hep-ph/0601162.

[109] E. Laenen and G. F. Sterman(1992).

[110] P. Bolzoni, Phys.Lett. **B643**, 325 (2006), arXiv:hep-ph/0609073 [hep-ph].

[111] M. Aicher, A. Schafer, and W. Vogelsang, Phys.Rev.Lett. **105**, 252003 (2010), arXiv:1009.2481 [hep-ph].

[112] G. Corcella and L. Magnea, Phys.Rev. **D72**, 074017 (2005), arXiv:hep-ph/0506278 [hep-ph].

[113] D. de Florian and R. Sassot, Phys. Rev. **D69**, 074028 (2004), arXiv:hep-ph/0311227.

[114] M. Gluck, E. Reya, and M. Stratmann, Eur.Phys.J. **C2**, 159 (1998), arXiv:hep-ph/9711369 [hep-ph].

[115] http://wwwcompass.chern.ch/compass/future_physics/drellyan/.

[116] H. Shimizu, G. Sterman, W. Vogelsang, and H. Yokoya, Phys. Rev. **D71**, 114007 (2005), arXiv:hep-ph/0503270.

[117] V. Ravindran, J. Smith, and W. van Neerven, Nucl.Phys. **B767**, 100 (2007), arXiv:hep-ph/0608308 [hep-ph].

[118] C. S. Li, Z. Li, and C.-P. Yuan, JHEP **0906**, 033 (2009), arXiv:0903.1798 [hep-ph].

[119] M. Bonvini, S. Forte, and G. Ridolfi, Nucl.Phys. **B847**, 93 (2011), arXiv:1009.5691 [hep-ph].

[120] M. Aicher, A. Schafer, and W. Vogelsang, Phys.Rev. **D83**, 114023 (2011), arXiv:1104.3512 [hep-ph].

[121] A. Bravar (Spin Muon Collaboration), Nucl.Phys. **A666**, 314 (2000).

[122] M. Alekseev *et al.* (COMPASS Collaboration), Phys.Lett. **B673**, 127 (2009), arXiv:0802.2160 [hep-ex].

[123] V. Alexakhin *et al.* (COMPASS Collaboration), Phys.Rev.Lett. **94**, 202002 (2005), arXiv:hep-ex/0503002 [hep-ex].

[124] A. Airapetian *et al.* (HERMES Collaboration), Phys.Rev.Lett. **103**, 152002 (2009), arXiv:0906.3918 [hep-ex].

[125] A. Airapetian *et al.* (HERMES Collaboration), Phys.Rev.Lett. **94**, 012002 (2005), arXiv:hep-ex/0408013 [hep-ex].

[126] A. Airapetian *et al.* (HERMES Collaboration), Phys.Rev.Lett. **84**, 4047 (2000), arXiv:hep-ex/9910062 [hep-ex].

[127] D. W. Sivers, Phys.Rev. **D41**, 83 (1990).

[128] D. W. Sivers, Phys.Rev. **D43**, 261 (1991).

[129] J. C. Collins, Nucl.Phys. **B396**, 161 (1993), arXiv:hep-ph/9208213 [hep-ph].

[130] P. Mulders and R. Tangerman, Nucl.Phys. **B461**, 197 (1996), arXiv:hep-ph/9510301 [hep-ph].

[131] D. Boer and P. Mulders, Phys.Rev. **D57**, 5780 (1998), arXiv:hep-ph/9711485 [hep-ph].

[132] D. Boer, P. Mulders, and F. Pijlman, Nucl.Phys. **B667**, 201 (2003), arXiv:hep-ph/0303034 [hep-ph].

[133] A. Efremov and O. Teryaev, Sov.J.Nucl.Phys. **36**, 140 (1982).

[134] A. Efremov and O. Teryaev, Phys.Lett. **B150**, 383 (1985).

[135] J.-w. Qiu and G. F. Sterman, Phys.Rev.Lett. **67**, 2264 (1991).

[136] J.-w. Qiu and G. F. Sterman, Nucl.Phys. **B378**, 52 (1992).

[137] J.-w. Qiu and G. F. Sterman, Phys.Rev. **D59**, 014004 (1999), arXiv:hep-ph/9806356 [hep-ph].

[138] X. Ji, J.-W. Qiu, W. Vogelsang, and F. Yuan, Phys.Rev.Lett. **97**, 082002 (2006), arXiv:hep-ph/0602239 [hep-ph].

[139] X. Ji, J.-w. Qiu, W. Vogelsang, and F. Yuan, Phys.Rev. **D73**, 094017 (2006), arXiv:hep-ph/0604023 [hep-ph].

[140] X. Ji, J.-W. Qiu, W. Vogelsang, and F. Yuan, Phys.Lett. **B638**, 178 (2006), arXiv:hep-ph/0604128 [hep-ph].

[141] A. Bacchetta, D. Boer, M. Diehl, and P. J. Mulders, JHEP **0808**, 023 (2008), arXiv:0803.0227 [hep-ph].

[142] A. Airapetian *et al.* (HERMES Collaboration), Phys.Rev. **D64**, 097101 (2001), arXiv:hep-ex/0104005 [hep-ex].

[143] A. Airapetian *et al.* (HERMES Collaboration), Phys.Lett. **B562**, 182 (2003), arXiv:hep-ex/0212039 [hep-ex].

[144] B.-Q. Ma, I. Schmidt, and J.-J. Yang, Phys.Rev. **D63**, 037501 (2001), arXiv:hep-ph/0009297 [hep-ph].

[145] B.-Q. Ma, I. Schmidt, and J.-J. Yang, Phys.Rev. **D66**, 094001 (2002), arXiv:hep-ph/0209114 [hep-ph].

[146] A. Efremov, K. Goeke, and P. Schweitzer, Phys.Lett. **B522**, 37 (2001), arXiv:hep-ph/0108213 [hep-ph].

[147] A. Efremov, K. Goeke, and P. Schweitzer, Eur.Phys.J. **C24**, 407 (2002), arXiv:hep-ph/0112166 [hep-ph].

[148] A. De Rujula, J. Kaplan, and E. De Rafael, Nucl.Phys. **B35**, 365 (1971).

[149] K. Hagiwara, K.-i. Hikasa, and N. Kai, Phys. Rev. **D27**, 84 (1983).

[150] J. G. Korner and G. Schuler, Z. Phys. **C26**, 559 (1985).

[151] J. G. Korner, B. Melic, and Z. Merebashvili, Phys. Rev. **D62**, 096011 (2000), arXiv:hep-ph/0002302.

[152] M. Ahmed and T. Gehrmann, Phys.Lett. **B465**, 297 (1999), arXiv:hep-ph/9906503 [hep-ph].

[153] B. Pire and J. P. Ralston, Phys.Rev. **D28**, 260 (1983).

[154] K. Hagiwara, K.-i. Hikasa, and N. Kai, Phys.Rev.Lett. **52**, 1076 (1984).

[155] R. D. Carlitz and R. Willey, Phys.Rev. **D45**, 2323 (1992).

[156] A. Mendez, Nucl.Phys. **B145**, 199 (1978).